



NTNU – Trondheim
Norwegian University of
Science and Technology

On Shear Wave Velocity Testing in Clay

Henrik Takle Eide

Civil and Environmental Engineering

Submission date: June 2015

Supervisor: Steinar Nordal, BAT

Norwegian University of Science and Technology
Department of Civil and Transport Engineering



| | | | | |
|---|---|---|--------------|--|
| Report Title: On Shear Wave Velocity Testing in Clay | Date: 09.06.2015 | | | |
| | Number of pages (incl. appendices): 145 | | | |
| | Master Thesis | X | Project Work | |
| Name: Henrik Takle Eide | | | | |
| Advisors: Amanuensis Arnfinn Emdal, Professor Steinar Nordal | | | | |
| Other external professional contacts/supervisors: Jean-Sebastien L'Heureux, NGI | | | | |

Abstract:

The soil stiffness at small strains is an important parameter for settlement predictions and for understanding soil behaviour under seismic/dynamic loading. The small strain stiffness is usually found from the shear wave velocity, V_s , obtained by wave propagation tests in field and laboratory. Results from laboratory testing have proved to be different from results obtained by in situ testing. The results from invasive and non-invasive tests in situ also tend to differ.

In this study, various wave propagation tests are carried out to obtain V_s in clay. The results from the various tests are compared and discussed. The assessed field tests are Seismic Cone Penetration Test (SCPT), Crosshole Test (CHT) and Multichannel Analysis of Surface Waves (MASW). Bender element testing on 54 mm samples is carried out in the laboratory. Testing is performed at various sites, but only the results from the Tiller site are presented in this thesis. The Tiller site is a NTNU research site consisting of low plasticity clay. Quick clay is expected below about 8 m depth. Two profiles, 50 m apart, are investigated at Tiller.

Full V_s -profiles to about 20 m depth are found using SCPT and MASW. The SCPT data are processed using both cross-correlation and crossover method. The crossover method, with a pseudo-interval spacing of 3 m or more, provide the best results. These results are considered to be the most accurate of all the assessed tests.

MASW surveys were carried out in two rounds. The original survey provides significantly higher V_s -results than expected at depths below 8 m. Lower frequencies are produced in the repeated survey. The repeated survey provides a V_s -profile similar to the result obtained from SCPT.

CHT is only performed at one profile and the equipment measures V_s at just one depth. Most of the received signals obtained at Tiller are unclear. V_s is however estimated from the received signals. A significant uncertainty is not expected. The result from CHT corresponds well to results from SCPT and MASW.

Eight samples are tested in a triaxial cell with bender elements. The results show significantly lower V_s compared to the field tests. Five samples from the same depth with various height are tested. No difference in V_s related to sample height are found. That suggest that there is no system time delay in the system.

Two samples are consolidated past the primary consolidation to investigate the aging effect. The bender element results are found to correspond fairly well with in situ measurements when they are adjusted for the aging effect.

The aging effect does however seem to be different in sensitive and non-sensitive clay samples.

A brief study on the consequences of variation in V_s in practical engineering is conducted with respect to settlement and earthquake engineering. Both the settlement and earthquake analyses show significant influence of variation in V_s .

Keywords:

1. Shear wave velocity
2. Wave propagation tests
3. Small strain stiffness
4. Earthquake engineering

Henrik Takle Eide

MASTER DEGREE THESIS

Spring 2015

for

Student: Henrik Takle Eide

On shear wave velocity testing in clay**Background**

The stiffness at small strains is an important parameter for settlement predictions and for understanding soil behaviour under seismic/dynamic loading. The small strain stiffness is usually found from the shear wave velocity, V_s , obtained by wave propagation tests in field and laboratory. Results from laboratory testing have proved to be different from results from in situ testing. The results from invasive and non-invasive tests in situ also tend to differ.

Task description

A complete shear wave velocity profile should be determined at the Tiller site using various wave propagation tests (SCPT, CHT, MASW and bender element). The results from the different test should be compared and evaluated. The accuracy and suitability of the tests for soft Norwegian low plasticity clays should be discussed. Brief calculations regarding the engineering consequences of using different values for V_s should be carried out and discussed.

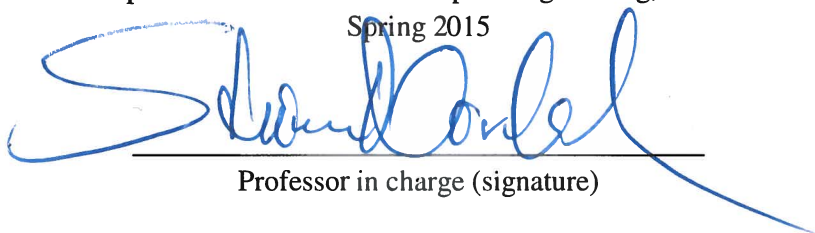
Objective and purpose

- Perform field and laboratory tests and in particular investigate the differences between V_s obtained from the tests
- Evaluate the various methods applied for assessing V_s
- Conduct a brief study and presentation on the engineering consequences of variation in V_s

Advisors: Amanuensis Arnfinn Emdal, Professor Steinar Nordal**Other supervisors: Jean-Sebastien L'Heureux, NGI**

Department of Civil and Transport Engineering, NTNU

Spring 2015



Professor in charge (signature)

Preface

This study is performed as a Master's Thesis in the specialization course TBA4900 Geotechnics. The thesis is part of the MSc in Civil and Environmental Engineering, and is written at the Geotechnical Division, Department of Civil and Transport Engineering at the Norwegian University of Science and Technology (NTNU).

Main supervisors of the study have been Doctor Jean-Sebastien L'Heuraux at NGI and Amanuensis Arnfinn Emdal and Professor Steinar Nordal at NTNU.

This study is performed in the Spring of 2015, with a duration of 20 weeks.

The report deals with the topic of geodynamics, particularly the shear wave velocity, V_s , which is an important dynamic soil property. Various wave propagation tests in field and laboratory have been carried out. A brief study on the consequences of variation in V_s is also conducted. The first part of the report presents basic theory regarding wave propagation and dynamic soil behavior. The second part of the report presents the laboratory and field testing which has been performed during the study. Subsequently, a discussion regarding test results is given. Lastly, the study consequences of variation in V_s on practical engineering is presented.

My interest in the subject has grown during the study, and the work has provided both practical and theoretical knowledge.

Trondheim, June 2015



Henrik Takle Eide

Acknowledgements

I would like to thank following persons for their great help during this study:

Jean-Sebastien L'Heuraux, for showing great interest in my work. He has put me in touch with both NGI and APEX, making this work possible. He has also given me great ideas and feedback.

Arnfinn Emdal, for organizing the field investigations and discussion of test results.

Steinar Nordal, for being available for interpretation and discussion of test results.

Per Asbjørn Østensen, for invaluable help and work. He has developed computer software for both bender element and crosshole testing, and additional equipment used for cross-hole testing. He has also been a great support in the laboratory, teaching me a lot regarding the triaxial setup. He has always made time for me, and I could not have done this study without his effort.

Geotechnical Field Department, with Gunnar Winther, Einar Husby and Jan Jønland, for their excellent work in the field and their general good spirits.

NGI, with Guillaume Sauvin, for his help with the SCPT in field and processing.

APEX Geophysical Services, with especially Greg Balding, for their great work with MASW testing and processing and allowing me to assist on some of the investigations.

Helge Tovslid, for helping me to get started in the laboratory.

Abstract

The soil stiffness at small strains is an important parameter for settlement predictions and for understanding soil behaviour under seismic/dynamic loading. The small strain stiffness is usually found from the shear wave velocity, V_s , obtained by wave propagation tests in field and laboratory. Results from laboratory testing have proved to be different from results obtained by in situ testing. The results from invasive and non-invasive tests in situ also tend to differ.

In this study, various wave propagation tests are carried out to obtain V_s in clay. The results from the various tests are compared and discussed. The assessed field tests are Seismic Cone Penetration Test (SCPT), Crosshole Test (CHT) and Multichannel Analysis of Surface Waves (MASW). Bender element testing on 54 mm samples is carried out in the laboratory. Testing is performed at various sites, but only the results from the Tiller site are presented in this thesis. The Tiller site is a NTNU research site consisting of low plasticity clay. Quick clay is expected below about 8 m depth. Two profiles, 50 m apart, are investigated at Tiller.

Full V_s -profiles to about 20 m depth are found using SCPT and MASW. The SCPT data are processed using both cross-correlation and crossover method. The crossover method, with a pseudo-interval spacing of 3 m or more, provide the best results. These results are considered to be the most accurate of all the assessed tests.

MASW surveys were carried out in two rounds. The original survey provides significantly higher V_s -results than expected at depths below 8 m. Lower frequencies are produced in the repeated survey. The repeated survey provides a V_s -profile similar to the result obtained from SCPT.

CHT is only performed at one profile and the equipment measures V_s at just one depth. Most of the received signals obtained at Tiller are unclear. V_s is however estimated from the received signals. A significant uncertainty is not expected. The result from CHT corresponds well to results from SCPT and MASW.

Eight samples are tested in a triaxial cell with bender elements. The results show significantly lower V_s compared to the field tests. Five samples from the same depth with various height are tested. No difference in V_s related to sample height are found. That suggest that there is no system time delay in the system.

Two samples are consolidated past the primary consolidation to investigate the aging effect. The bender element results are found to correspond fairly well with in situ measurements when they are adjusted for the aging effect. The aging effect does however seem to be different in sensitive and non-sensitive clay samples.

A brief study on the consequences of variation in V_s in practical engineering is conducted with respect to settlement and earthquake engineering. Both the settlement and earthquake analyses show significant influence of variation in V_s .

Samandrag

Jordstivleik ved små tøyingar er ein viktig parameter for å anslå setningar og for å forstå korleis jord oppfører seg under seismisk/dynamisk last. Småtøyingsstivleiken er vanlegvis funnen frå skjærbølgjesnøggleiken, V_s , som er innhenta frå bølgeforsplantingstestar i felt og laboratorium. Resultat frå testing i laboratorium har vist seg å gje ulike resultat samanlikna med in situ testar. Resultata frå invasive og ikkje-invasive testar in situ har også ein tendens til å avvike.

I dette studiet er ulike bølgeforsplantingstestar utførte for å finna V_s i leire. Resultata frå dei ulike testane er samanlikna og diskuterte. Dei omhandla felttestane er Seismic Cone Penetration Test (SCPT), mellomholmetoden (CHT) and Multichannel Analysis of Surface Waves (MASW). Bender element testing er utført på 54 mm prøvar i laboratoriet. Dei ulike testane er utførte på fleire stader, men berre resultat frå Tiller er presentert i denne avhandlinga. Tiller er eit forsøksfelt for NTNU som består av leire med låg plastisitet. Kvikkleire er forventa under omtrent 8 m djupn. To profil, 50 m frå kvarandre, er undersøkt på Tiller.

Fullstendige V_s -profilar ned til ei djupn på omlag 20 m er funnen frå SCPT og MASW. Data frå SCPT er prosessert ved hjelp av både krysskorrelasjons- og crossover-metoden. Crossover-metoden, med eit pseudo-intervall på 3 m eller meir, gav dei beste resultatane. Resultata frå SCPT ved dei to profila var noko ulike. Truleg skyldas skilnaden variasjon i jordparametrar.

MASW undersøkingar er utført i to omgangar. Den originale undersøkinga gav markant høgare V_s -resultat under om lag 8 m, enn forventa. Lågare frekvensar vart laga i den repeterte undersøkinga. Den gav V_s -profilar som er liknande resultatane frå SCPT.

CHT er berre utført ved det eine profilet. Utstyret målar berre V_s på ei djupn. Dei fleste mottekne signala frå Tiller er uklære. V_s er likevel anslått frå dei mottekne signala. Det er ikkje venta ei betydingfull usikkerheit. Resultatet frå CHT samsvarar godt med resultatane frå SCPT og MASW.

Åtte prøvar er testa i ei treaksial celle med benderelement. Testing med benderelement gjer betrakteleg lågare V_s -resultat enn felttestane. Fem prøvar frå same djupn, men med ulik høgde, er testa. Ingen skilnad i V_s grunna prøvehøgde er funnen. Det indikerer at det ikkje er ei tidsforseinking i systemet.

To prøvar er konsoliderte forbi primærkonsolideringa for å undersøkje aldringseffekten. Resultata frå testinga med benderelement samsvarar temmeleg bra med in situ målingar, om dei vert justerte for aldringseffekten. Basert på resultata frå laboratoriet verkar det som om aldringseffekten er ulik i sensitive og ikkje-sensitive prøvar.

Ei kortfatta studie på ingeniørmessige konsekvensar av variasjon i V_s er utført. Studiet bestod av enkle setnings- og jordskjelvanalysar. Funna frå studiet viste at variasjon av V_s hadde stor påverking på både resultata i setnings- og jordskjelvanalysane.

Table of Contents

| | |
|---|------|
| Preface..... | i |
| Acknowledgements | iii |
| Abstract | v |
| Samandrag..... | vii |
| Table of Contents | ix |
| List of Symbols | xiii |
| Chapter 1 Introduction | 1 |
| 1.1 Background..... | 1 |
| 1.2 Scope and Aim for this Study | 1 |
| 1.2.1 Objectives..... | 1 |
| 1.3 Approach | 2 |
| 1.4 Thesis Structure | 2 |
| Chapter 2 Theoretical Background | 5 |
| 2.1 Wave Propagation..... | 5 |
| 2.1.1 Shear Waves..... | 6 |
| 2.1.2 Primary Waves | 7 |
| 2.1.3 Surface Waves..... | 8 |
| 2.1.4 Damping | 9 |
| 2.1.5 Anisotropy | 9 |
| 2.2 Small Strain Stiffness | 11 |
| 2.3 Parameters Affecting V_s and G_{\max} | 12 |
| Chapter 3 Tiller Site | 19 |

| | | |
|-----------|--|----|
| 3.1 | Site Characterization and Engineering Properties | 19 |
| 3.2 | Previous Shear Wave Measurements | 22 |
| Chapter 4 | Field and Lab Methods..... | 23 |
| 4.1 | Seismic Cone Penetration Test (SCPT)..... | 23 |
| 4.1.1 | Testing Procedure..... | 24 |
| 4.1.2 | Processing..... | 26 |
| 4.2 | Crosshole Test (CHT)..... | 27 |
| 4.2.1 | Testing Procedure..... | 27 |
| 4.3 | Multichannel Analysis of Surface Waves (MASW) | 31 |
| 4.3.1 | Testing Procedure..... | 31 |
| 4.4 | Bender Element Testing | 34 |
| 4.4.1 | Testing Procedure..... | 35 |
| Chapter 5 | Results and Interpretation..... | 41 |
| 5.1 | SCPT..... | 41 |
| 5.2 | CHT | 44 |
| 5.3 | MASW | 45 |
| 5.4 | Bender Element | 50 |
| 5.4.1 | Tests with Various Height..... | 50 |
| 5.4.2 | Time Effect..... | 51 |
| Chapter 6 | Discussion | 57 |
| 6.1 | Accuracy..... | 57 |
| 6.2 | Suitability..... | 61 |
| 6.3 | Sources of Errors | 62 |
| 6.3.1 | SCPT | 62 |
| 6.3.2 | Crosshole | 63 |
| 6.3.3 | MASW | 66 |
| 6.3.4 | Bender Element..... | 67 |

| | | |
|-----------------|--|------|
| Chapter 7 | Engineering Consequences | 73 |
| 7.1 | Settlement Calculations | 73 |
| 7.1.1 | Drained Analysis | 76 |
| 7.1.2 | Undrained Analysis | 80 |
| 7.1.3 | Discussion on Settlement Calculations | 81 |
| 7.2 | Earthquake Engineering | 82 |
| 7.2.1 | Earthquake Calculations..... | 85 |
| 7.2.2 | Results from Tiller | 88 |
| 7.2.3 | Discussion on Earthquake Calculations | 89 |
| Chapter 8 | Conclusions | 91 |
| Chapter 9 | Further Work and Recommendations | 93 |
| Bibliography | | 95 |
| List of Figures | | 100 |
| List of Tables | | 103 |
| Appendix | | I |
| Appendix A | | I |
| A.1 | Conducted Field and Laboratory work..... | I |
| Appendix B | | II |
| B.1 | P-wave | II |
| Appendix C | | III |
| C.1 | Bender Element Results..... | III |
| C.2 | Noticeable Incidents during Testing..... | VI |
| C.3 | Signal Interpretation | VIII |
| Appendix D | | IX |
| D.1 | Other Tests | IX |
| D.2 | Electrical Resistivity Tomography (ERT)..... | XI |
| Appendix E | | XII |

| | |
|--|-------|
| E.1 Multifunction DAX Specifications | XII |
| E.2 Accelerometer Specifications | XV |
| Appendix F | XVI |
| F.1 Settlement Calculations..... | XVI |
| Appendix G | XVIII |
| G.1 Westerlund on Diagenesis | XVIII |
| G.2 Aging Effect | XIX |
| Appendix H | XX |
| H.1 Anisotropy in Gault Clay | XX |
| Appendix J..... | XXI |
| J.1 Empirical Correlations..... | XXI |

List of Symbols

| | |
|----------------|--|
| γ | <i>Shear strain</i> |
| $\gamma_{0.7}$ | <i>Shear strain at $G/G_{max} = 0.7$</i> |
| θ | <i>Rotational angle</i> |
| λ | <i>Wavelength, correction factor</i> |
| ν | <i>Poisson's ratio</i> |
| ρ | <i>Density</i> |
| σ'_h | <i>Effective horizontal stress</i> |
| σ'_v | <i>Effective vertical stress</i> |
| τ | <i>Shear stress</i> |
| a_g | <i>Design ground acceleration</i> |
| C_t | <i>Moment bracing factor</i> |
| d_g | <i>Design ground displacement</i> |
| e_0 | <i>Initial void ratio</i> |
| E | <i>Young's modulus</i> |
| EOP | <i>End of primary consolidation</i> |
| f | <i>Frequency</i> |
| G | <i>Shear modulus</i> |
| G_0 | <i>Maximal shear modulus</i> |
| G_{max} | <i>Maximal shear modulus</i> |
| G_s | <i>Secant shear modulus</i> |
| G_t | <i>Tangent shear modulus</i> |
| H | <i>Height</i> |
| I_p | <i>Plasticity index</i> |
| I_G | <i>Coefficient of shear modulus increase with time</i> |
| I_{Vs} | <i>Coefficient of shear wave velocity increase with time</i> |
| K'_0 | <i>Coefficient of lateral stress</i> |
| m | <i>Modulus number, mass</i> |
| M | <i>Constrained modulus</i> |
| n | <i>Porosity</i> |

| | |
|------------|--|
| N_G | <i>Normalized shear modulus increase with time</i> |
| N_{V_s} | <i>Normalized shear wave velocity increase with time</i> |
| OCR | <i>Overconsolidation ratio</i> |
| p' | <i>Effective mean stress</i> |
| p'_c | <i>Preconsolidation pressure</i> |
| S | <i>Soil factor</i> |
| s_u | <i>Undrained shear stress</i> |
| t | <i>Time</i> |
| T | <i>Torque</i> |
| T_1 | <i>Fundamental period of vibration</i> |
| u | <i>Displacement</i> |
| V_s | <i>Shear wave velocity</i> |
| V_p | <i>Compressional (primary) wave velocity</i> |
| $V_{s,30}$ | <i>Average shear wave velocity</i> |

Chapter 1 Introduction

1.1 Background

The soil stiffness at small strains is an important parameter for settlement predictions and for understanding soil behaviour under seismic/dynamic loading. The small strain stiffness is usually found from the shear wave velocity, V_s , obtained by wave propagation tests in field and laboratory. Results from laboratory testing have proved to be different from results from in situ testing. The results from invasive and non-invasive tests in situ also tend to differ.

Earthquake engineering in Norway has had increased focus the latest years, especially after the introduction of Eurocode 8 in March 2010. Eurocode 8 requires the seismic ground type to be classified when designing a structure. The most relevant parameter to use when choosing ground type is the average shear wave velocity, $V_{s,30}$.

1.2 Scope and Aim for this Study

The aim of this study is to conduct and compare various wave propagation tests (SCPT, CHT, MASW and bender element) in clay. The assumed accuracy and suitability of the tests at soft Norwegian low plasticity clays are discussed. Brief calculations regarding the consequences of using different values for V_s in practical geotechnical engineering are carried out and discussed.

1.2.1 Objectives

- Perform field and laboratory tests and in particular investigate the differences between V_s obtained from the tests
- Evaluate the various methods applied for assessing V_s
- Conduct a brief study and presentation on the engineering consequences of variation in V_s

1.3 Approach

The author studied the subject of small strain stiffness in his project work during the autumn of 2014.

The first part of this work consisted of studying literature on small strain stiffness, wave propagation and various wave propagation tests. Kramer (1996) and Benz (2007) are the main sources of literature.

Subsequently, testing in field and laboratory and processing of the associated data were performed. Several challenges regarding different equipment have occurred during the testing, but all the tests were eventually conducted. The bender element testing and processing were performed by the author himself. The SCPT test at Esp was led by Guillaume Sauvin, but at Tiller and Klett the author led the investigations. The SCPT data used are mostly processed by the author. The MASW surveys were mostly conducted and processed by APEX Geophysical Services. The author did however assist during some of the performed testing. The crosshole test was carried out by the author and Per Asbjørn Østensen. The author conducted the processing of the crosshole data.

A brief study on the consequences of using variation in V_s in practical geotechnical engineering was then conducted.

Lastly, the results were discussed and the report was written and put together.

1.4 Thesis Structure

This thesis consist of 8 chapters.

- Chapter 1 presents the background and objectives for this study
- Chapter 2 presents theoretical background on wave propagation and small strain stiffness. Parameters affecting shear wave velocity and small strain stiffness in clay are briefly presented
- Chapter 3 describes the investigated Tiller site. Only the most important parameters and previous investigations for this work are given.

- Chapter 4 describes the field and lab tests carried out in this work. Brief general descriptions of the tests are presented in addition to more specific descriptions of the test procedures at Tiller
- Chapter 5 presents the results obtained from testing and interpretations of these results
- Chapter 6 presents a brief study on consequences of varying shear wave velocity in practical geotechnical engineering. Simple settlement analyses are conducted using PLAXIS. A simple earthquake analysis using Eurocode 8. The analyses are presented and discussed briefly
- Chapter 7 presents the conclusions from this work
- Chapter 8 suggest further work and recommendations on this subject. Some beneficial modifications to the equipment is also suggested

Chapter 2 Theoretical Background

The stiffness at small strains is an important parameter in term of settlement predictions and understanding of soil behaviour under seismic/dynamic loading. This is highlighted in e.g. Burland (1989) Bjerrum Memorial lecture and Simpson (1992) and Atkinson (2000) Rankine lecture. Using a relation to the shear wave velocity is the most common way to obtain the stiffness at small strains.

In this chapter, basic theory on wave propagation and small strain stiffness in soil are presented. Different wave types are presented due to their significance to shear wave velocity measurements. Subsequently, basic theory on small strain stiffness is presented, as this is the parameter used in engineering. Finally, the most important parameters affecting shear wave velocity and small strain stiffness are presented. The focus is on clay material.

2.1 Wave Propagation

"It is the continuous nature of geologic materials that causes soil dynamics and geotechnical earthquake engineering to diverge from their structural counterparts. While most structures can readily be idealized as assemblages of discrete masses with discrete sources of stiffness, geologic materials cannot. They must be treated as continua, and their response to dynamic disturbances must be described in the context of wave propagation." - Kramer (1996)

In an unbounded elastic medium there exist only two kinds of waves, primary wave (p-wave) (sometimes referred to as compressional wave) and shear wave (s-wave). The p- and s-wave is referred to as body waves. The particle motion for the body waves are illustrated in Figure 2.1.

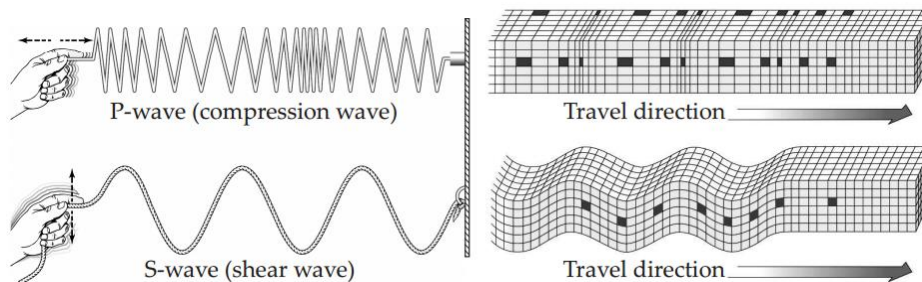


Figure 2.1 Particle movement of body waves Benz (2007)

2.1.1 Shear Waves

The s-wave particle motion is perpendicular to the direction of wave propagation. Thus, the s-wave involve shearing, but no volumetric deformations. As the s-wave propagates by shearing, it may only travel in material that transfer shear. In soils, this means that the shear wave travels in the soil skeleton, rather than the pore water.

The s-wave velocity is subdivided based on direction of propagation and particle motion. A horizontal propagated s-wave may have both horizontal $V_{s(hh)}$ and vertical $V_{s(hv)}$ particle motion. A vertical propagated s-wave has horizontal particle motion, $V_{s(vh)}$.

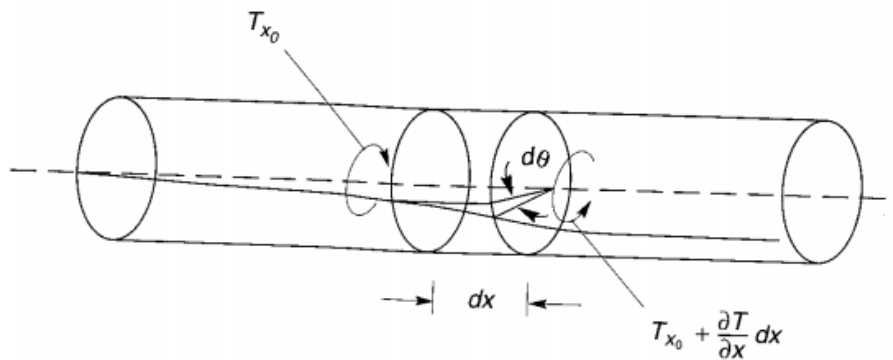


Figure 2.2 Torque and rotation of a one dimensional rod (Kramer 1996)

The relation between the shear wave velocity and small strain stiffness is derived by assuming a constrained infinite rod, with only torsional deformation, as shown in Figure 2.2, the equilibrium equation is given as:

$$(T_{x_0} + \frac{\delta T}{\delta x} dx) - T_{x_0} = \rho J \frac{\delta^2 \theta}{\delta t^2} dx \quad (2.1)$$

which may be simplified into the one-dimensional equation of motion:

$$\frac{\delta T}{\delta x} = \rho J \frac{\delta^2 \theta}{\delta t^2} \quad (2.2)$$

by using the Torque-rotation relation: $T = GJ \frac{\delta \theta}{\delta x}$, eq.(2.2) may be written as:

$$\frac{\delta(GJ \frac{\delta\theta}{\delta x})}{\delta x} = GJ \frac{\delta^2\theta}{\delta x^2} = \rho J \frac{\delta^2\theta}{\delta t^2} \quad (2.3)$$

An alternative way of writing the one-dimensional equation of motion is:

$$\frac{\delta^2\theta}{\delta t^2} = \frac{G}{\rho} \frac{\delta^2\theta}{\delta x^2} \quad (2.4)$$

Hence, following relation may be made between the rod stiffness, density and wave propagation:

$$V_s^2 = \frac{G}{\rho} \quad (2.5)$$

Note that the shear wave velocity is only dependent on material properties, not amplitude, frequency or any other wave property.

2.1.2 Primary Waves

The p-wave propagates through compression and rarefaction of the material, thus the particle motion is parallel to the direction of wave propagation. In contrast to the s-wave, p-waves may travel in both soil and water.

The one dimension p-wave propagation velocity may be derived similar to the V_s (The full derivation may be found in Appendix B), and results in following relation:

$$V_p^2 = \frac{M}{\rho} \quad (2.6)$$

Where M is the constrained modulus defined as: $M = \frac{1-\nu}{(1+\nu)(1-2\nu)} E$.

The p-wave propagates with a greater velocity than the s-wave. This may lead to interference between the signals from s- and p- waves in tests to determine V_s . By combining equation (2.5) and (2.6) the relation between s-wave and p-wave velocity may be described in terms of the poisons ratio, ν .

$$\frac{V_p}{V_s} = \sqrt{\frac{2(1-\nu)}{1-2\nu}} \quad (2.7)$$

2.1.3 Surface Waves

Near the surface there are two other types of waves with importance to earthquake engineering that may occur, Rayleigh waves and Love waves (Kramer 1996). Other types of surface waves exist, but are not of significance to this thesis.

Rayleigh waves

The Rayleigh waves (r-waves) occur near the surface of a homogenous elastic half-space. The r-wave may be described as a combination of p- and s-waves with particle movement as both compression/rarefaction and perpendicular displacement, as shown in Figure 2.3. The propagation velocity of the r-waves are approximately like the s-waves.

The r-wave velocity is not depending on frequency, but low frequency r-waves penetrate the surface deeper than high frequency r-waves. The soil stiffness, and thus the wave velocity, increase with stress, giving the r-wave a dispersive character with depth. This property is used in non-invasive investigations like SASW and MASW to find the s-wave velocity.

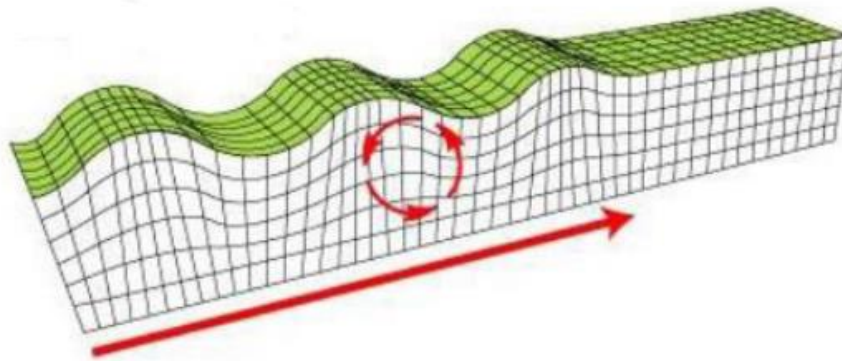


Figure 2.3 Particle movement in a Rayleigh wave (Eiksund 2013)

Love waves

While p-, s- and r-waves exist in homogenous half-space, the Love-waves only appear if the half-space is overlain by a layer of material with lower body-wave velocity. The Love-wave consist mostly of horizontally propagating s-waves reflected within the upper layer and are

clearly dispersive. The Love waves are not considered to be of particular importance to this work and will not be explained further.

2.1.4 Damping

As a shear wave propagates through soil, its amplitude will gradually be reduced. The damping effect is usually divided into two contributions, material and radial damping. The material damping is due to some part of the travelling wave elastic energy being converted to heat (Kramer 1996). In order to model this damping in soils mathematically, a Kelvin-Voigt viscoelastic solid is often used. The stress-strain relation is given in equation (2.8), and consist of an elastic and a viscous part as shown in Figure 2.4.

$$\tau = G\gamma + \mu \frac{\delta\gamma}{\delta t} \quad (2.8)$$

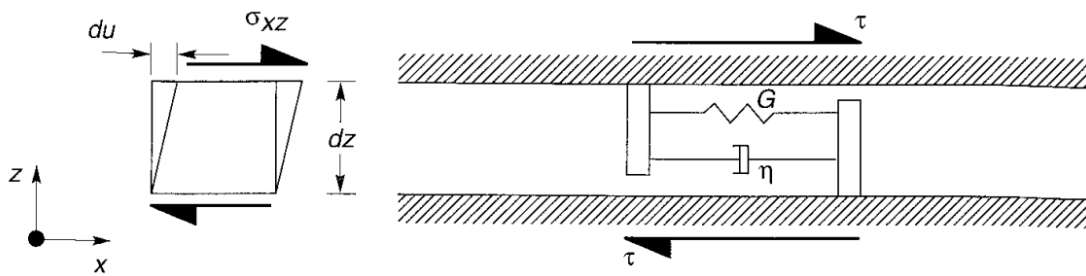


Figure 2.4 Schematic figure of a thin element in a Kelvin-Voigt solid (Kramer 1996)

The radial damping is simply due to the wave energy being distributed over a larger volume as it travels away from the source. The geometric damping of the amplitude of a spherical wave front may be shown to decrease with a rate of $1/r$. However, Bullen (1953) shows that the surface waves amplitude attenuate with a rate of $1/\sqrt{r}$. Hence, body waves are damped more quickly than the surface waves. The radial damping often dominate in problems with a finite energy source (Kramer 1996).

2.1.5 Anisotropy

Soil material is known for its uncertainty in measured soil properties. The soil has inherent anisotropy, due to the soil ‘fabric’ or particle orientation/arrangement. The soil is generally

considered to be cross-anisotropic, which means the soil has no preferred direction in the horizontal planes, but behaves differently in the vertical planes.

The stress condition in soil is generally also anisotropic, where the ratio between the vertical and horizontal stress is defined by the coefficient of lateral earth pressure at rest, K_0' .

A shear wave produces particle motion perpendicular to the direction of wave propagation. Thus a shear wave with horizontal propagation may have either horizontal ($V_{s(hh)}$) or vertical ($V_{s(hv)}$) particle motion. A vertical propagated shear wave however, will only have horizontal ($V_{s(vh)}$) particle motion.

In a perfect cross-anisotropic material, $V_{s(vh)} = V_{s(hv)}$. However, $V_{s(hh)}$ would be expected to differ.

2.2 Small Strain Stiffness

"The limit of classical laboratory testing coincides at the same time with characteristic shear strains that can be measured near geological structures. However, the soil stiffness that should be used in the analysis of geotechnical structures is not the one that relates to these final strains. Instead, very-small strain soil stiffness and its non-linear dependency on strain amplitude should be properly taken into account in all analysis that strive for reliable predictions of displacement." - Benz (2007)

Soil stiffness varies significantly with strain level. At very small strain level, the soil is found to behave elastic. According to Atkinson and Salfors (1991), the strain range that the soil display this elastic behaviour is for $\gamma_s < 10^{-6}$. This is believed to be a fundamental property independent of geotechnical material, loading and drainage conditions, and it is called the very-small strain range. For larger strains, the soil behaves in a non-linear manner. Strain in the range $10^{-6} < \gamma_s < 10^{-3}$ is defined as small strains by Atkinson and Salfors (1991). The limit of 10^{-3} is roughly the strain level that may be reliably measured in traditional laboratory tests like the oedometer or triaxial test. Strains larger than 10^{-3} is called large or larger strains. The definition of strain ranges and typical strain ranges of structures and testing are given in Figure 2.5.

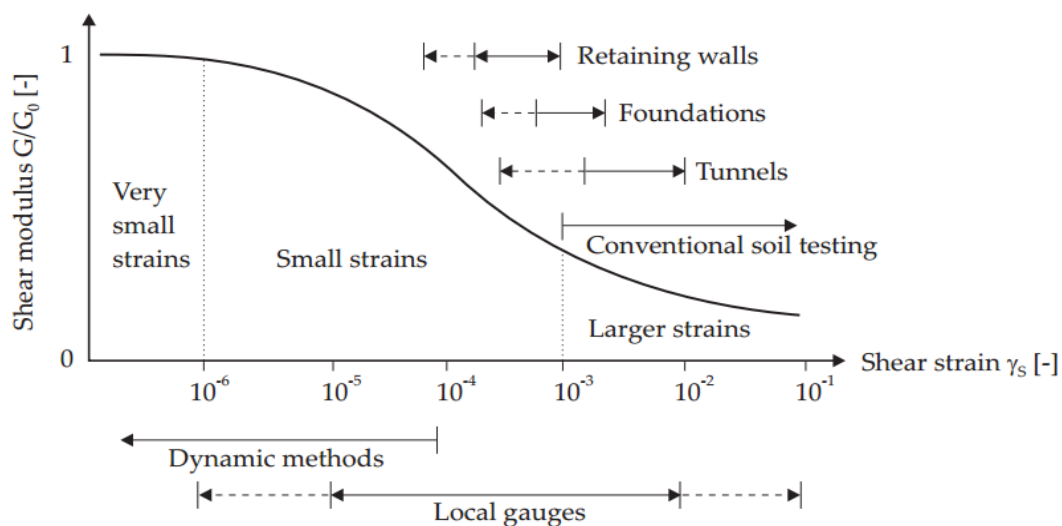


Figure 2.5 Characteristic stiffness-strain behaviour and definition of strain ranges (Atkinson and Salfors 1991)

The greatest shear stiffness, denoted G_{max} or G_0 , occurs in the very-small strain range. However, it is often included for measurements in the small strain range as well.

The shear strains produced by a shear wave is in the small or very-small strain range. Thus, equation (2.5) may be rewritten in terms of G_{max} :

$$G_{max} = \rho V_s^2 \quad (2.9)$$

2.3 Parameters Affecting V_s and G_{max}

There are several parameters affecting V_s and G_{max} . Benz (2007) suggests the importance of different parameters in respect to G_{max} and $\gamma_{0.7}$ based on previous recommendations from Hardin and Drnevich (1972). $\gamma_{0.7}$ is the strain level at which $G/G_{max} = 0.7$. His results may be seen in Table 2.1. According to Benz (2007), the most important parameters for V_s and G_{max} in cohesive soils are:

- Strain amplitude (since last load reversal)
- Confining stress
- Void ratio
- Plasticity index
- Degree of saturation
- Diagenesis

Only the most important parameters regarding V_s and G_{max} in clays are discussed further in this thesis.

| Parameter | Importance to ^a | | | |
|---|----------------------------|----------------|----------------|----------------|
| | G_0 | | $\gamma_{0.7}$ | |
| | Clean sands | Cohesive soils | Clean sands | Cohesive soils |
| Strain amplitude | V | V | V | V |
| Confining stress | V | V | V | V |
| Void ratio | V | V | R* | V |
| Plasticity index (PI)* | - | V | - | V |
| Overconsolidation ratio | R | L | R | L |
| Diagenesis* | V* | V* | R* | R* |
| Strain history* | R | R | V | V |
| Strain rate | R | R | R | R* |
| Effective material strength | L | L | L | L |
| Grain Characteristics (size,shape,gradation) | L* | L* | R | R |
| Degree of saturation | R | V | L | L* |
| Dilatancy | R | R | R | R |

^a V means Very Important, L means Less Important, and R means Relatively Unimportant
* Modified from the original table presented in Hardin & Drnevich[53]

Table 2.1 Parameters affecting G_{max} (Benz, 2007)

Strain Amplitude

G_{max} only occur in the very-small strain range. At larger strains, the shear modulus number decreases. A frequently used method to describe the relation between the small-strain stiffness and large strain stiffness is given by Hardin and Drnevich (1972):

$$\frac{G}{G_{max}} = \frac{1}{1 + \left| \frac{\gamma}{\gamma_r} \right|} \quad (2.10)$$

where G is the shear stiffness at current strain level, γ is the shear strain (since last load reversal) and γ_r is the threshold shear strain quantified as:

$$\gamma_r = \frac{\tau_{max}}{G_{max}} \quad (2.11)$$

This results in a S-shaped curve when $\frac{G}{G_{max}}$ is plotted against $\log(\gamma)$, as shown in Figure 2.5.

Confining Stress

A typical way of describing the relation between stiffness and confining stress at large strains is by using a Janbu (1963) type power law. The relation at small strains has been shown to be similar and is often described using a similar type of power law;

$$G_{max} \propto p'^m \quad (2.12)$$

where

p' = Average confining stress

m = Module number, normally $0.5 < m < 1.0$ for cohesive soils

Void Ratio

The void ratio give an idea of the density of the soil. Denser soil means more contact between grains, which again means higher stiffness. Hardin and Richart Jr (1963) present equations to describe the relation between void ratio and small strain shear modulus. They are mostly valid for non-cohesive soil, but equation (2.13) has also proven to be applicable for clays with low surface activity (Hardin and Black 1969).

$$G_{max} \propto \frac{(2.97 - e)^2}{1 + e} \quad (2.13)$$

Plasticity Index

The plasticity index, I_p , is often used as an indicator of the stiffness of a cohesive material. High plasticity usually lead to low stiffness in overconsolidated soils. The stiffness reduction curve is also in the highest degree depending on the soil plasticity. Vucetic and Dobry (1991) present a chart describing the effect of I_p on the damping curve in soils (Figure 2.6).

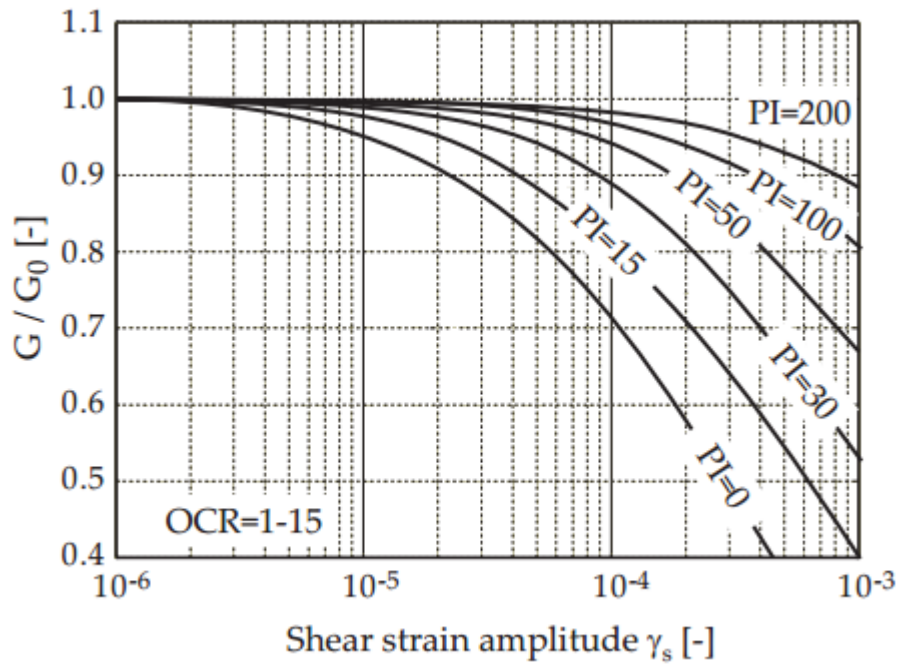


Figure 2.6 PI-chart of the stiffness reduction curve (Vucetic and Dobry 1991)

Aging Effect (Diagenesis)

“Everything on this earth has one thing in common – everything changes with time. All soils age and change.” – Schmertmann (1991).

Diagenesis is the process of changing sediments and sediment rocks into a different sediment rock. The changes are due to weathering and chemical, physical and biological processes. This process happens slowly over time, and is often referred to as aging effect.

During secondary compression/consolidation water is expelled and thus the void ratio is lowered and effective stress increased. The total increase in G_{\max} with time is however significantly greater than what can be explained by this. Diagenesis has been suspected to account for most of the increase in shear stiffness with time. This effect has been investigated by several researchers for decades (e.g. Stokoe and Richart (1974), Anderson and Woods (1976)). Anderson and Stokoe (1978) present two ways of describing the effect of diagenesis. Equation (2.14) give the coefficient of shear modulus increase with time, I_G , which give the

absolute increase of the shear modulus in given time interval. Equation (2.15) give the normalized shear modulus increase with time.

$$I_G = \frac{\Delta G_{max}}{\log t_2/t_1} \quad (2.14)$$

where

$t_1, t_2 =$ Times after primary consolidation

$\Delta G_{max} =$ Change in small-strain shear modulus from t_1 to t_2

$$\frac{G_{max,SC}}{G_{max,EOP}} = [1 + N_G \log(\frac{t}{t_{EOP}})] \quad (2.15)$$

where

$G_{max,SC} =$ Small-strain shear modulus under secondary compression

$G_{max,EOP} =$ Small-strain shear modulus at end of primary consolidation

$t, t_{EOP} =$ Time and time at end of primary consolidation

$N_G =$ Normalized shear modulus increase with time

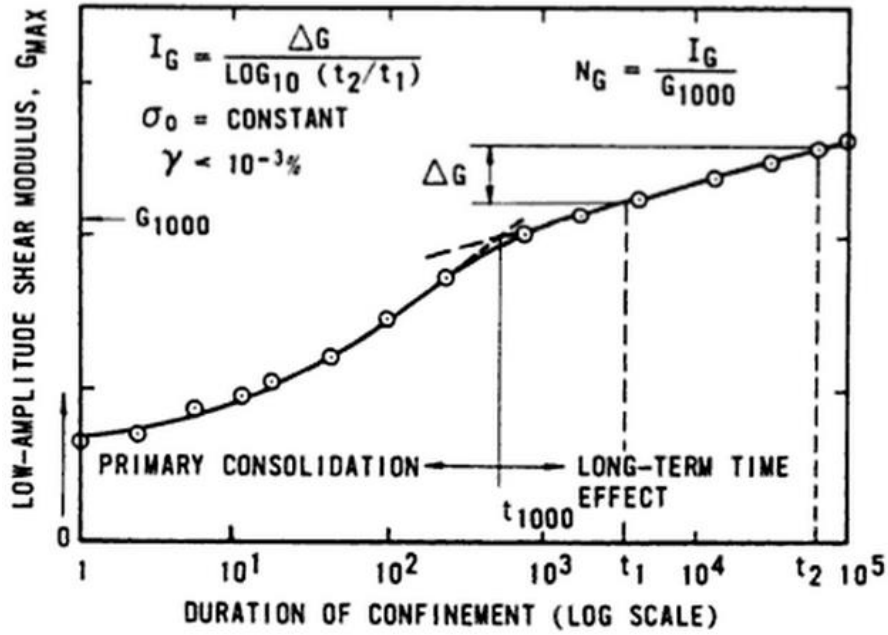


Figure 2.7 Phases and modulus-time response (Anderson and Stokoe, 1978)

Similar relations may also be made for the shear wave velocity.

$$I_{V_s} = \frac{\Delta V_s}{\log(t_2/t_1)} \quad (2.16)$$

where

$t_1, t_2 =$ Times after primary consolidation

$\Delta V_s =$ Change in shear wave velocity from t_1 to t_2

$$N_{V_s} = \frac{I_{V_s}}{V_{s,1000}} \quad (2.17)$$

where

$N_{V_s} =$ Normalized shear wave velocity increase with time

Anderson (1974) presents the following empirical formula for clay:

$$N_{V_s} (\%) = e^{2.0-0.46s_u+0.25e_0} \quad (2.18)$$

where

s_u = Undrained shear strength in kg/cm^2

e_0 = Initial void ratio

The values for N_{V_s} is normally in the range of 5-25% for clays. By setting $t_1 = 1000 \text{ min}$ in equation (2.18), the V_s after several years of consolidating could in theory be estimated.

Previous research on this topic is presented in Appendix G.

Chapter 3 Tiller Site

3.1 Site Characterization and Engineering Properties

The Norwegian University of Science and Technology (NTNU) has used the Tiller site as a research site since the early 1980's. Hence, a detailed characterization of the site has been made. The Tiller site is chosen as research site in this work due to the thickness and uniformity of the clay deposit, its availability and its proximity to the city of Trondheim. The Tiller site is located some 10 km south-east of the center of Trondheim in Sør-Trøndelag, Mid Norway.



Figure 3.1 Location of the Tiller site

Gylland et al. (2013) presents a detailed characterization of the quick clay at the Tiller site. Only the most relevant and important properties to this thesis will be presented in this section.

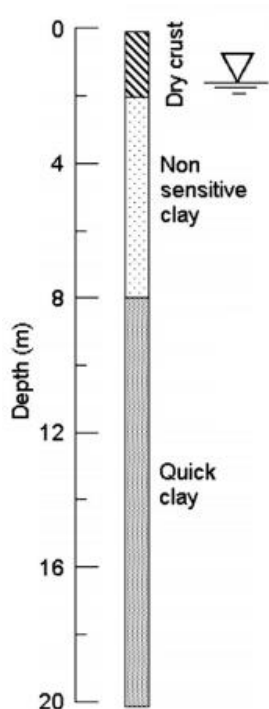


Figure 3.2 Suggested layering at the Tiller site (Gylland et al. 2013)

The suggested layering is given in Figure 3.2. Between 2.5 m and 13.5 m depth the material is believed to be very consistent, with an average of 38 % clay content and the remainder of the material to be made up of approximately equal percentages of fine, medium and coarse. This layer should be termed "clay" according to standard Norwegian practice, (Norges Geoteknisk Forening 1982). Below 13.5 m depth the clay content decrease with depth to about 20 % at 17.5 m.

The water content range between 25 % and 45 %, and averages of 37.8 % below the dry crust. There is no tendency of decreasing water content with depth, hence the material is considered to be homogeneous below the dry crust. The material is also found to be fully saturated below the dry crust.

The average Plasticity index (I_p) is around 6.3 % which makes the material classified as low plasticity (Norges Geoteknisk Forening 1982). There are some tendency of decreasing plasticity index with depth.

The undrained shear strength, s_u , is found to fit fairly well with the $0.25\sigma_{v0}'$ line.

The clay is slightly overconsolidated with an overconsolidation ratio OCR varying from 3 to 2 at 5 and 10 m depth, respectively.

| | | |
|-----------------|-----------|------------|
| ρ | 1.9 | $[kg/m^3]$ |
| OCR | 2 – 3 | $[-]$ |
| K_0' | 0.7 | $[-]$ |
| z_w | 1.5 | $[m]$ |
| e_0 | 1.07 | $[-]$ |
| E_{oed}^{ref} | 2 | $[MPa]$ |
| E_{50}^{ref} | 2 | $[MPa]$ |
| E_{ur}^{ref} | 6 | $[MPa]$ |
| $\gamma_{0.7}$ | 10^{-4} | $[-]$ |
| φ' | 29 | $[^\circ]$ |
| c' | 6 | $[kPa]$ |
| ν_{ur} | 0.2 | $[-]$ |
| m | 1.0 | $[-]$ |

Table 3.1 Tiller soil parameters used in this work (Gylland et al. 2013) and (Tovslid 2015)

The approximate location of the investigations at Tiller are presented in Figure 3.3.



Figure 3.3 Overview of Tiller and approximate locations of performed site investigations

3.2 Previous Shear Wave Measurements

From a spectral analysis of surface waves (SASW) survey (Long and Donohue 2010), the shear wave velocity is found to increase from about 100 m/s at 0.5 m depth to 225 m/s at 10 m depth.

Knutsen (2014) performed a triaxial test with bender elements on a block sample from 9.1 m depth. The sample was put to an in situ stress condition and left to consolidate drained for 42 hours. Then the stress was increased (still lower than the preconsolidation stress) and left to consolidate for 58 hours. During consolidation of the in situ stress condition the shear wave velocity increased from 110 m/s to 118 m/s. At the higher stress level, the shear wave velocity increased from 118 m/s to 126 m/s.

Chapter 4 Field and Lab Methods

Shear wave velocity measurements are carried out both in field and in the laboratory. There are several methods used to determine the shear wave velocity.

The shear strain amplitude from in situ seismic testing is usually in the order of 10^{-6} (Robertson et al. 1986), hence G_{\max} may be found. Field methods are generally divided into two groups, invasive and non-invasive methods. Invasive methods usually measures the shear wave velocity directly by putting a shear wave receiver and/or source in boreholes. In a non-invasive method both the shear wave source and receivers are placed above ground. By measuring refracted seismic waves, the shear wave velocity may be found. Invasive methods are generally considered more accurate, but are not free of uncertainty.

A sample being tested in the laboratory have been affected by several factors, such as unloading and sample disturbance from sampling and bedding. Generally, shear wave velocity measured in the laboratory give lower shear wave velocity compared to in situ measurements.

In this chapter, the methods used to obtain data in this work are described. Other methods commonly used to determine V_s (e.g. resonant column in lab and downhole method in situ) will not be discussed further, but are briefly described in Appendix D. Some empirical correlations used to obtain V_s are given in Appendix J. Note: In this work, Z is defined in the vertical direction and X and Y have arbitrary perpendicular directions in the horizontal plane.

4.1 Seismic Cone Penetration Test (SCPT)

Robertson et al. (1986) introduce the Seismic Cone Penetration Test to determine in situ shear wave velocity, V_s . The SCPT combine an ordinary Cone Penetration Test (CPT) and the downhole method by integrating an accelerometer in the cone. An energy source is located at the surface and measurements are taken with desired spacing. The energy source should preferentially produce shear waves rather than compressional waves. In order to make this, a beam is often clamped to the ground by the rig and hit horizontally by a sledgehammer. Some SCPT equipment measure the true V_s by having two accelerometers in the probe, located with

some distance between them. When only one accelerometer, a pseudo-interval travel time has to be used to determine the shear wave velocity.

4.1.1 Testing Procedure

The testing was performed in the period of 6.-10. March 2015 at three different sites; Esp, Klett and Tiller. Only the results from Tiller will be discussed further. At Tiller two SCPT boreholes are conducted (S5 and S6), about 50 m apart. At these locations previous MASW-data are available for comparison.

An Envi seismic cone belonging to NGI is penetrated into the soil. The Envi cone consist of a normal Memocone with three accelerometers installed in the cable tube 770 mm above the cone tip. The accelerometers measure movements in three directions (X, Y and Z). The drilling rig used are NTNU's GeoTech GEORIG607. At every 0.5 m depth the rig is stopped and a wooden beam is hit horizontally by a sledgehammer to generate a shear wave. The wooden beam is clamped to the ground by the rig. A wooden beam is chosen as it makes a signal with less noise than a metal beam. A magnetic trigger-microphone is placed at the rig. The trigger microphone determine the zero time and starts the sampling. The cone and rig are produced by different producers, which made the cone and rig incompatible. Thus, the depth is measured manually and no CPTu data are being logged in this study. At each depth four hits are made to lower the uncertainty and improve the signal to noise ratio. Two hits are made on each side of the wooden beam to generate opposite polarized waves. The signals are recorded using a PicoScope oscilloscope and PicoScope6 software. At every hit, the trigger starts the time and a file with signal recordings of 0.5 s is saved. A typical output signal is given in Figure 4.1. As the shear wave propagates vertically, the soil movement from the shear wave is found in the XY-plane.

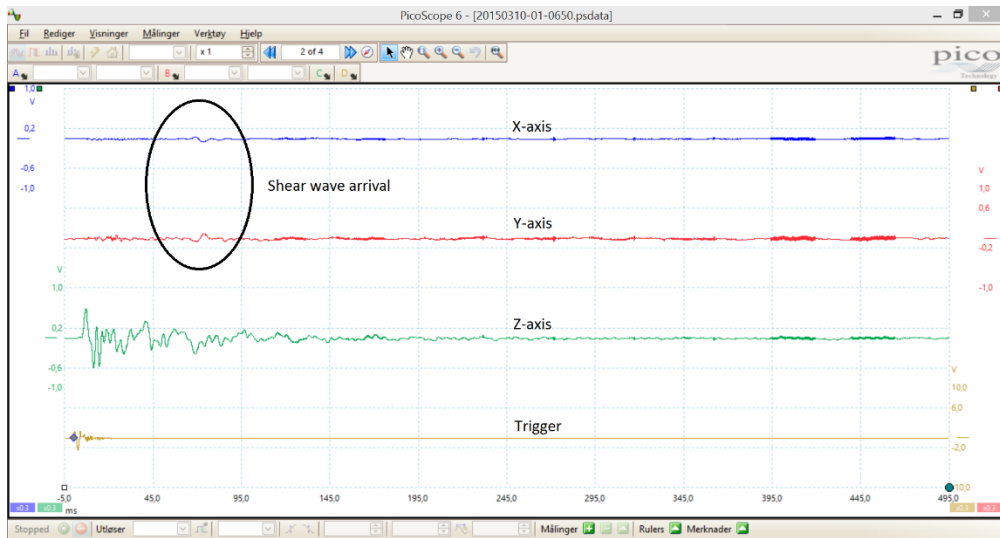


Figure 4.1 Signal output from one hit using SCPT



Figure 4.2 Setup of the SCPT (Photo: Eide, H)

4.1.2 Processing

The signal to noise ratio is not as desired at all depths, thus processing proved to be a challenge. Two different methods of processing the data are carried out, cross-correlation and crossover.

Cross-Correlation Method

The cross-correlation method compares signals from different depths. The lower signal is shifted relative to the upper signal to get the best match using the least square method. The shift represent the interval travel time of the shear wave. NGI, by Guillaume Sauvin, applied this method by putting the data into already existing scripts.

Crossover Method

The Crossover method (Tanimoto and Kurzeme 1973) superimpose oppositely polarized shear wave traces to determine the shear wave arrival. The processing is carried out using Microsoft Excel 2013. There are signals in both X and Y direction available from every hit. They are calculated separately. Four hits are made at each depth. Two at each side of the wooden beam to generate opposite polarized waves. The two equal polarized signals are summarized. The first crossover point of the oppositely polarized shear wave is identified (see Figure 4.3). With only one receiver in the SCPT probe, a pseudo-interval method is used to estimate the shear wave velocity.

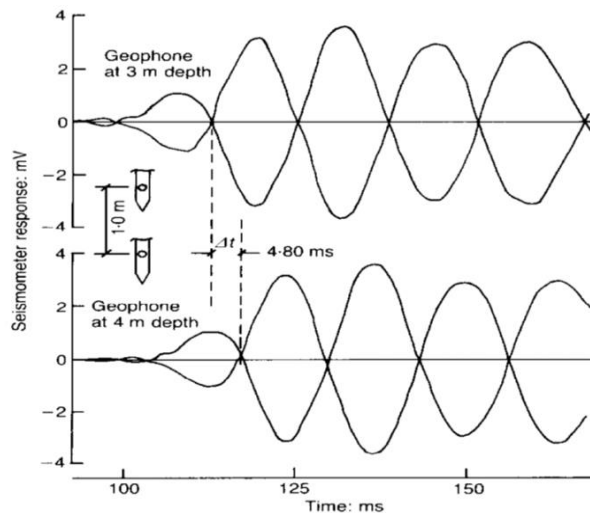


Figure 4.3 Illustration of polarized waves and usage of crossover method (Sully and Campanella 1995)

4.2 Crosshole Test (CHT)

Stokoe and Woods (1972) present the crosshole test. The crosshole test require at least two boreholes. A shear wave source is placed in one borehole, while a receiver is placed in the other. Alternatively, three boreholes are used with receivers in two of the boreholes. Then, the travel time is measured between these two boreholes (see Figure 4.4). The receivers are placed at the same depth as the shear wave source to make it possible to find the horizontal shear wave velocity. The soil is generally layered horizontally, which means the crosshole test often measure V_s accurately. If several receivers are placed at different depths in the same borehole, the test is called Crosshole Tomography.

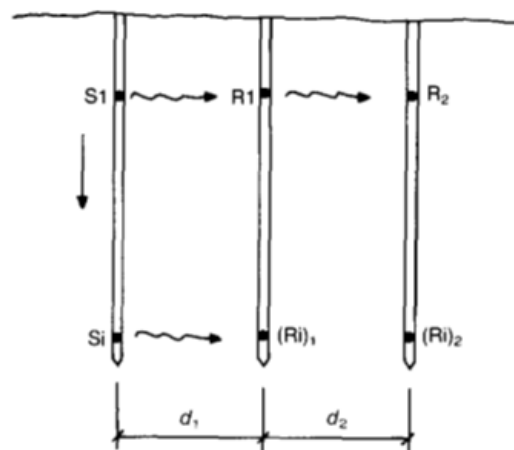


Figure 4.4 Schematic figure of the crosshole method using two receivers (Sully and Campanella 1995)

4.2.1 Testing Procedure

The crosshole test was performed at two sites, Esp and Tiller in the end of May 2015. At Tiller, the test are performed in the profile S6. Two accelerometers are placed inside two separate plastic tubes. The 3-axis accelerometer is produced by Analog Devices (specifications are found in Appendix E). The accelerometers measure deformation in three directions (X, Y and Z). The tubes are lowered into pre-drilled holes at 8.0 m depth and with 5.0 m spacing. A steel rod is penetrated into the soil in line with the two plastic tubes. Figure 4.5 shows the relevant measures used in the crosshole test. Shear waves are generated by hitting the steel rod with a sledgehammer from various directions. The rod is hit with 20 vertical hits and 5 hits both

parallel and normal to the propagation direction. A vertical hit is expected to produce a shear wave with mainly vertical particle motion. Horizontal strikes on the steel rod is expected to produce waves with more horizontal particle motion. No trigger system is installed, thus one operator starts the recording shortly before another operator hits the steel rod. The signals are sent to a multifunction data acquisition (DAQ) device, produced by National Instruments, that is ran by LabVIEW software. Details on the DAQ device is found in Appendix E. LabVIEW is a graphical programming software developed and provided by National Instruments. From every hit, 42000 signal samples within 1,0 s from every direction are saved into a file. The received signals are also plotted on the computer screen, but no shear wave travel time is suggested. Figure 4.6 displays a clear output signal from one hit. The corresponding signals are compared from each hit, and the signal from accelerometer 1 is shifted to match the received signal in accelerometer 2. The best match is found manually and focused on the shear wave arrival at the two accelerometers. Microsoft Excel 2013 is used to process the data.

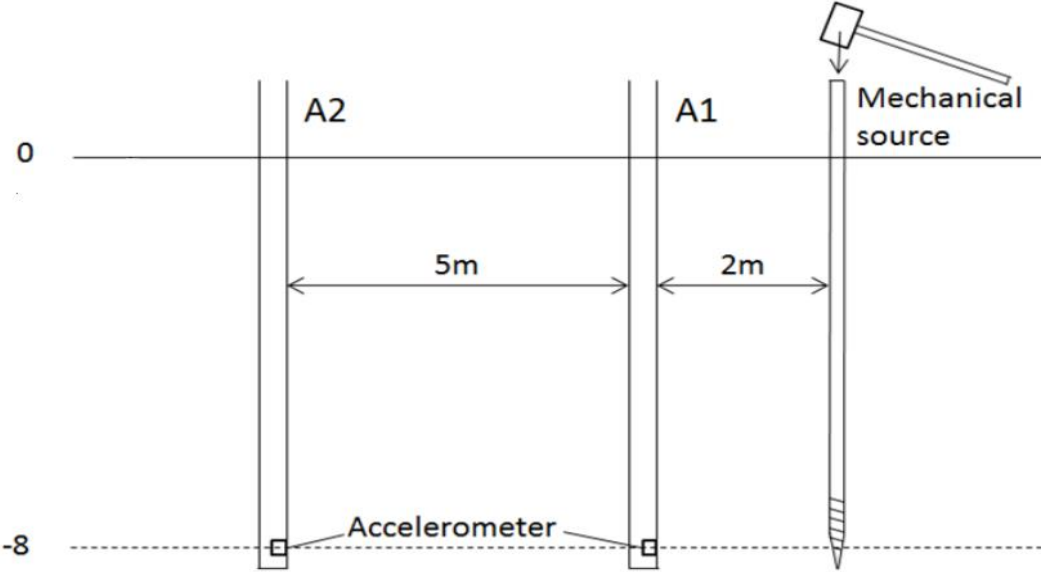


Figure 4.5 Schematic figure of the crosshole test (Knutsen, 2014)

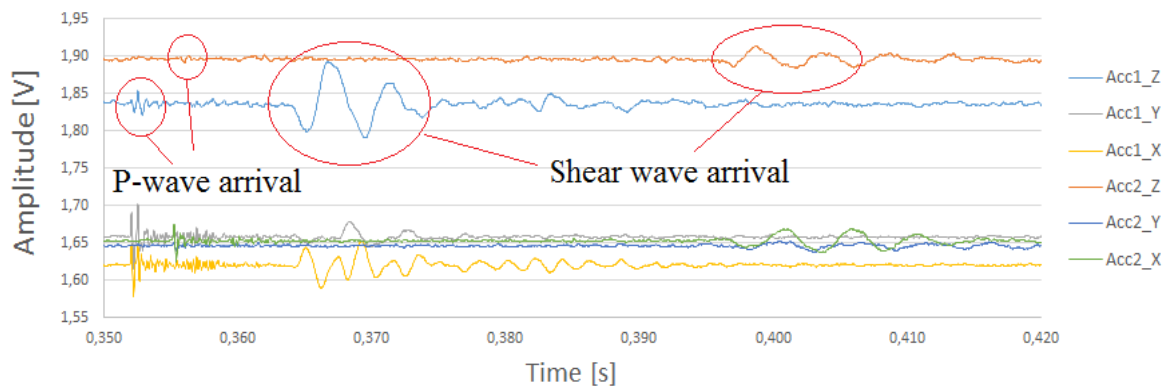


Figure 4.6 Clear signals from the crosshole test



Figure 4.7 Setup of the crosshole test at Tiller (Photo: Eide, H)

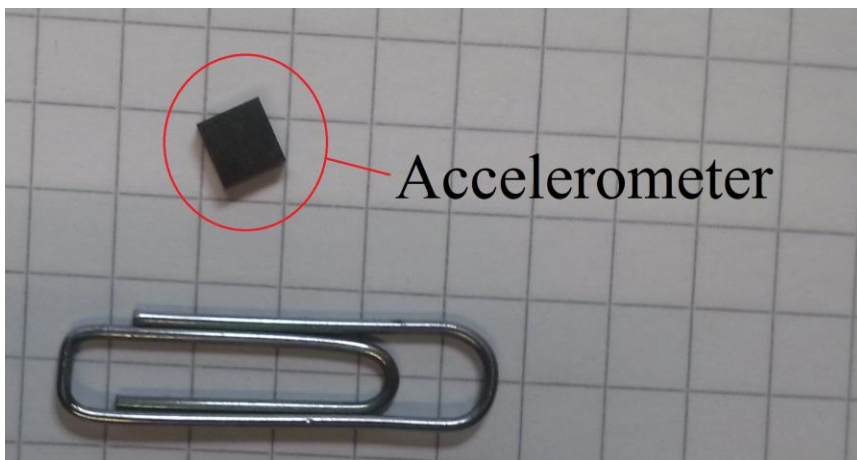


Figure 4.8 The accelerometer used in the crosshole test (Photo: Eide, H)

4.3 Multichannel Analysis of Surface Waves (MASW)

In the late 1990s, the MASW technique was introduced (Park et al. 1999) as a development of the spectral analysis of surface waves (SASW) method. MASW is an effective non-intrusive geophysical method to determine the shear wave velocity, V_s , based on surface waves. An impulse source and several geophones are placed in line with suitable distance as shown in Figure 4.9. The impulse source is often a vertical strike with a sledgehammer. Rayleigh waves with a wide range of frequencies (and thus wavelengths) propagates from the source. Due to the dispersive character of the Rayleigh waves, correlations between velocity and frequency can be made from the received signals. These correlations are called experimental dispersion curves. To obtain V_s , the experimental dispersion curve has to be iteratively matched to theoretical dispersion curves. V_s -profiles from MASW for clay sites have given consistent and repeatable results that are similar to those obtained from other techniques (Long and Donohue 2007).

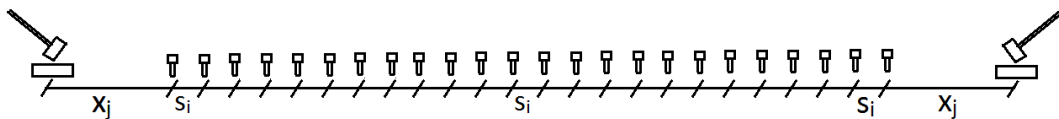


Figure 4.9 Schematic figure of the MASW setup

4.3.1 Testing Procedure

The two MASW surveys at Tiller were carried out at different times. The original survey was conducted in August 2014. The results from the original survey show considerable uncertainty, hence a repeated survey is carried out in the same profiles. The repeated survey was conducted in May 2015. The profiles are named S5 and S6 and S5A and S6A for the original and repeated survey, respectively.

The field work is performed by Greg Balding from APEX Geophysics. However, the author assisted three MASW-profiles at the Klett site, using the same procedure and equipment in May 2015. The data processing is also mainly carried out by APEX. Only the procedure of the

repeated survey is presented in this chapter. The procedure is however rather similar to the original survey. The main difference is that a 5 kg sledgehammer and 1.0 m spacing were used during the original survey. They are increased at the repeated survey with the aim of producing lower frequencies waves. Lower frequencies waves allow measurements at greater depths.

At each profile 24 no. 10 Hz vertical geophones are lined up with a spacing of 3.0m. That results in a 69 m spread. The resulting V_s -profile is located in the centre of the spread. A 24 take-out cable connects the geophones with a Geode 24 channel digital seismograph. The energy source is a 10 kg sledgehammer hit vertically at a hard plastic plate. A trigger system is connected to the sledgehammer and the seismograph. At each profile, five hits are made 4.0 m, 8.0 m and 12.0 m away from both the first geophone (G1) and last geophone (G24) of the line.

From the first survey, the data are processed using Win_MASW software, and Win_MASW and NGI inversion routine based on LAYSAC forward modelling.

The processing by APEX is carried out by using the SURFSEIS processing package developed by Kansas Geotechnical Survey. This package is designed to generate shear wave velocity profiles. A dispersion curve is produced for almost all the vertical hits. The dispersion curves with the best result from each profile are inverted and they produce the shear wave profile. Best result means the dispersion curve with the smoothest frequency against phase velocity curve at a wide and well defined frequency range.

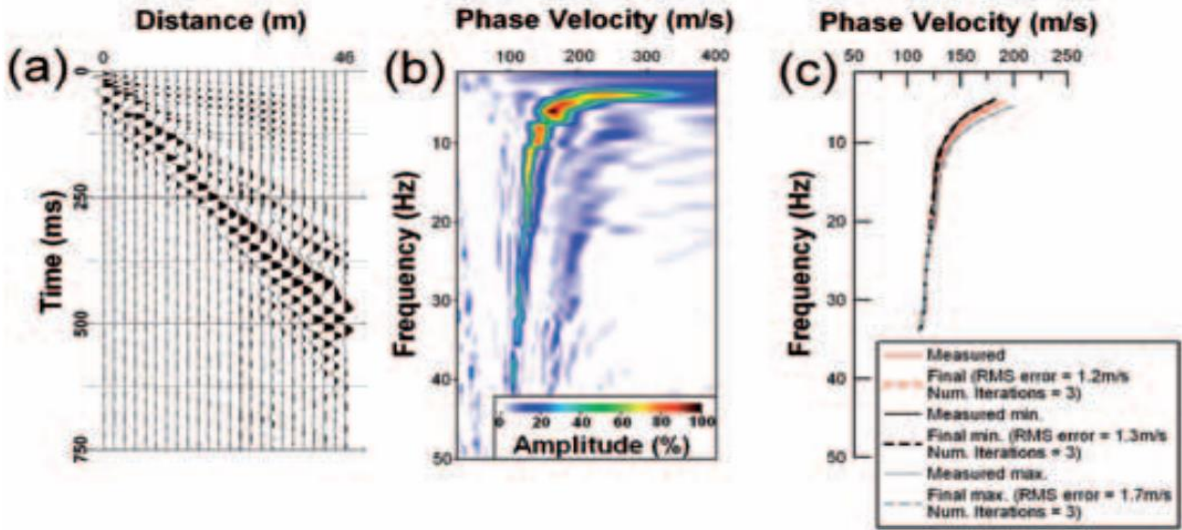


Figure 4.10 Example of shot gather (a), dispersion image (b) and dispersion curves with associated root mean square error (c) from a MASW (Donohue et al. 2012)



Figure 4.11 MASW setup at Klerr (Photo: Eide, H)

4.4 Bender Element Testing

Bender element testing was introduced by Dyvik and Madshus (1985) and is one of the most popular laboratory methods used to determine the shear wave velocity, V_s . The bender element is easily incorporated into conventional testing apparatus such as triaxial, oedometer, resonant column and simple shear box. This makes shear wave velocity measurements possible in a variety of conditions. A bender element is a short cantilever beam made out of a two-layer piezoelectric transducer. When a voltage pulse is applied one layer will contract while the other expands, making the bender element bend. This movement creates shear waves that are registered at the other end of the soil sample by another bender element. The shear wave velocity is then simply found from the distance and travel time between the transmitting and receiving bender elements.

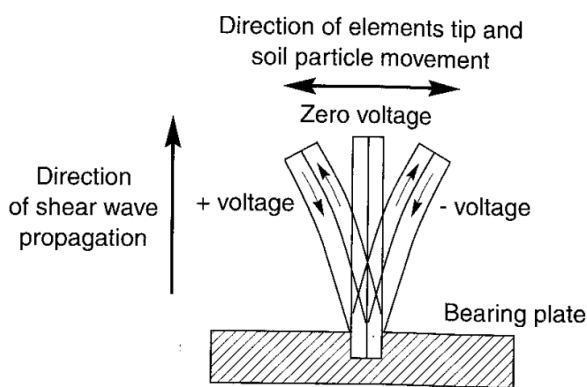


Figure 4.12 Movement of a piezoelectric bender element (Kramer 1996)

The two-layer piezoelectric transducer consist of two conductive outer electrodes, two piezoceramic sheets, and a conductive metal shim at the center (Lee and Santamarina 2005). Depending on the poling directions of the two piezoelectric layers, the bender element is either series- or parallel-type. With opposite poling directions the bender element is a series-type, while with same poling direction the

bender element is a parallel-type. For the same applied voltage, the parallel-type connection provide twice the displacement of the series-type (Lee and Santamarina 2005). Hence, the transmitter is recommended to be a parallel-type connection and the receiver a series-type connection.

The bender elements are usually embedded into the platens of a triaxial or oedometer cell, and penetrate the sample with about 3mm (see Figure 4.13).

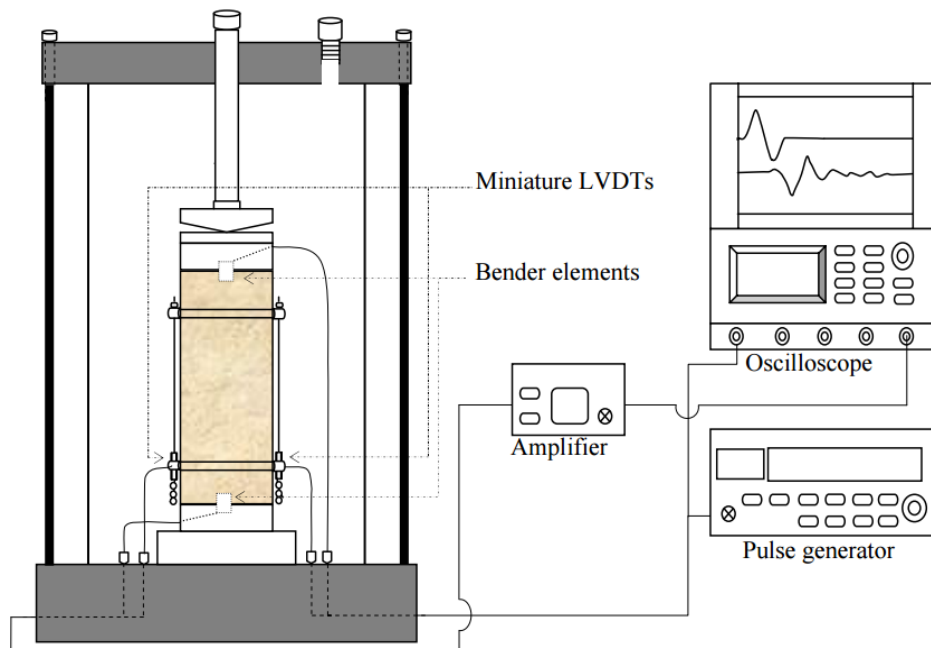


Figure 4.13 Schematic figure of a bender element setup in a triaxial-cell (Ibrahim et al. 2011)

4.4.1 Testing Procedure

The samples are all from the area around profile S5. Sample #1-5 were tested in the following days after being taken out of the ground the 19th of February 2015. Sample #6-8 were tested about three months after. They had been stored in a refrigerator packed in aluminum foil, wet paper and a plastic bag. The samples are bedded in the same way as ordinary triaxial samples, with a paper string around the sample. A rubber skin is pulled over the sample and clamped by O-rings to make it water tight. Because the bender elements protrude the sample, the normal filters are replaced by annulus shaped paper filters.

The bender elements used in this study are purchased from GDS Instruments and mounted by Per Asbjørn Østensen at NTNU. One of the elements is specified as a s-wave transmitter, the other one as a s-wave receiver. These have different poling directions of the piezoelectric plates. The transmitter is a parallel type bender element, the receiver a series type. The bender elements are mounted in the top and bottom platens of a (“normal”) triaxial cell and protrude the samples with about 2.5mm.



*Figure 4.14 Piezoelectric bender element fitted into modified pedestal
(Photo: Eide, H)*

During consolidation shear wave travel time is measured at least once every minute. The stages of consolidation for the different samples are described later. The input signal and software for interpretation of results are built up using LabVIEW. The program makes a multifunction data acquisition (DAQ) device send out a single sine signal automatically in every measurement. Specifications on the DAQ device is found in Appendix E. The transmitter element is connected to a power amplifier and the receiver element to a voltage amplifier, giving a better output signal. The amplitude of the transmitted signal is 5 V. The frequency is varied until the received signal is of the same shape as the transmitted sine signal. A frequency between 1.5 and 3.5 kHz is used in the tests, which results in a wavelength of about 0.15-0.35 m. The software uses cross-correlation between the transmitted and received signal to determine the shear wave travel time. The transmitted signal, received signal and best match from every measurement are presented at the computer (Figure 4.15). However, only the calculated shear wave travel time is saved in the output file. The system has a time resolution of 5.0 μ s. The shear wave velocity is then found by using equation (4.1).

$$V_s = \frac{H_s - u}{t_s} \quad (4.1)$$

where

H_s = Distance between the two bender elements, $H_{tot} - 5mm$

u = Deformation during consolidation

t_s = Shear wave travel time

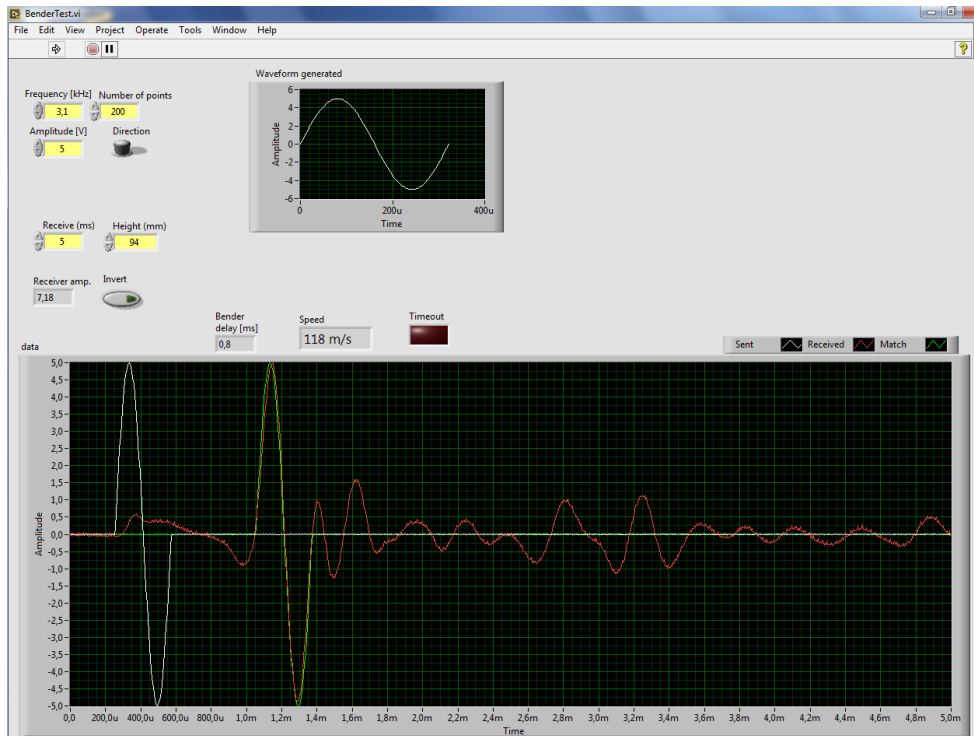


Figure 4.15 Screenshot during bender element testing

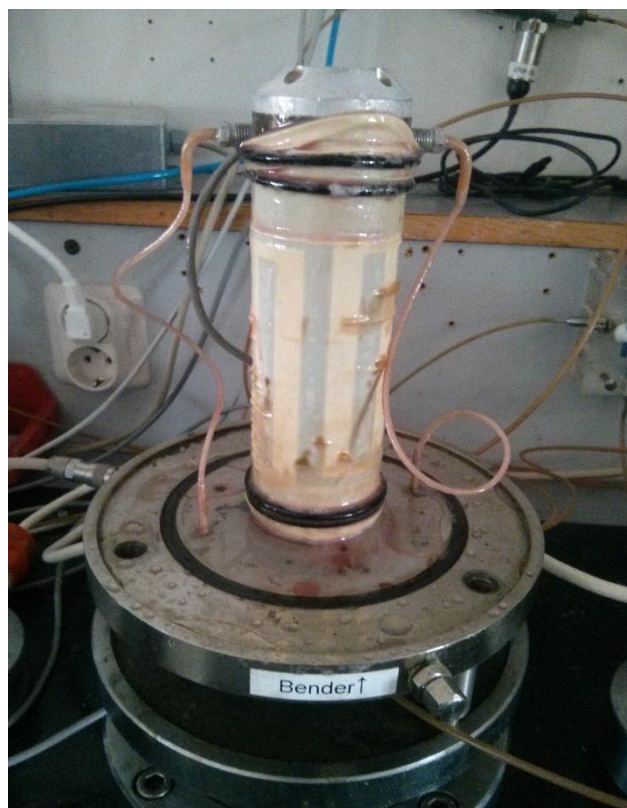


Figure 4.16 Example of sample after testing (Photo: Eide, H)

Consolidation

The in situ pressures are calculated using eq.(4.2) and (4.3).

$$\sigma'_1 = \rho z_w + (\rho - \rho_w)(z - z_w) \quad (4.2)$$

$$\sigma'_3 = K'_0 \sigma'_1 \quad (4.3)$$

The OCR is assumed to be about 3, hence the vertical preconsolidation stress is about 3 times greater than the in situ pressure.

The first five samples are consolidated in the same way; first to in situ pressure (1), then to preconsolidation pressure (2) and back to in situ pressure (3).

| Stage | σ'_1 [kPa] | σ'_3 [kPa] |
|-------|-------------------|-------------------|
| (1) | 43 | 30 |
| (2) | 150 | 105 |
| (3) | 43 | 30 |

Table 4.1 Stages of consolidation for sample #1-5

Sample #6 was supposed to follow the same procedure, but failed during loading to preconsolidation pressure.

| Stage | σ'_1 [kPa] | σ'_3 [kPa] |
|-------|-------------------|-------------------|
| (1) | 117 | 82 |
| (2) | 150 | 105 |
| (3) | 117 | 82 |

Table 4.2 Stages of consolidation for sample #7

Sample #8 is also consolidated for a long time to in situ pressure in stage (1). The rest of the consolidation stages is found in Table 4.3. At the end of stage (1), the applied amplitude of the shear wave is set to 2 V in some measurements to investigate a possible effect.

| Stage | σ'_1 [kPa] | σ'_3 [kPa] |
|-------|-------------------|-------------------|
| (1) | 74 | 52 |
| (2) | 150 | 105 |
| (3) | 74 | 52 |
| (4) | 185 | 130 |

Table 4.3 Stages of consolidation for sample #8

Any important incidents in the various samples during testing are described in Appendix C

Chapter 5 Results and Interpretation

5.1 SCPT

Cross-Correlation Method

In Figure 5.1 the results from cross-correlation are presented. Only the obtained V_s -values between 70 and 400 m/s are plotted. In addition a smooth average from the crossover method with 0.5 m pseudo-interval spacing is included as a reference.

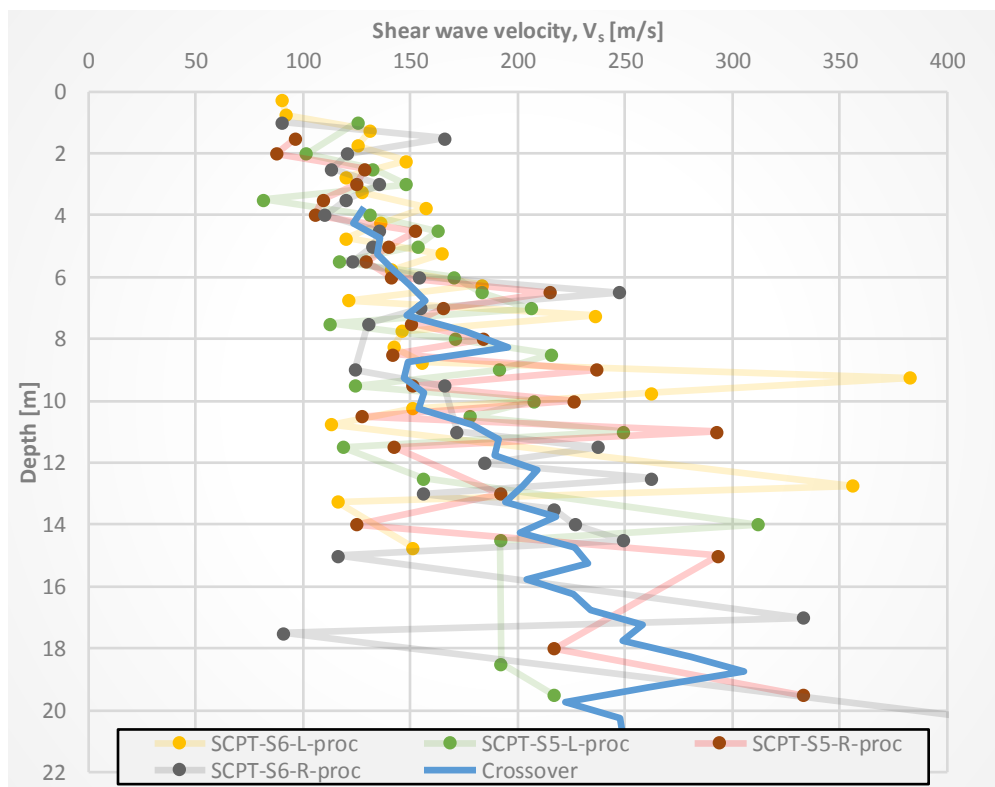


Figure 5.1 SCPT-results using cross-correlation method in processing

The results from cross-correlation processing produced an irregular scatter of results. The scatter is greater than results using the crossover method with 0.5m pseudo-interval spacing. It is very hard to find a trend based on these results, especially below 8m.

Crossover Method

The results using the crossover method with pseudo-interval spacing of 0.5 and 5 m are presented in Figure 5.2. At both profiles (S5 and S6) the received signal in both x- and y-direction (ch.1 and ch.2) are interpreted.

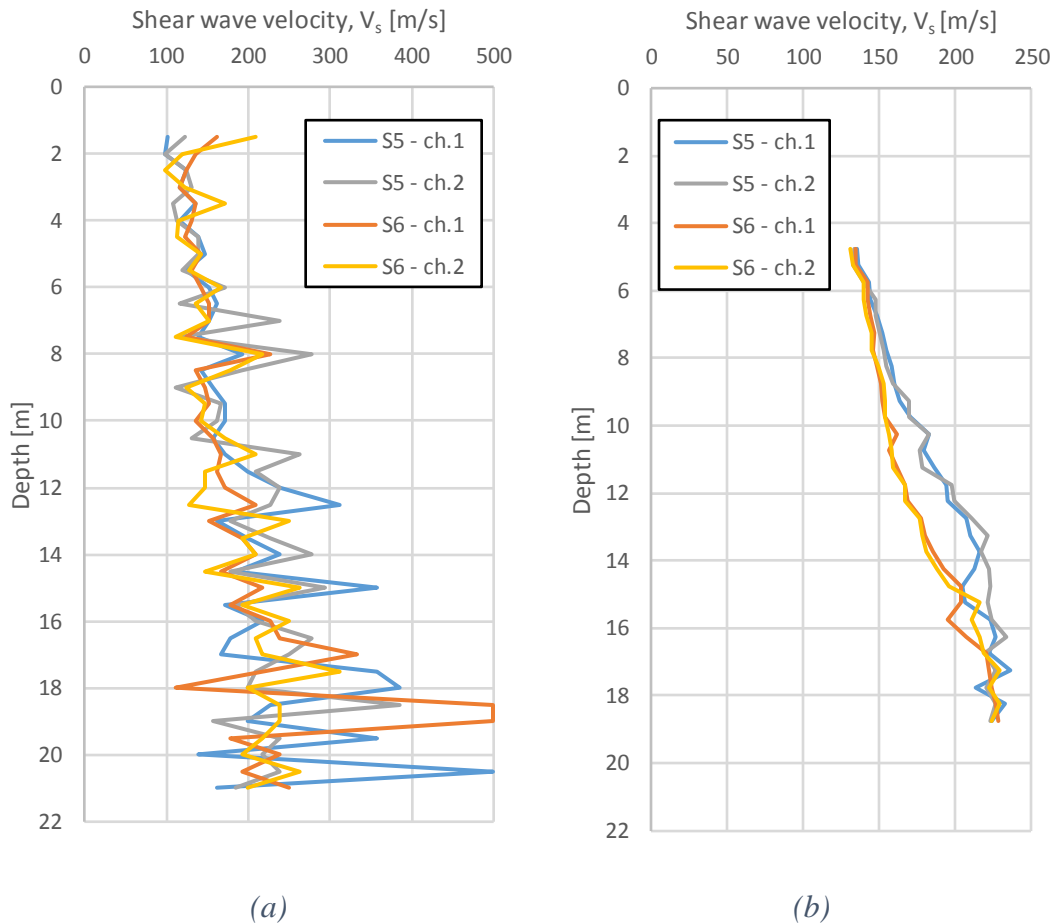


Figure 5.2 SCPT-results using crossover method and 0.5m (a) and 5m (b) pseudo-interval spacing

The results were fluctuating using 0.5 m pseudo-interval spacing, with great uncertainty. A trend of a linear increase with depth could however be implied. The zigzag pattern suggest that the fluctuation probably is due to inaccuracy in determination of shear wave arrivals and depth measurements. By measuring the shear wave velocity of a larger interval, these errors get less significant. However, sharp changes in the V_s due to different layers with different would not be found.

By using a 5m pseudo-interval spacing, a rather smooth V_s -profile is presented. The results at profile S5 and S6 differ between approximately 9 and 17 m depth. The difference has a maximum magnitude of 36 m/s (about 20 %) at 13 m depth. The distance between the profiles is around 50 m, and some difference in the soil properties are possible. The results from ch. 1 and ch. 2 provides very similar profiles at their respective profile. That supports that the processing did not cause the difference.

The average value of results from both profile S5 and S6 with 3m pseudo-interval spacing is given in Figure 5.3.

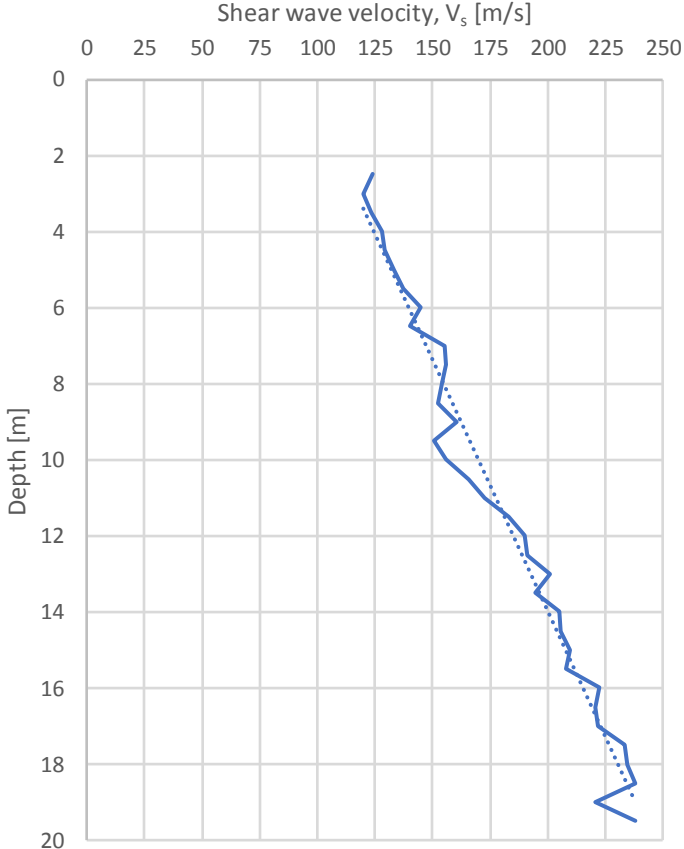
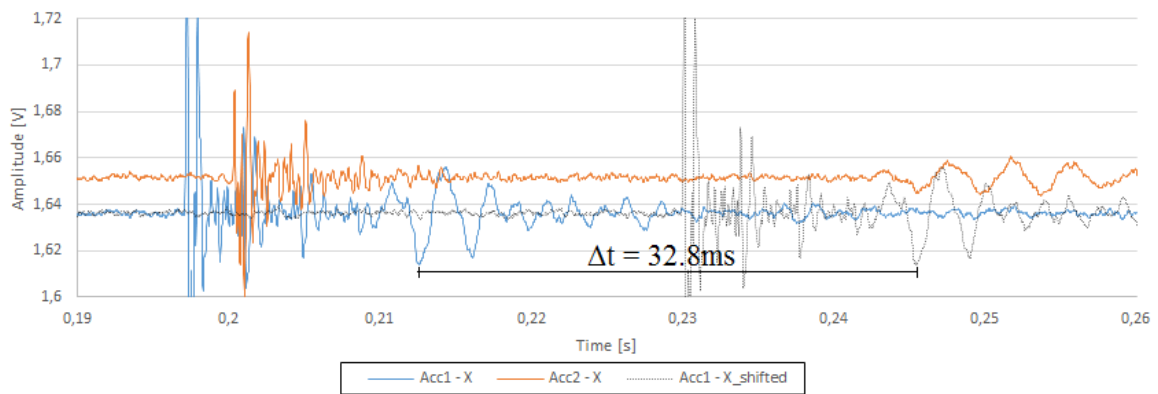


Figure 5.3 Average values from SCPT investigations from crossover method with 3.0 m pseudo-interval spacing

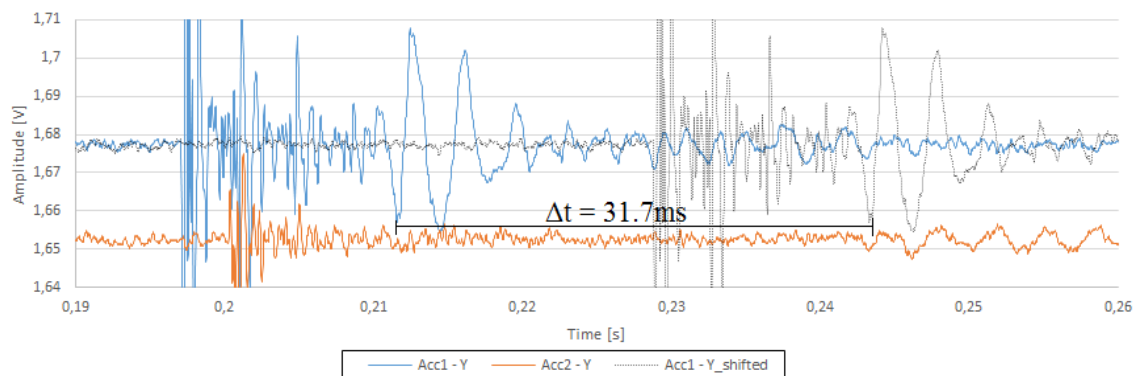
The average value of the two SCPT-profiles provides an almost linearly increase with depth. From 125 m/s at 4 m to 230 m/s at 18 m. This profile is trusted to represent the shear wave velocity at Tiller. As the shear wave arrival is picked manually at every depth, no major error is expected. The accuracy is estimated to be about 10 %.

5.2 CHT

Observed shear wave travel time vary roughly between 31.7 ms and 33.1 ms. Assuming a distance of exactly 5.0 m between the rods results in V_s varying between and 151 m/s and 158 m/s. Most results suggest a Δt around 33.0ms giving a V_s of 152 m/s. Some of the clearest signals and corresponding time shifts are presented below. One time shift equals the shear wave travel time.



(a)



(b)

Figure 5.4 Signals from the first vertical hit in x- (a) and y-direction (b)

In principle, the crosshole test is the most reliable in situ V_s testing method (Benz 2007). However, the crosshole test at Tiller did not produce as clear signals as expected. To determine the arrival of the shear wave proved to be difficult. Some signals are better, and the shear wave velocity is roughly estimated from these. The uncertainty in determining the shear wave arrival

is estimated to be in the order of 3 ms (about 10 %). That results in a V_s range of 14 m/s, which is not too bad in itself, but the fact that no clear signals are obtained is worrying.

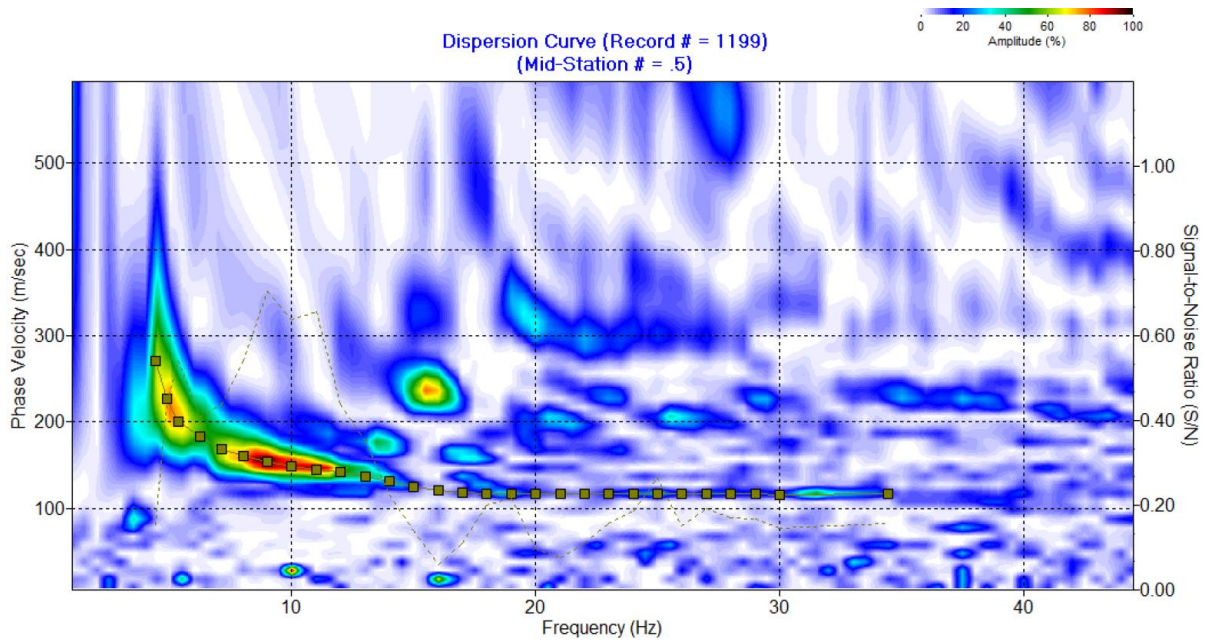
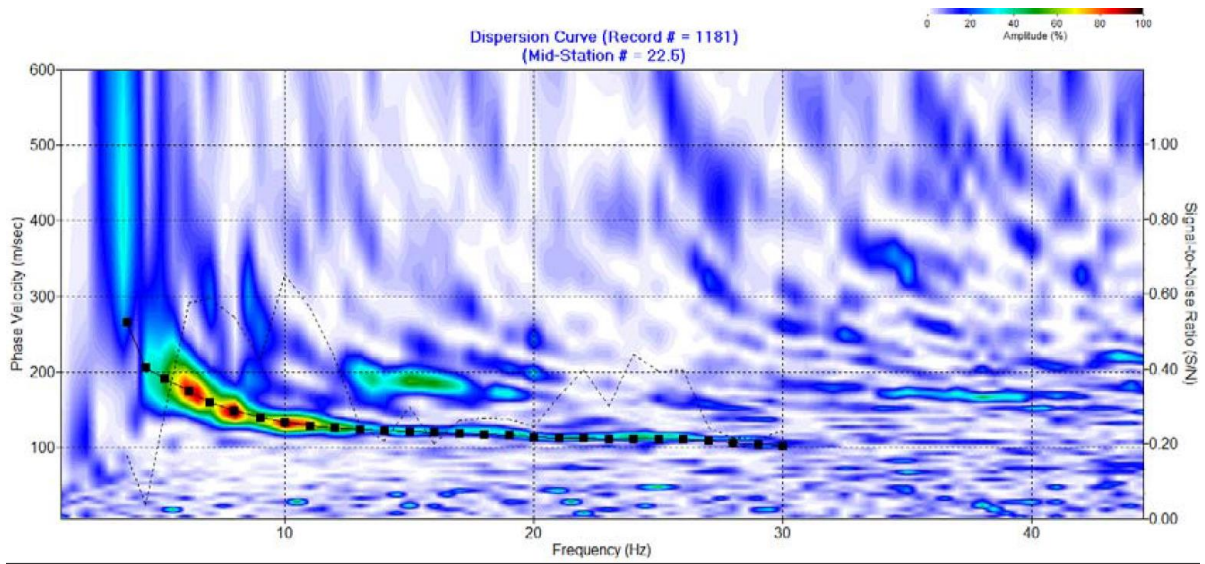
5.3 MASW

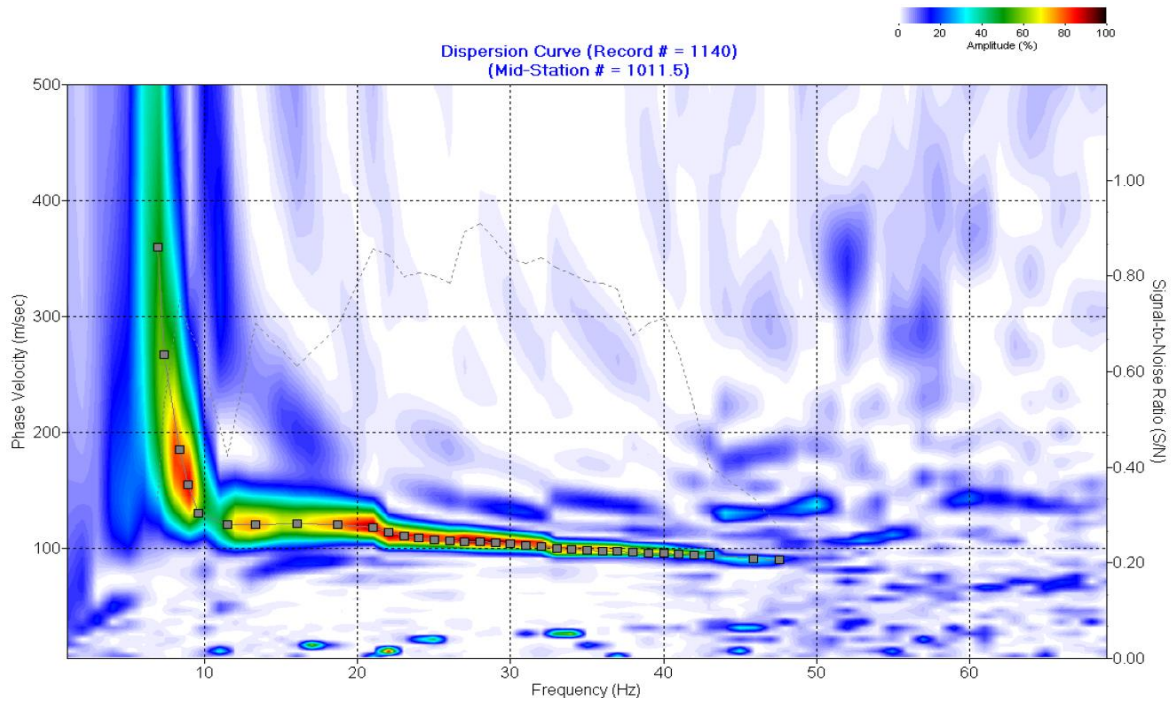
The results from both the original survey in August 2014 and the repeated survey in May 2015 are presented in O'Rourke (2015). The best dispersion curves from both surveys are presented in Figure 5.5.

The best result from S5 and S6 is obtained by shots 8 m off G24 and 4 m off G24, respectively. S5 and S6 have a frequency range of about 7-48 and 8-47Hz, respectively.

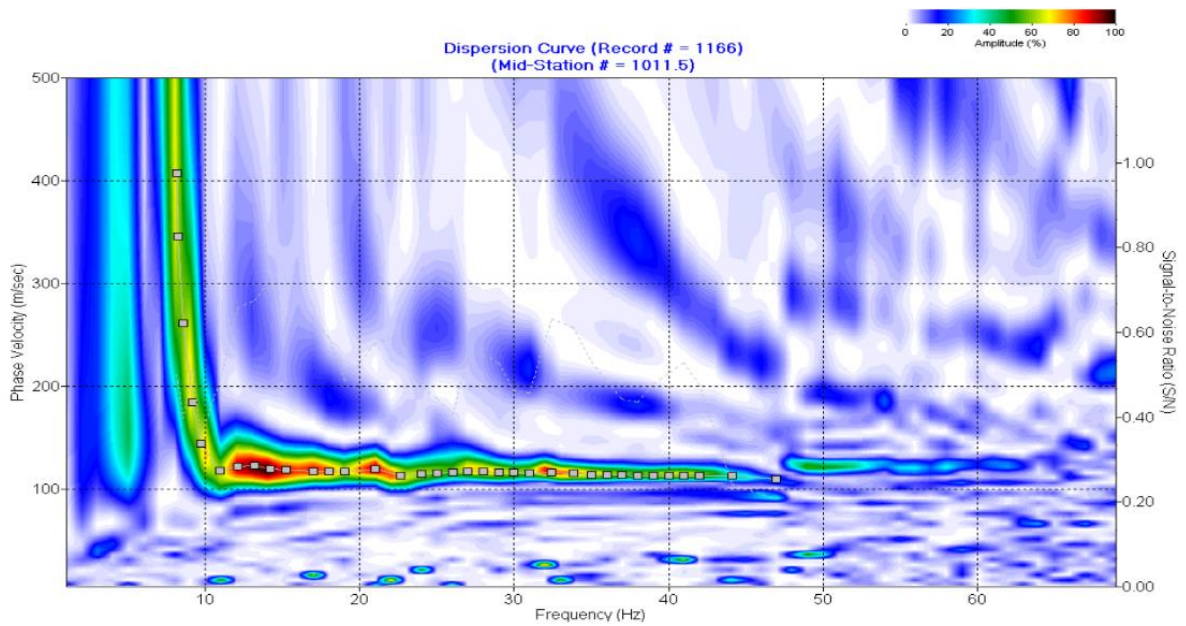
For profile S5A and S6A, a shot 8 m off G1 and 12 m off G24, respectively, produced the best result. The dispersion curve at profile S5A and S6A have a frequency range of about 3-30Hz and 4-35Hz, respectively.

The aim of producing lower frequencies using a heavier sledgehammer and larger geophone spacing is successful.





(c)



(d)

Figure 5.5 Dispersion curve from best shot at profile S5A (a), S6A (b), S5 (c) and S6 (d) at Tiller (O'Rourke 2015)

The V_s profiles at S5 and S6 from both the original and repeated surveys are presented in Figure 5.6. In addition to the APEX processing results, the results from NGI processing of the original survey are presented.

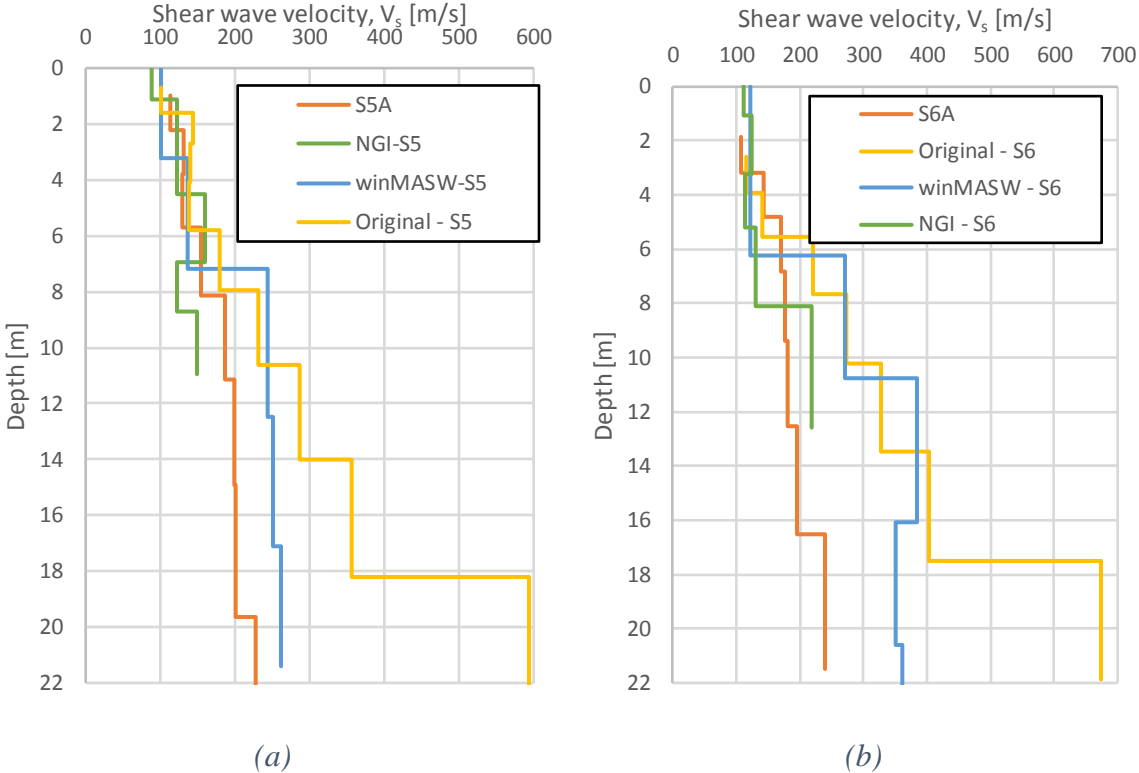


Figure 5.6 Comparison between original (with several methods of processing) and repeated MASW results at profile S5 (a) and S6 (b)

The original results show a V_s -value increasing from about 100 m/s at the surface to 670 m/s at 20 m depth. However, the results differ when using other ways of processing. Win_MASW give a V_s at S5 increasing from 100 to 260 m/s at the surface and at 20 m depth, respectively. At S6 the V_s is increasing from 120 to 360 m/s at the depths using Win_MASW. The NGI processing does not provide values to the same depth. The NGI processing gave V_s increasing from 90 to 150 m/s and 110 to 220 m/s at the surface and 12m depth for profile S5 and S6, respectively.

The V_s in the two repeated profiles are mostly in accordance. Compared to the original MASW investigation the repeated MASW results are quite similar down to about 8 m depth. Below this depth the new results are considerable lower and closer to a level that would be expected. The profiles in the repeated survey are presented by themselves in Figure 5.7.

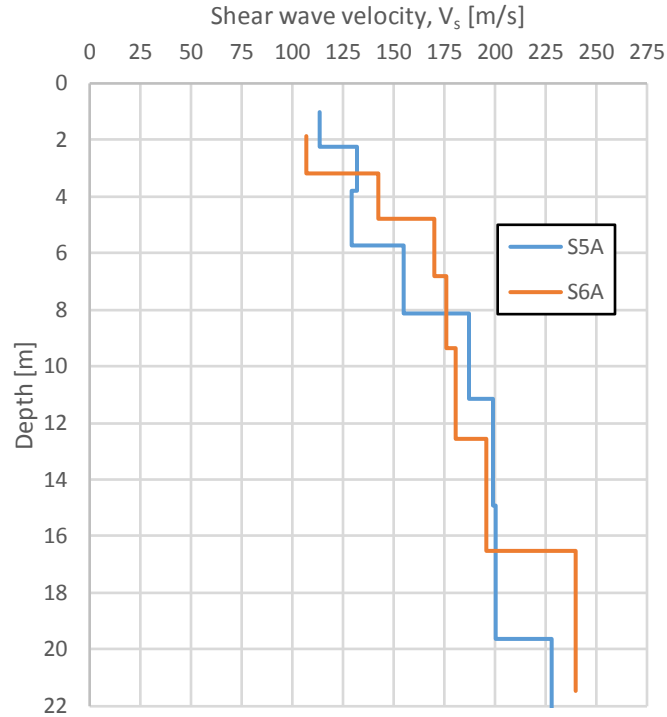


Figure 5.7 Result from the repeated MASW survey

The repeated MASW results at profile S5A and S6A are very similar. The MASW-results may be summarized as increasing V_s from about 110 m/s at 1.0 m depth to about 230 m/s at 20 m depth, with a slightly greater increase in the top clay layer (above 8m). Compared to the original results the repeated V_s -results is in a more expected range and they are used in the comparison in this work. However, the accuracy of the MASW is not trusted, especially at depth greater than about 12 m. Based on the different results obtained from the original survey using various processing, the uncertainty remains great.

5.4 Bender Element

More detailed data from the different samples may be found in Appendix C.

5.4.1 Tests with Various Height

A summary of the results from the bender element testing on samples with various height are given in Table 5.1. The development of V_s during consolidation is presented in Figure 5.8.

| Sample # | Height [mm] | $V_{s,1}$ [m/s] | $V_{s,2}$ [m/s] | $V_{s,3}$ [m/s] |
|----------|-------------|-----------------|-----------------|-----------------|
| 1 | 100 | 93,4 | 138,3 | 121,8 |
| 2 | 100 | 98 | 141,2 | 112 |
| 3 | 50 | 109,3* | 139,3 | 113,1 |
| 4 | 120 | 96,6 | 139,3 | 113,8 |
| 5 | 50 | 110,2* | 138,4 | 112,2 |

Table 5.1 Result from bender element test on samples from same depth with various height

where

$V_{s,1}$ = Shear wave velocity when the samples are consolidated to in situ pressure (1)

$V_{s,2}$ = Shear wave velocity when the samples are consolidated to preconsolidation pressure (2)

$V_{s,3}$ = Shear wave velocity when the samples are consolidated back to in situ pressure (3)

*The cross-correlation program had problems identifying the first arrival on the 50 mm samples after some time during stage (1), hence the results given are based on rough estimates from pictures of the received signal (Appendix C).

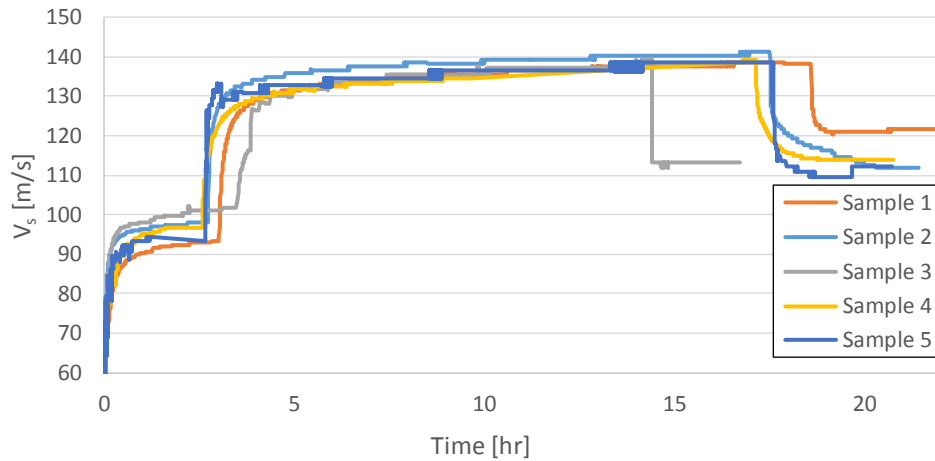


Figure 5.8 Development of V_s during consolidation for sample #1-5

The in situ shear wave velocity from these test is not easily determined. From stage (1) the V_s -results are not very consistent, but it seem to be around 97 m/s. However, in stage (3) V_s is around 113 m/s. The true value is probably in between these values. Sample #8 (described in the next section) was consolidated in stage (1) for over 20hr and the result is trusted. The increase in V_s from stage (1) to stage (3) is 5 m/s. Samples #1-5 are assumed to have a greater increase, as the stress level in stage (1) is lower. Based on the results from sample#8, a V_s of 105 m/s is assumed as in situ value in sample #1-5.

5.4.2 Time Effect

The effect of long term consolidation is investigated on three samples from various depths. Sample #6 and #7 consist of quick clay, and the quality of these tests are considered to be poor. However, a clear tendency can be seen. The shear wave velocity in the quick clay samples “consolidated” significantly slower.

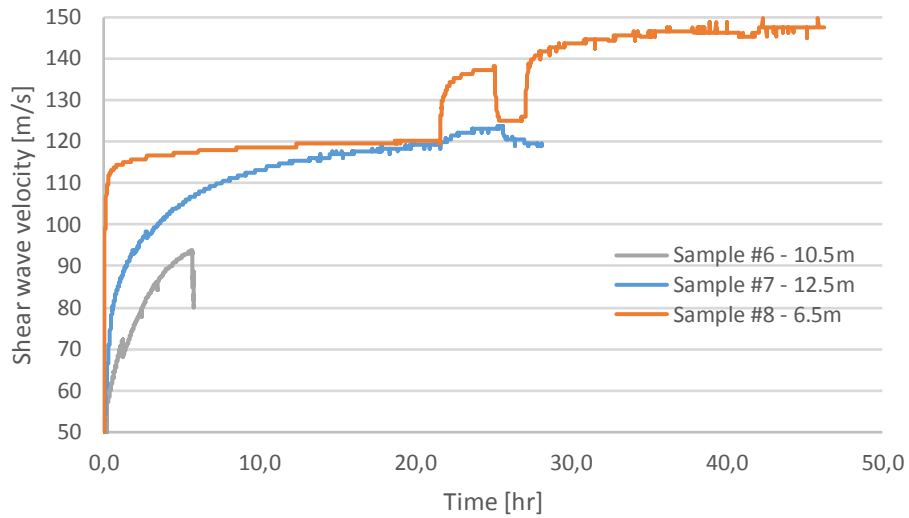


Figure 5.9 Development of V_s during consolidation for sample #6-8

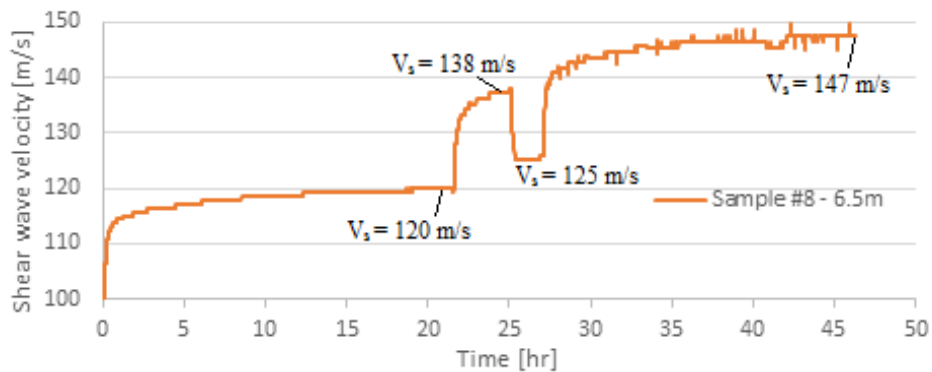


Figure 5.10 Development of V_s for sample#8 during consolidation

After the end of primary consolidation the shear wave velocity increased with about 4 m/s in the next 20 hr. When unloading from a higher stress level, the V_s has increased. No difference in result is found when using a signal amplitude of 2 V.

An interesting discovery is that the samples of non-sensitive clay give consistent V_s -value when consolidated to $\sigma'_1 = 150kPa$ and $\sigma'_3 = 105kPa$. The quick clay sample however, did not. An interesting investigation would be to consolidate a sample stepwise. Maybe a total shear wave profile could be made from one sample in soils with homogeneous layering.

To find values for the time effect after primary consolidation, the shear wave velocity is plotted against the logarithm of time (Figure 5.11).

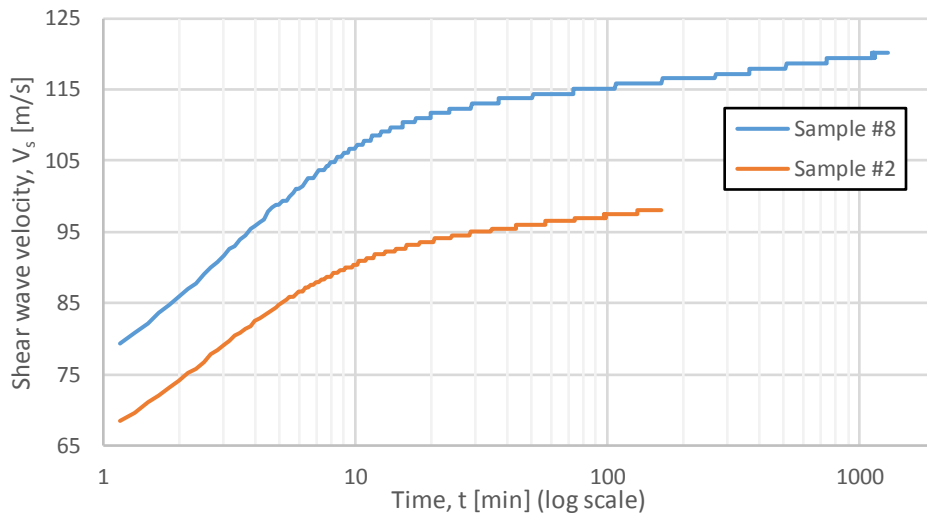


Figure 5.11 Shear wave velocity development vs. log time

In both samples, the V_s starts increasing linearly until they bend after about 15 min and starts increasing linearly again at a lower rate. It is believed that the increase of V_s after the bend is due to aging effects.

In Figure 5.12 the development of sample #8 after 80 min is presented.

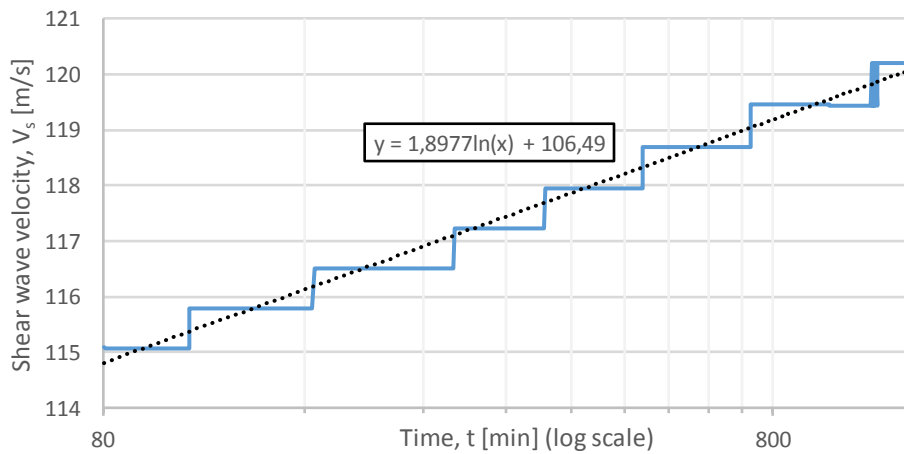


Figure 5.12 Shear wave velocity development of sample #8 after the end of primary consolidation

The reason for the stepwise increase of V_s is the bender element time resolution of 5.0 μ s. However, a linear increase in the log scale is a good estimate.

The normalized development of the shear wave velocity after the end of primary consolidation of sample #8 is presented in Figure 5.13.

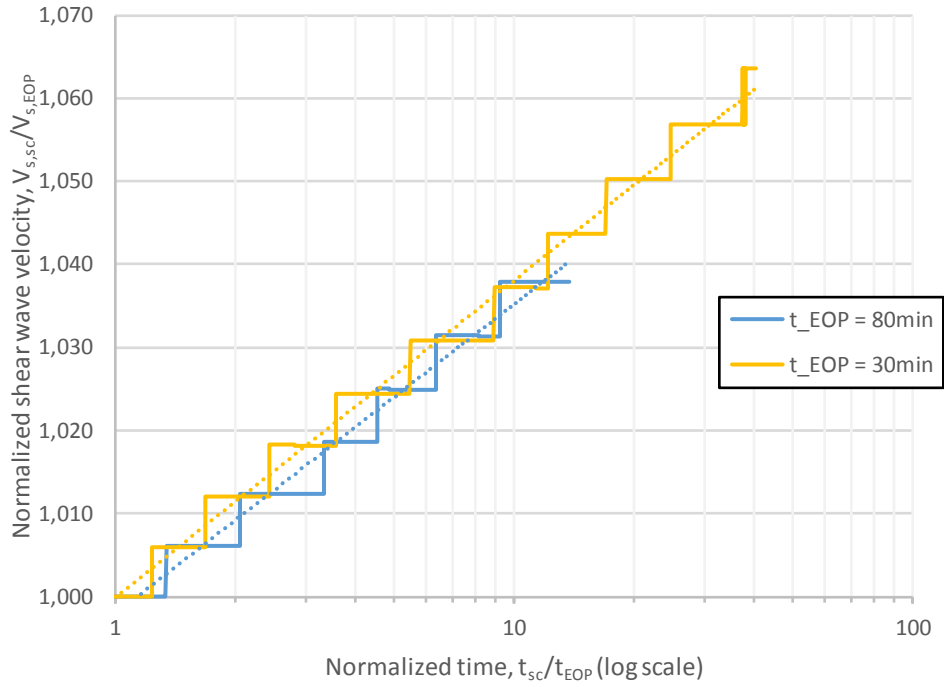


Figure 5.13 Normalized development of the shear wave velocity after end of primary consolidation of sample #8

Assuming end of consolidation after 30 or 80 min does not influence the inclination significantly.

Using equation (2.16) and (2.17) on results from sample #8 give:

$$I_{V_s} = 4.37 \text{ m/s}$$

$$N_{V_s} = 3.65 \%$$

Using the empirical equation (2.18) from Anderson (1974), N_{V_s} is found to be:

$$N_{V_s} = e^{2.0 - 0.46 \cdot 0.19 + 0.25 \cdot 1.07} = 8.86\%$$

Now, ΔV_s from t_{1000} to any given time can be estimated using equation (2.16) and (2.17) and $V_{s,1000} = 120 \text{ m/s}$. The results are given in Table 5.2.

| | From data | | From empirical eq. | |
|-------------|--------------------|-------------|--------------------|-------------|
| Time [min] | ΔV_s [m/s] | V_s [m/s] | ΔV_s [m/s] | V_s [m/s] |
| 1000 | 0.0 | 120 | 0.0 | 120 |
| 1200 | 0.3 | 120 | 0.8 | 120 |
| 2000 | 1.3 | 121 | 3.2 | 123 |
| 5000 | 3.1 | 123 | 7.4 | 127 |
| 7000 | 3.7 | 123 | 9.0 | 129 |
| Time [days] | ΔV_s [m/s] | V_s [m/s] | ΔV_s [m/s] | V_s [m/s] |
| 7 | 4.4 | 124 | 10.6 | 130 |
| 14 | 5.7 | 125 | 13.8 | 133 |
| 30 | 7.1 | 127 | 17.3 | 137 |
| 60 | 8.5 | 128 | 20.5 | 140 |
| 180 | 10.5 | 130 | 25.6 | 145 |
| Time [yr] | ΔV_s [m/s] | V_s [m/s] | ΔV_s [m/s] | V_s [m/s] |
| 1 | 11.9 | 131 | 28.8 | 148 |
| 2 | 13.2 | 133 | 32.0 | 152 |
| 5 | 14.9 | 135 | 36.2 | 156 |
| 10 | 16.2 | 136 | 37.8 | 157 |
| 20 | 17.6 | 137 | 39.4 | 159 |
| 50 | 19.3 | 139 | 41.3 | 161 |
| 100 | 20.6 | 140 | 42.6 | 162 |
| 1000 | 25.0 | 145 | 46.8 | 166 |
| 10000 | 29.3 | 149 | 50.0 | 170 |

Table 5.2 Predicted aging effect using values from both laboratory data and an empirical equation

Sample #7 did not seem to get to the end of primary consolidation as no bend is found in Figure 5.14, even after 1000 min. The curve from sample #7 results in a $N_{V_s} \approx 22\%$. At 10.5 m depth, that would result in a ΔV_s of 106 m/s after 20 years (almost 90% increase). One possible reason is that sensitive clays are more subjected to sample disturbance during sampling and testing.

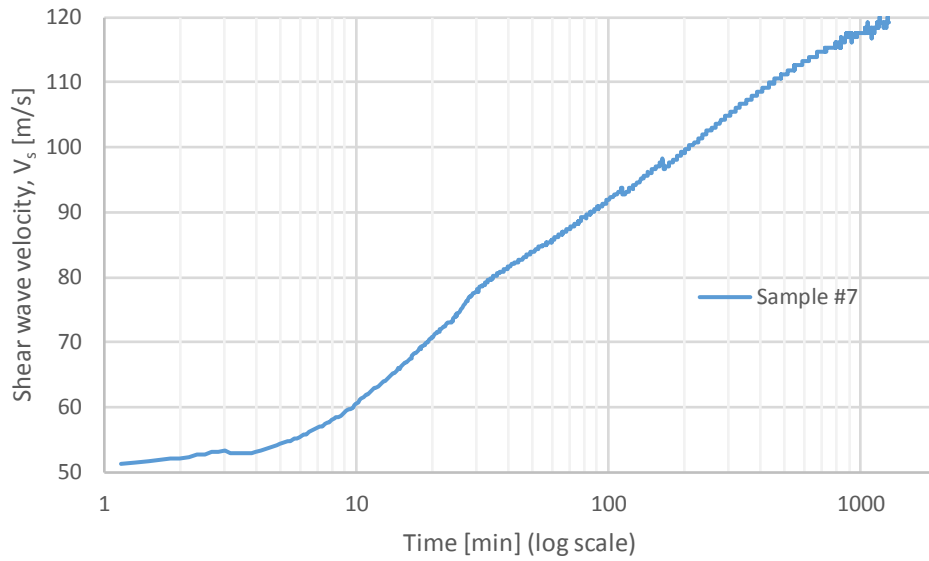


Figure 5.14 Development of the shear wave velocity in sample #7 against log time

Based on the calculated values for secondary aging effect from sample #8, $V_{s,20yr}$ is calculated for all the samples. The empirical formula gives a significantly greater increase in shear wave velocity with time, compared to the results from laboratory data.

| Depth [m] | $V_{s,1000}$ [m/s] | $V_{s,20yr,data}$ [m/s] | $V_{s,20yr,empiri}$ [m/s] |
|--------------|-----------------------|----------------------------|------------------------------|
| 4,5 | 105 | 123 | 149 |
| 6,5 | 120 | 138 | 163 |
| 9,1 | 118 | 136 | 160 |
| 10,5 | 119 | 137 | 160 |

Table 5.3 Shear wave velocity from bender element and its predicted development based on laboratory data and empirical formulas

Chapter 6 Discussion

6.1 Accuracy

All shear wave velocity investigations carried out at Tiller is presented in Figure 6.1. In addition to the bender element results found in the laboratory, results with estimated aging effect are presented. The aging effect is divided in two. One based on laboratory data and the other from empirical formulas (Anderson 1974).

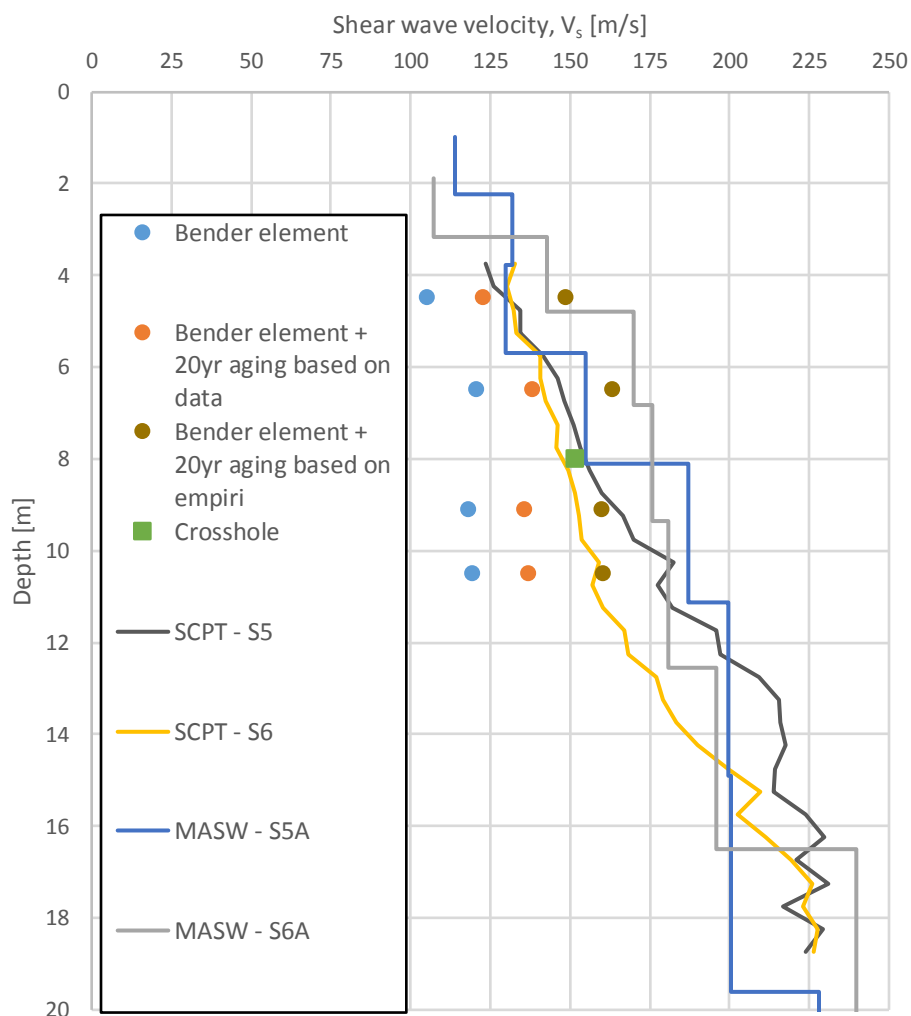


Figure 6.1 Summary of all obtained data from Tiller

The results from the in situ tests show a fairly good agreement, increasing from about 125 to 225 m/s at 3 and 19 m depth, respectively. Some variation in results is present along the profile, but no more than about 20 %. The SCPT results have higher resolution compared to the MASW results as the SCPT is plotted with one point every 0.5 m while the MASW give average values in steps ranging from about 1.5 m to 4.7 m. Despite not giving any clear signals, the V_s from the crosshole test is very similar to the average SCPT result. This supports the assumption that SCPT is more accurate than the MASW test.

The bender element results are however considerably lower (20-60 %) if no aging effect is considered. By using formulas from Anderson (1974), the aging effect can be estimated by extrapolating the consolidation time to 20 years. The results fits reasonably well with the in situ measurements when adding the aging effect. In the top soil layer (above 8 m depth) the aging effect based on laboratory data seem to give the best fit compared to the SCPT results, only underestimating V_s with about 6 %. If aging effect based on the empirical formulation is used, V_s in the upper non-sensitive clay layer is overestimated with about 10-15 %. In the quick clay layer, the aging effect based on empirical formulation are most compliant. Compared to the SCPT in profile S5 these results underestimate V_s with 4-10 %. However, if compared to SCPT in profile S6, they overestimate V_s with 1-5 %.

In Figure 6.2 the results are divided with respect to the two profiles. The laboratory samples are taken from the area close to profile S5. Note that the bender element point at 9.1 m is from a block sample tested by Knutsen (2014).

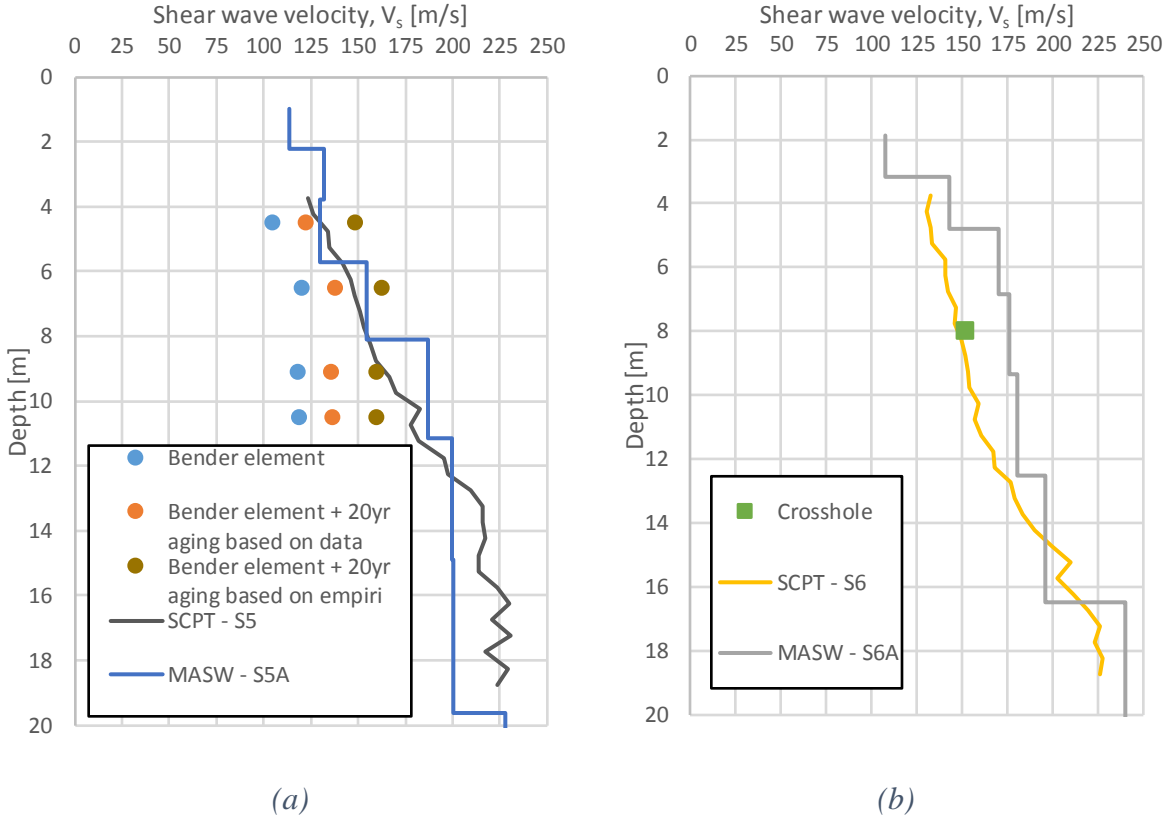


Figure 6.2 Comparison of results from profile S5 (a) and S6 (b)

In Figure 6.3 the average SCPT and MASW V_s -profiles are plotted with results from crosshole and the “best corrected” bender element results. The “best corrected” bender element results are the V_s -results from the laboratory corrected for the aging effect. In the upper clay layer (above 8m) aging effect based on laboratory data is used. Below 8m is the Anderson (1974) empirical formula used to estimate the aging effect.

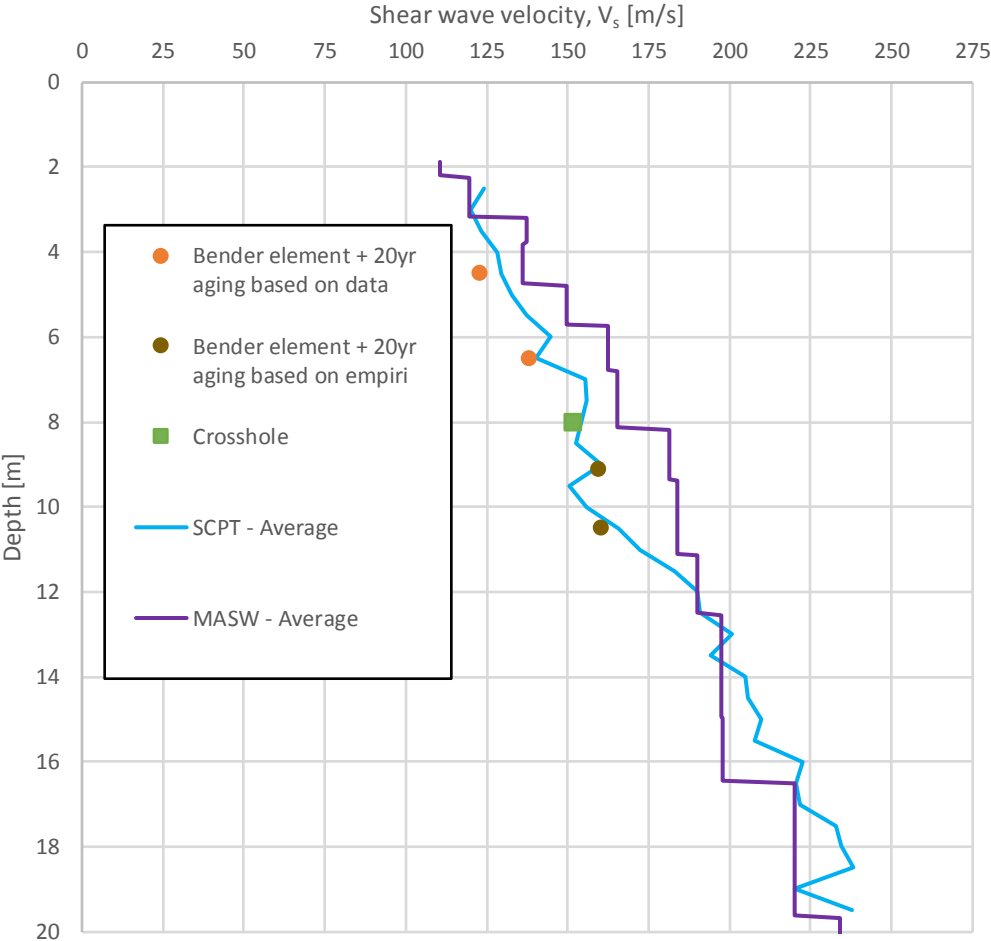


Figure 6.3 Average shear wave velocity results from Tiller

All the results given in Figure 6.3 match fairly well, with a maximum deviation of about 20 %. The accuracy is considered to be best from the SCPT method. The sensitivity in results due to interpretations of the MASW dispersion curves, makes the uncertainty of the MASW method considerable.

6.2 Suitability

In this section, the suitability of the tests for soft Norwegian low plasticity clays are discussed.

All the tests are rather simple to perform in field and laboratory. All of the tests can also be implemented into already standard equipment (e.g. drilling rig, triaxial cell). The challenge is processing of the data. If the signals from SCPT, CHT and bender element are clear, the data could be quickly processed by scripts. If the signals have a significant level of noise, manual interpretation may be needed. The results from the performed tests reminds that there is no guarantee for obtaining clear signals. To get trustable results from MASW with depth, the frequency range on the dispersion curve has to be sufficiently clear and low. Using a 10 kg sledgehammer and 3 m geophone spacing in field provide sufficiently quality of the dispersion curves in this study. However, more study on getting and interpreting dispersion curves in soft clays are required.

CPTU is often performed in areas with soft Norwegian low plasticity clays. SCPT may be combined with an ordinary CPTU without increasing the consumed time significantly. SCPT is able to identify rather thin layers if the measurement interval is sufficiently small. If combined with Electrical Resistivity Tomography (Appendix D), SCPT may also be used effectively to determine the shear wave velocity of a large area.

CHT test is rather time consuming, and is thus mostly recommended at sites with uniform layering.

MASW is the most effective method if a large area is to be investigated. However, it may have problems identifying thin layers

Samples are often tested in the laboratory if a site consist of soft Norwegian low plasticity clay. In this study, the results deviate significantly from in situ testing. The aging effect and other factors affecting V_s should to be better understood before bender element testing is included as standard laboratory testing. Bender element testing is very time consuming. One test only give information about one position at one depth. If a sample can be loaded stepwise to produce a full profile, that would increase its effectiveness and suitability significantly.

6.3 Sources of Errors

Uncertainties related to the different tests are discussed in this section.

6.3.1 SCPT

Processing

The signal to noise ratio is not as desired at some depths. In general, the ratio decreased with depth. Hence, damping is assumed to be the main reason. The shear wave arrival is picked manually at every depth, and some minor errors might be expected. The magnitude of these errors are expected to be in the order of $\mp 0.2ms$. Some single measurements however, may have a greater error. Manual determination of shear waves ensures that the correct waves are picked for comparison.

An unexpected major signal in the vertical z-direction, arriving before the shear wave, is found at all hits. It is probably due to direct and refracted p-waves. It is however not considered to have any considerable effect on the shear wave.

Depth Measurements

The depths are measured manually by marking the rods every 0.5m. The drilling rig is stopped when these marks are at the ground level. The accuracy is assumed to be on cm level. In addition, there are no measurements of the rods verticality down the borehole, thus some inclination is to be expected. However, it is not considered to cause a considerable error as the measurements are made on short intervals. As the shear wave source is placed next to the rods, the travel distance is slightly longer than the vertical distance. This error is decreasing with depth, and considered negligible after the top three meters.

Shear Wave Source

The hits with the sledgehammer are performed by the operators, and the applied energy varied. According to theory however, the wave frequency and amplitude should not affect the propagation velocity.

Soil Disturbance

The effect on V_s from having a steel rod penetrated into the soil is unknown. Disturbance and stress increase are induced to the surrounding soil. In addition the shear wave travel path may be influenced. It is however considered to be of less importance to this test.

6.3.2 Crosshole

Common Pitfalls

Butler and Curro Jr (1981) presents some common pitfalls in the crossover method. The use of too large borehole spacing in a layered soil may give erroneous results due to the shear wave travels in the adjacent layer with highest V_s , giving a shorter travel time. At Tiller there are no layers with considerable higher V_s . A distance of 5.0 m is not considered to give any considerable error.

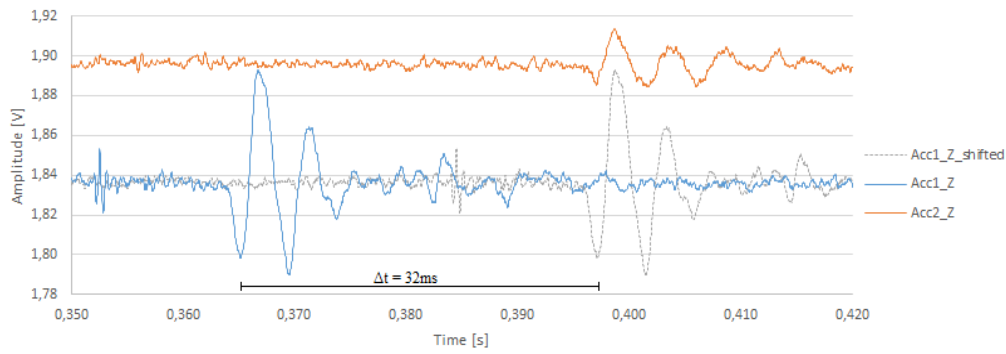
Butler and Curro Jr (1981) also warn against using two receivers to determine the V_s -profile. They claim that “*the first arrivals at the two receivers probably do not represent the direct-path arrivals at the two receivers through the same unit or even refracted arrivals along the same interface*”. This is important to keep in mind when processing the results. The processing in this study does however not only focus on the first arrival, but also the shape of the waves. Using one receiver is not assumed to increase the accuracy in this test.

Processing

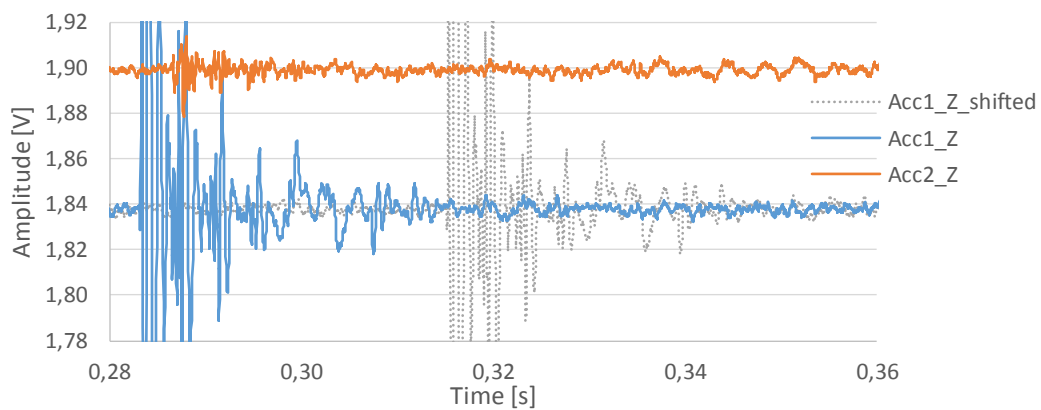
A small error in shear wave travel time may be decisive. Thus, the signal interpretation is vital in order to get good results.

During the first test on the Esp site, vertical hits provide distinct signals in the vertical z-direction at both accelerometers. Although the signals are not equal at the two accelerometers, the first arrival is rather simple to find. Also in the x- and y-direction quite clear signals are obtained. Horizontal strikes give weaker and more unclear signals at the farthest accelerometer.

The received signals from the second test, at the Tiller site, are not of the same quality. At the closest accelerometer, the signal from the p-wave is dominant, making the shear wave arrival hard to determine. The signal at the farthest accelerometer is also much weaker at the second test. Horizontal strikes do not improve the results.



(a)



(b)

Figure 6.4 Crosshole signal in z -direction from Esp (a) and Tiller (b)

There is no apparent reason why the signals at the two sites are so different. The same equipment are used and the soil material is expected to be rather similar. Some possible explanations are given in this section. Knutsen (2014) also experience problems getting a clear signal, especially in the vertical direction. She use the same equipment. The main explanation suggested by Knutsen (2014) is high attenuation effect of the plastic tubes. To cope with this problem, the tubes are pushed a bit too deep and pulled up again a couple of cm. The steel rod at Esp has been staying in the ground for about a year. At Tiller the steel rod is placed in the ground only days before the testing. The signals are also found to be clearer using softer hits.

Shear Wave Source

By using a steel rod as shear wave source, shear waves propagates from the whole length of the rod. The V_s in steel is about 5000 m/s. Figure 6.5 illustrates some possible wave paths. The time

difference between the start of the shear waves from the top and bottom of the rod are about 1.5 ms. However, as the distance is significantly longer, the horizontal travel path is assumed to give first arrival at both accelerometers.

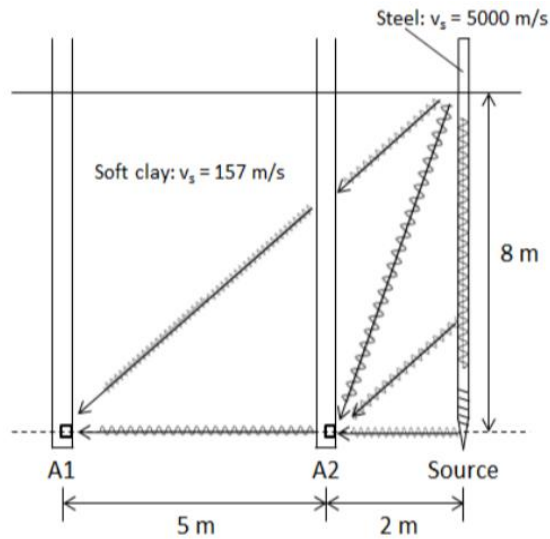


Figure 6.5 Illustration of different signal paths (Knutsen 2014)

Horizontal Distance

The plastic tubes are lowered 8 m into predrilled holes. No inclinometers or other positional devices are used. Thus, the accurate horizontal distance between the two accelerometers is hard to determine. A small inclination on the borehole may give considerable offset at 8 m depth. However, the error is assumed to be less than 5-10 %.

Anisotropy

In contrast to the other methods, the crosshole method measure horizontal propagating shear waves. Waves with both $V_{s(hh)}$ and $V_{s(hv)}$ are measured without any considerable difference in result. Due to the relative low OCR, the stress difference is not major in this clay. Anisotropy is not considered to cause a significant error.

6.3.3 MASW

Retrieving Good Dispersion Curves

The obtained frequency range from the original MASW survey is too high to evaluate V_s at great depths. Using heavier sledgehammer and greater geophone spacing allow lower frequencies to be found. However, 10 Hz vertical geophones are used in the tests. Frequencies lower than 10 Hz are to be used with caution.

Processing

Unless the soil profiles are simple, the processing of the dispersion curves require knowledge and experience. The same data may give very different results, based on the processing. Significant user experience and knowledge is needed for complex soil profiles to determine suitable dispersion curves (Long and Donohue 2007). The major part of the uncertainty is related to picking the dispersion curve. Comina et al. (2010) find that the differences of $V_{s,30}$ due to the inversion of the dispersion curve are of minor importance (within approximately 2%). They also state that with a maximum retrieved wavelength greater than 60 m, the final result is approximately close to the one of invasive tests.

The MASW-method may be significantly influenced by the data processing. An example is the original MASW survey on Tiller. Three different ways of processing the same data are presented in Figure 6.6. The results are varying substantially. The uncertainty of the dispersion curves are also increasing at lower frequencies (Lai et al. 2005). Hence, the uncertainty of V_s increases at greater depths.

Moss (2008) underlines that surface wave measurements tends to overestimate V_s in soft soils.

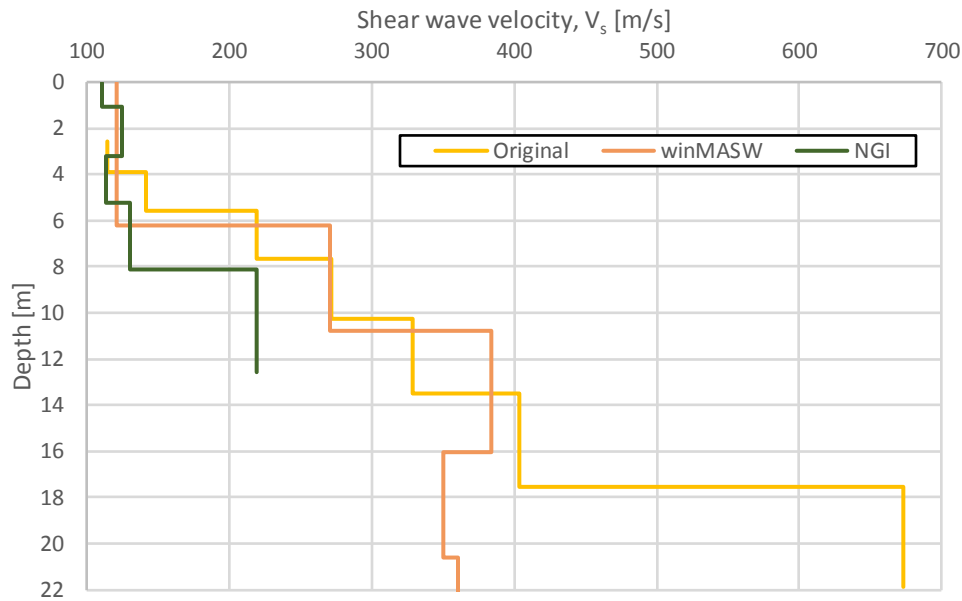


Figure 6.6 MASW-data from Tiller S6 with different processing

6.3.4 Bender Element

Signal Interpretation

The travel time and distance are the two measurements that are given by the bender elements. There are generally few problems finding the distance between the transmitter and the receiver. The travel time however, has shown to be more problematic to determine. The output signals are generally quite different from the input signals.

The bender element does not only generate shear waves. When the bender element bends, two pressure waves (one in compression and the other in rarefaction) are generated. These waves may cause trouble when identifying the arrival of the shear waves. Pressure waves propagate generally with a greater velocity than shear waves, hence a pressure wave reflected off the wall of the sample may arrive before the shear wave. This effect is called the near-field effect, as the problem is known to occur when the distance between the transmitter and receiver is short. To avoid such near-field effect, certain ratios between the distance to the receiver (d) and shear-wavelength (λ) have been suggested. A commonly used limit is $d/\lambda > 2$, suggested by Sanchez-Salinerio et al. (1986). The necessary frequency to satisfy this limit for different sample heights is given in Table 6.1 and Table 6.2 for a V_s of 100 and 200 m/s, respectively.

$$V_s = 100\text{m/s}$$

Sample height, d Wavelength, λ Frequency, f

| <i>[mm]</i> | <i>[mm]</i> | <i>[kHz]</i> |
|-------------|-------------|--------------|
| 50 | 25 | 4.0 |
| 100 | 50 | 2.0 |
| 120 | 60 | 1.7 |

Table 6.1 Suggested minimum frequency to avoid near-field effect with $V_s=100$ m/s

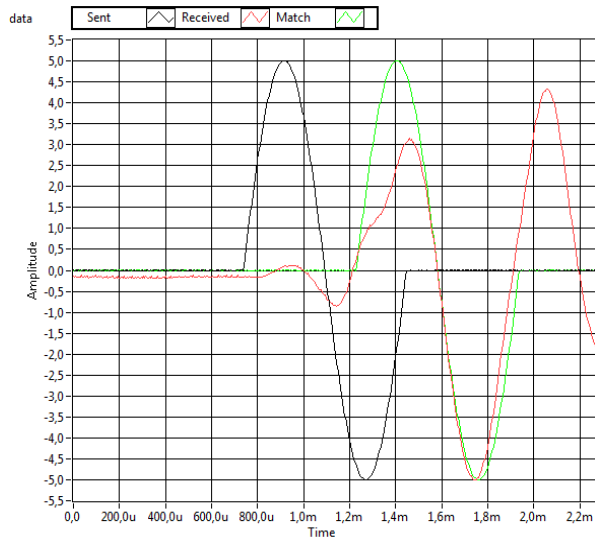
$$V_s = 150\text{m/s}$$

Sample height, d Wavelength, λ Frequency, f

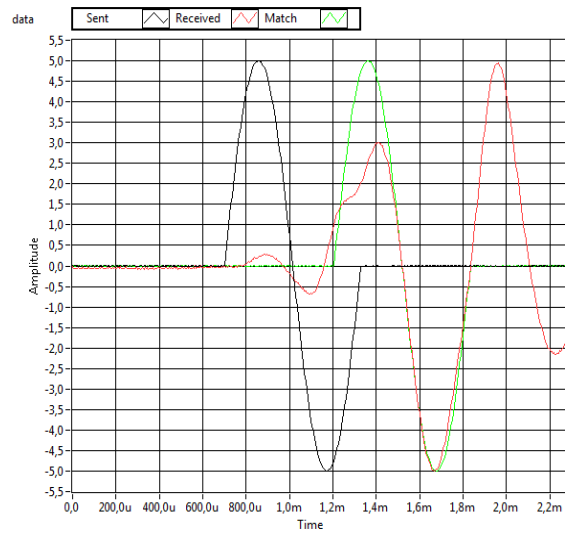
| <i>[mm]</i> | <i>[mm]</i> | <i>[kHz]</i> |
|-------------|-------------|--------------|
| 50 | 25 | 6.0 |
| 100 | 50 | 3.0 |
| 120 | 60 | 2.5 |

Table 6.2 Suggested minimum frequency to avoid near-field effect with $V_s=150$ m/s

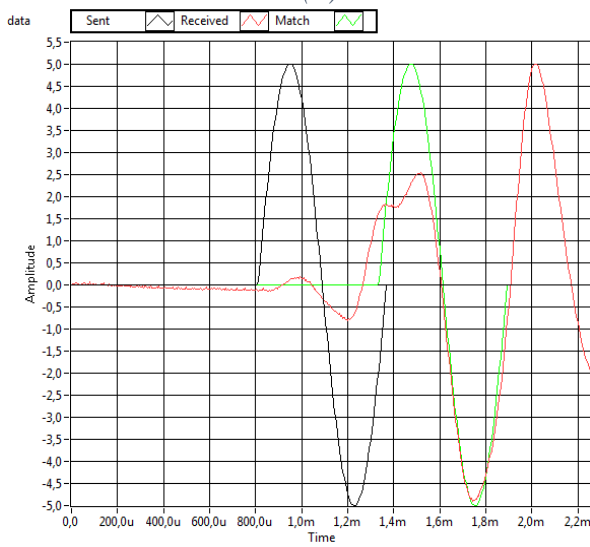
The biggest challenge during the testing is getting and evaluating the received signals. The received signal changes significantly when the frequency is changed. This may indicate near/far-field problems. However, the received signal mostly showed a better match with the input signal at lower frequencies than those suggested by Sanchez-Salinero et al. (1986). That is probably because the natural frequency of the system is in this lower range. The program automatically use the cross-correlation method between transmitted and received signal to determine the travel time. In some cases, mostly using high frequency, the cross-correlation failed to determine the first arrival. An example from sample #8 is given in Figure 6.7. It is clear that some signal interference is present.



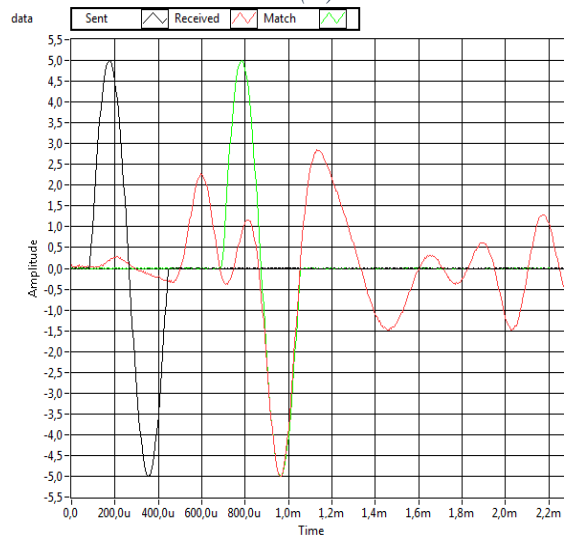
(a)



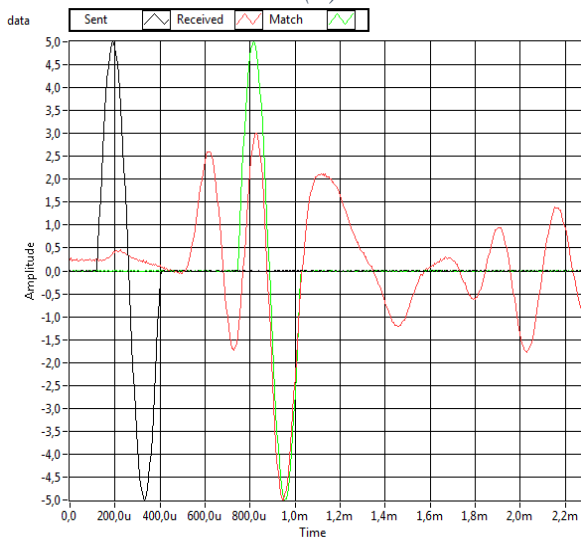
(b)



(c)



(d)



(e)

Figure 6.7 Received signals from sample #5 at frequencies 1.4 kHz (a), 1.6kHz (b), 1.8 kHz (c), 2.8kHz (d) and 3.6 kHz (e)

System Time Delay

Wang et al. (2007) investigate system delay in the bender element. They find that the time delay may be focused at the transfer function at the receiving bender element. The practice in bender element testing is to use a signal with a frequency equal to the eigenfrequency of the system to improve the signal to noise ratio. However, Wang et al. (2007) argue that this also cause a significant time delay and phase lag, mainly due to inertia effect and waveform distortion by the frequency-dependent response and phase lag. This time delay has to be quantified and taken into account when calculating the shear wave velocity.

Knutsen (2014) performe Bender element tests on both 50mm and 100mm samples from the Esp clay. The results showed an about 20 % higher V_s -value for the 100mm samples, and both V_s -values from the bender element testing was significantly lower than the result from using the cross-hole method. One possible explanation was that the system itself had a time delay (Wang et al. 2007), which would result in lower V_s for short samples as it would be a bigger part of the total time (equation (6.1)). Two equations with two unknowns was set up and solved based on the result from Knutsen (2014). The results are given in Table 6.3.

$$t_\epsilon + \frac{H_i}{V_s} = t_i \quad (6.1)$$

$$V_s = \frac{H_i - H_j}{t_i - t_j} \quad (6.2)$$

$$t_\epsilon = t_i - \frac{H_i}{V_s} \quad (6.3)$$

| $V_{s,100}$ | $V_{s,50}$ | $V_{s,corr}$ | $V_{s,CH}$ | t_ϵ |
|-------------|------------|--------------|------------|--------------|
| 120 m/s | 105 m/s | 142 m/s | 157 m/s | 0.15 ms |

Table 6.3 Results from Knutsen (2014) and corrected V_s -value assuming system delay

The results from sample #1-5 are quite consistent for $V_{s,2}$ and $V_{s,3}$, regardless of sample height. This suggests that a considerable system delay is not apparent.

Ground Water Level

The ground water level, z_w , was set to 0.5 m when calculating in situ pressure. However, values up to 1.5 m have been measured. That equals a difference of about 10kPa in effective vertical stress.

Sample Quality

Bedding and installation will disturb the sample to some extent. Chan et al. (2010) find the effect of installation of bender elements to be negligible. Local disturbance/remoulding due to the movement of the bender element may be another problem.

The change in pore volume relative to initial pore volume, $\Delta e/e_0$, when consolidated to in situ stress, is used as a measure to quantify the sample quality. This method is used by NGI since 1995 on several onshore and offshore consulting projects. Lunne et al. (2006) states that this method of measuring sample quality is mainly based on marine clays with plasticity index 6% – 43%, water content 20% – 67%, OCR=1-4 and depth 0m – 25m. With properties outside these ranges, the method should be used with caution. The Tiller clay fits within these limits. The suggested limits of sample quality is presented in Table 6.4.

| <i>Sample quality category</i> | | | | |
|--------------------------------|-------------------------------|---------------------|----------------|------------------|
| <i>OCR</i> | <i>Excellent to very good</i> | <i>Good to fair</i> | <i>Poor</i> | <i>Very Poor</i> |
| | $\Delta e/e_0$ | $\Delta e/e_0$ | $\Delta e/e_0$ | $\Delta e/e_0$ |
| 1 – 2 | < 0.04 | 0.04 – 0.07 | 0.07 – 0.14 | > 0.14 |
| 2 – 4 | < 0.03 | 0.03 – 0.05 | 0.05 – 0.10 | > 0.10 |

Table 6.4 Sample quality based on $\Delta e/e_0$ (Lunne et al. 2006)

The result using this measure is presented in Figure 6.8.



Figure 6.8 Measure of sample quality based on relative dissipation of pore waver

In respect to sample quality, the measure give quality varying from very good to very poor. According to this measure, the samples from the quick clay layer give the worst quality. In the non-sensitive clay layer, the quality seems to improve with greater sample height.

However, using this measure on samples with different heights and time of consolidation do not give a clear view of the sample quality. Higher samples needs more time to consolidate. The final V_s -results in the non-sensitive clay layer did not suggest to be influenced by differences in sample quality.

The quick clay samples are assumed to be of low quality.

Time Effect

N_{V_s} calculated from laboratory data is 3.65 %, which is lower than the normal range of clays (5-25 %). By using the empirical formulas, N_{V_s} is calculated to be 8.86 %. That is in the normal range of clays. The aging effect is in general greater for heavily overconsolidated clays. Thus, N_{V_s} in the lower range is expected. Based on the measure of sample quality it is not considered unlikely that sensitive and non-sensitive samples behave differently.

Chapter 7 Engineering Consequences

Comparison of MASW, CHT, SCPT and bender elements results (Chapter 6) show that for a given clay site, the collected V_s may vary depending on the techniques. For a geotechnical engineer it is of great importance to understand how such differences in V_s could impact on resulting geotechnical design and engineering calculations. To this aim, some simple analysis on settlement and earthquake engineering are conducted using different values for V_s . The results are discussed briefly.

7.1 Settlement Calculations

Most soil models assume elastic behaviour during unloading and reloading. As shown in chapter 2.2, the soil only behave elastic for very small strains. This is taken into account in the Hardening Soil Model with Small-Strain Stiffness (HS Small) in the geotechnical finite element program PLAXIS. The following section summarize how the HS Small model is described in PLAXIS Manual Material Models (Brinkgreve and BROERE 2006).

The small strain stiffness is controlled by two additional input parameters, G_{max}^{ref} and $\gamma_{0.7} \cdot G_{max}^{ref}$ is the reference shear modulus at stress level $p_{ref} = 100 \text{ kPa}$. $\gamma_{0.7}$ is the shear strain where the secant shear modulus, G_s , is about 70 % of the G_{max} . Hence, the equation may be written as:

$$\frac{G_s}{G_{max}} = \frac{1}{1 + a \left| \frac{\gamma}{\gamma_{0.7}} \right|} \quad (7.1)$$

where

$$a = 0.385$$

To determine the shear strain, γ , following scalar value presented by Benz (2007) is used: $\gamma = \sqrt{3} \frac{\|\underline{H}\Delta\mathbf{e}\|}{\|\Delta\mathbf{e}\|}$, where $\Delta\mathbf{e}$ is the true deviatoric strain increment and \underline{H} is a symmetric deviator that represent the deviatoric history of the material. Whenever a strain reversal is detected the tensor \underline{H} is partially or fully reset before the actual strain increment, $\Delta\mathbf{e}$, is added. The tangent shear

modulus, G_t , may be found from taking the derivate of the shear stress relation with respect to the shear strain.

$$G_t = \frac{G_{max}}{(1 + 0.385 \left| \frac{\gamma}{\gamma_{0.7}} \right|)^2} \tag{7.2}$$

Equation (7.2) is used well into the plastic material domain, but has a lower limit when $G_t = G_{ur}$, where $G_{ur} = \frac{E_{ur}}{2(1+\nu_{ur})}$. The cut-off stain level is given by:

$$\gamma_{cut-off} = \frac{1}{0.385} \left(\sqrt{\frac{G_{max}}{G_{ur}}} - 1 \right) \gamma_{0.7} \tag{7.3}$$

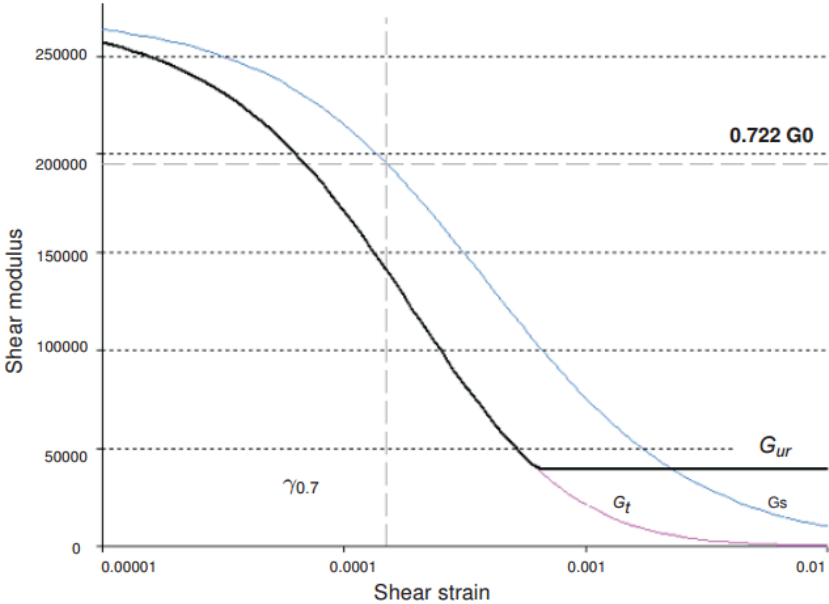


Figure 7.1 Tangent and secant reduction curves used in PLAXIS material model Hardening Soil with Small-Strain Stiffness (Brinkgreve and BROERE 2006)

A PLAXIS analyses is carried out to simulate settlements with V_s varying from 100 to 250 m/s. In Figure 7.2, the tangent shear modulus reduction curves are given for the different V_s .

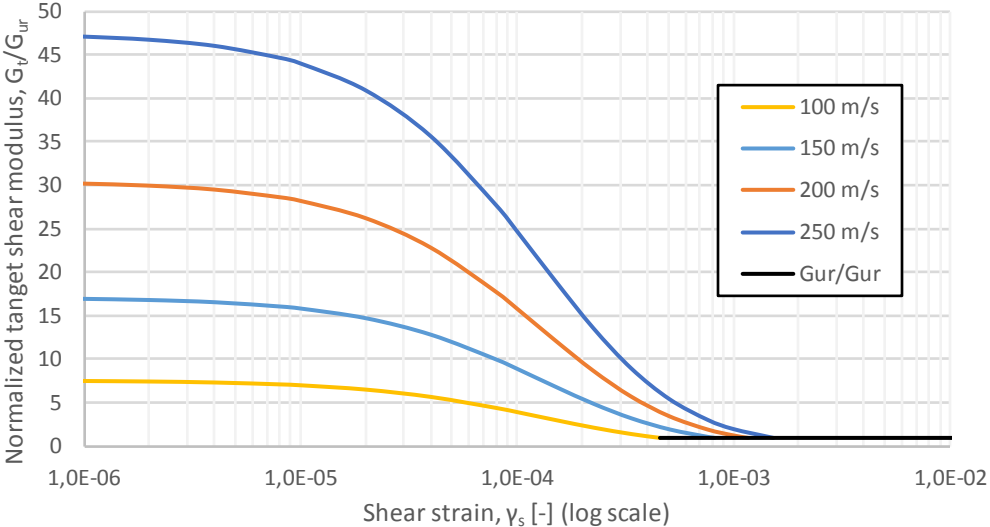


Figure 7.2 Normalized tangent shear modulus reduction curve for different shear wave velocities

The setup of the PLAXIS model is given in Figure 7.3. Four drained and undrained analysis are performed using the Hardening Soil with Small-Strain Stiffness (HSSmall) soil model. V_s -values of 100, 150, 200 and 250 m/s are used in the four analyses. They are taken into account by the model by adjusting G_{max} . In addition, one drained and undrained analysis using the soil model Hardening Soil (HS) are conducted. This soil model does not take the small-strain stiffness into account.

A simple setup with only one soil layer and a line load, $q = 200$ kPa, are used in the model. The soil parameters used are similar to what is expected at the Tiller site. The parameters are given in Table 3.1 and Figure 7.3. All input parameters are identical, besides G_{max}^{ref} . In the undrained analysis is drainage type “Undrained (A)” used and the q is lowered to 10kPa.

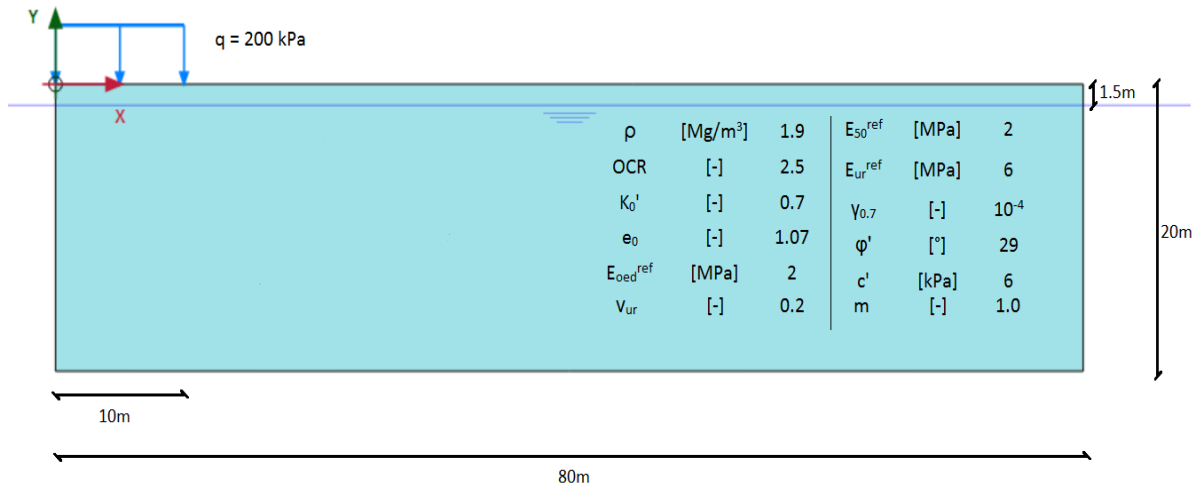


Figure 7.3 PLAXIS model setup and soil parameters

7.1.1 Drained Analysis

An example of a deformed mesh from one of the drained analysis is presented in Figure 7.4. The displacement under the line load is mainly vertical, while in the rest of the soil mainly horizontal displacement away from the line load is present.

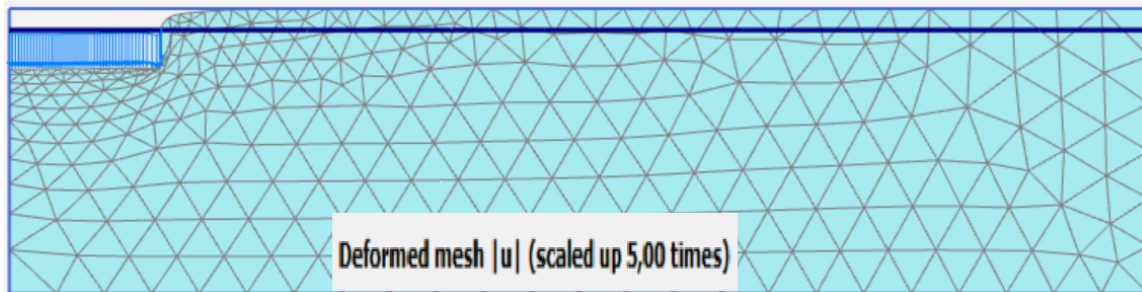


Figure 7.4 Example of deformed mesh of the drained analysis

The small strain stiffness proved to be a decisive parameter when calculating settlement in this manner. The difference in maximum deformation $|u|$ due to selection of V_s is presented in Table 7.1. Results show that an increase in shear wave velocity leads to less settlement. The effect of increasing V_s with 50 m/s is greater at high V_s . Increasing V_s with 50 % from 100 m/s to 150 m/s leads to 11 % less settlement. However, increasing V_s with 25 % from 200 m/s to 250 m/s leads to 19 % less settlement.

| Soil Model | Maximum total deformation $ u $ | Percentage of $ u _{HS}$ |
|-------------------|---------------------------------|--------------------------|
| HS | 1.10m | 100 % |
| HSSmall – 100 m/s | 0.99m | 90 % |
| HSSmall – 150 m/s | 0.88m | 80 % |
| HSSmall – 200 m/s | 0.74m | 67 % |
| HSSmall – 250 m/s | 0.60m | 55 % |

Table 7.1 Maximum deformation using different V_s in a drained analysis

The development of total displacement in the point (0,0) during loading is given in Figure 7.5. At greater load, the displacement increase linearly with applied load. Results show that high V_s settles in a non-linear pattern for a greater applied load. The difference in $|u|$ between two models increases with increasing load. However, the ratio between them decreases. For example, the difference between $|u|$ in the models with 150 and 200 m/s is 6, 10, 14 and 17mm at 50, 100, 150 and 200 kPa applied load, respectively. The corresponding relative differences ($\Delta|u|/|u|_{200\text{ m/s}}$) are 40, 26, 23 and 20 %.

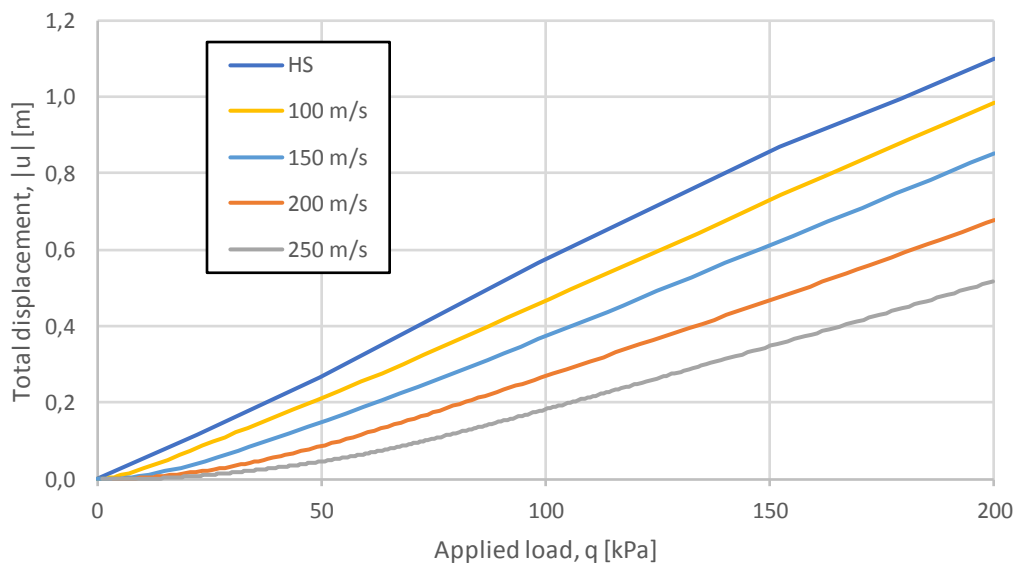


Figure 7.5 Development of total displacement $|u|$ in point (0,0) during loading

In Table 7.2 is the horizontal displacement in a point at the surface 20 m from the center (10 m from the end of the line load), given.

| Soil Model | Horizontal displacement u_x | Percentage of $u_{x,HS}$ |
|-------------------|-------------------------------|--------------------------|
| HS | 83 mm | 100 % |
| HSSmall – 100 m/s | 60 mm | 72 % |
| HSSmall – 150 m/s | 26 mm | 31 % |
| HSSmall – 200 m/s | 10 mm | 12 % |
| HSSmall – 250 m/s | 4 mm | 5 % |

Table 7.2 Horizontal displacement in point (20m, 0m)

The results show that every increase of V_s with 50 m/s causes u_x in point (20m, 0m) to reduce by about 60 %.

The development of horizontal displacement in the same point during loading is plotted in Figure 7.6. The difference in stiffness at low strains is evident.

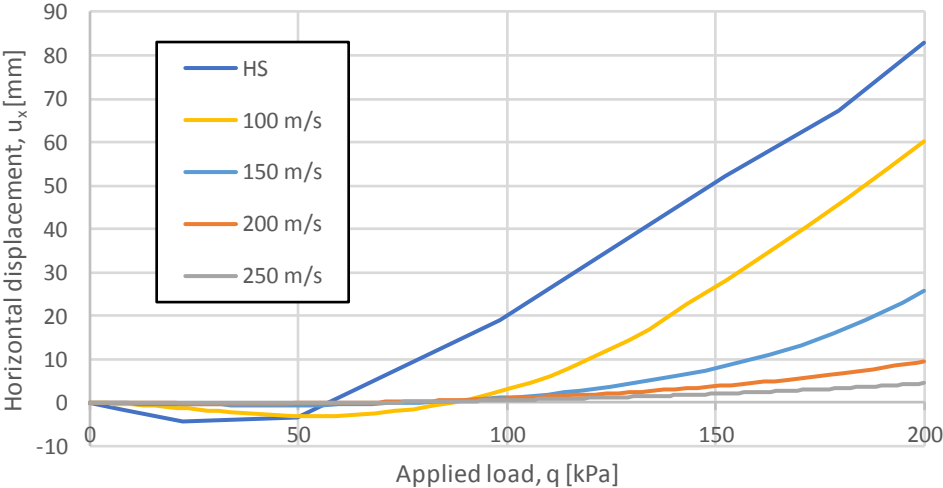


Figure 7.6 Development of horizontal displacement in point C (20m, 0m)

In Figure 7.7, the horizontal displacements in the three of the analysis plotted are against distance from the center.

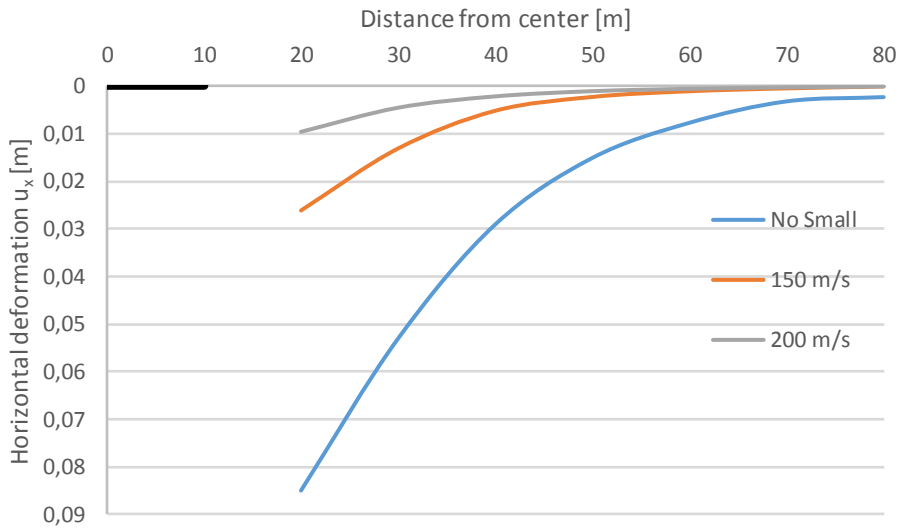


Figure 7.7 Horizontal displacement in the drained analysis

An interesting parameter to evaluate is the $\frac{G_t}{G_{ur}}$ after consolidation. In Figure 7.8, the $\frac{G_t}{G_{ur}}$ after consolidation is displayed for V_s of 150 and 200 m/s, respectively. If compared to the reduction curve (see in Figure 7.2), it seems like the maximum shear modulus is reached in both cases. The general strain level is nevertheless significantly higher in the case with V_s of 150m/s.

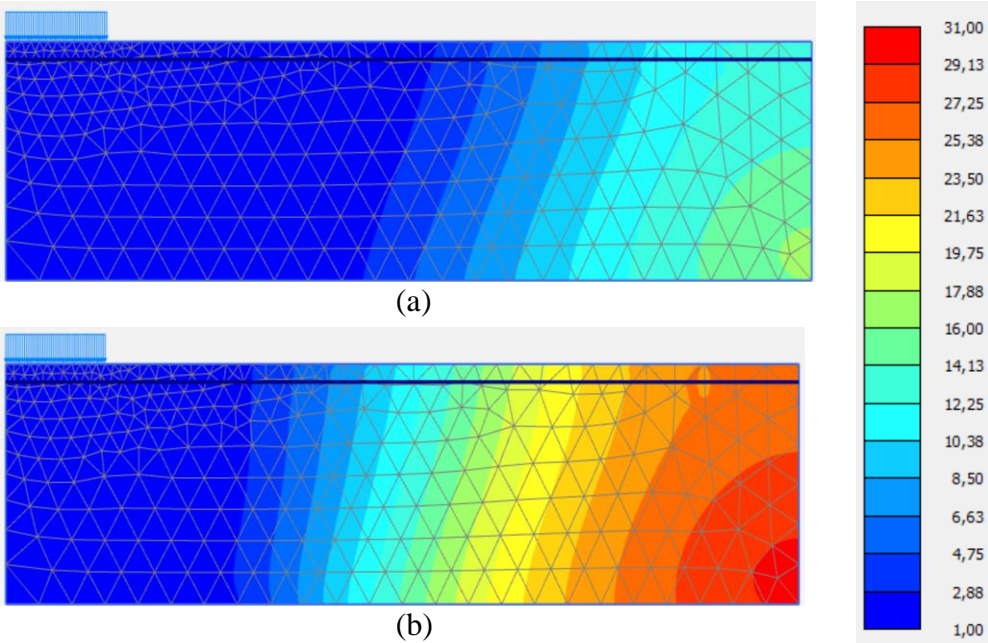


Figure 7.8 G_t/G_{ur} after consolidation with $V_s=150$ m/s (a) and $V_s=200$ m/s (b)

7.1.2 Undrained Analysis

In an undrained analysis there is no change in soil volume (see example of deformed mesh in Figure 7.9). Hence, the horizontal displacement is small. However, the effect of using HSSmall proved to be significant for the maximum total displacement $|u|$. The results are presented in Table 7.3.

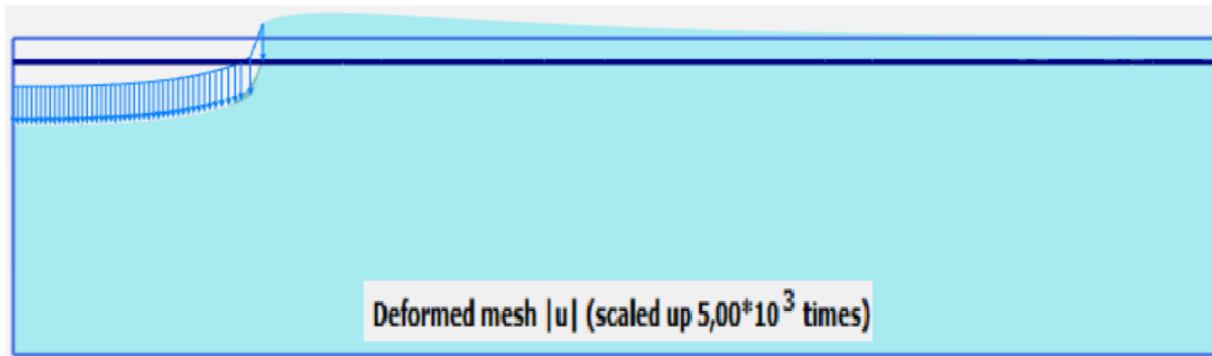


Figure 7.9 Example of a deformed mesh $|u|$ of an undrained analysis

| Soil Model | Maximum total deformation $ u $ | Percentage of $ u _{HS}$ |
|-------------------|---------------------------------|--------------------------|
| HS | 16,4 mm | 100,0 % |
| HSSmall – 100 m/s | 5,2 mm | 31,8 % |
| HSSmall – 150 m/s | 1,3 mm | 7,9 % |
| HSSmall – 200 m/s | 0,6 mm | 3,7 % |
| HSSmall – 250 m/s | 0,4 mm | 2,3 % |

Table 7.3 Maximum deformation using different V_s in a undrained analysis

Changing the V_s did not affect the development of excess pore pressure significantly (Figure 7.10). That implies that a change in V_s will not affect the stability. An undrained test was run to failure by applying $q=200$ kPa. All tests failed at about 54 kPa, supporting that different V_s do not affect the stability significantly.

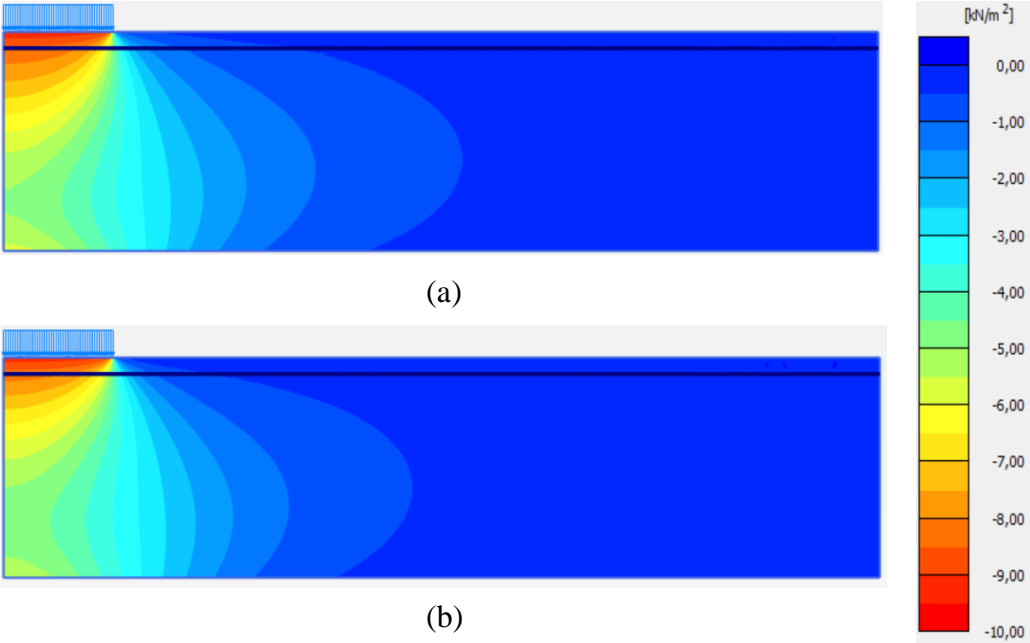


Figure 7.10 Excess pore pressure in undrained loading using $V_s=100$ m/s (a) and $V_s=250$ m/s (b)

Note: There seemed to be a numerical problem in the analysis regarding the stiffness when loading to failure. More about this test is found in Appendix F.

7.1.3 Discussion on Settlement Calculations

It is important to note that this analysis is very simple and is only supposed to roughly show the effect of using different V_s .

Calculating effects on nearby structures in densely urbanized areas is becoming more and more important. The small strain stiffness proves to be very important in calculating displacement some distance away from the loading.

This example was initially planned to focus on the consequences in the small strain area. However, varying V_s showed greater significance on the total settlement at large strains than expected. This is probably due to the support the loaded ground gets from the surrounding soil.

Results show that various V_s does not affect the undrained stability significantly. An important note is that only the G_{\max} is changed in this analysis. V_s is often correlated with other parameters influencing the stability, e.g. s_u and e_0 .

Note: The PLAXIS Material Manual the Hardening Soil with Small-Strain Stiffness states: “...the maximum ratio E_0/E_{ur} or G_0/G_{ur} permitted in the HSSmall soil model is limited to 10.” In these analyses G_0/G_{ur} varies between 7.5 and 47, but does not seem to be limited. If the model is not valid at such ratios it may explain the great influence of V_s in this example.

7.2 Earthquake Engineering

For the purpose of this work, a simple earthquake engineering example is made to show how the shear wave velocity could be used in earthquake engineering and the consequence of using different values for the shear wave velocity. The example is based on earthquake calculation on a building using an elastic analysis. For the sake of this study, the earthquake calculation will compare the effect of varying the average shear wave velocity from 100 - 200 m/s. The results from the tests carried out in this study are then characterized into to suitable ground types.

In Eurocode 8, the average shear wave velocity, $V_{s,30}$, is recommended as the best parameter to determine the ground type as in Table 7.4. The average shear wave velocity should be calculated using following equation:

$$V_{s,30} = \frac{30m}{\sum_{i=1,N} \frac{h_i}{v_i}} \quad (7.4)$$

where

h_i = Thickness of layers i in meter

v_i = Shear wave velocity of layers i

Table NA.3.1 – Ground types ¹⁾

| Ground type | Description of stratigraphic profile | Parameters ^{2), 3)} | | |
|-------------|--|------------------------------|------------------------|-------------|
| | | $V_{s,30}$ (m/s) | N_{SPT} (blows/30cm) | c_u (kPa) |
| A | Rock or other rock-like geological formation, including at most 5 m of weaker material at the surface. | > 800 | – | – |
| B | Deposits of very dense sand, gravel, or very stiff clay, at least several tens of metres in thickness, characterised by a gradual increase of mechanical properties with depth. | 360 – 800 | > 50 | > 250 |
| C | Deep deposits of dense or medium-dense sand, gravel or stiff clay with a thickness from several tens to many hundreds of metres. | 180 – 360 | 15 - 50 | 70 – 250 |
| D | Deposits of loose-to-medium cohesionless soil (with or without some soft cohesive layers), or of predominantly soft-to-firm cohesive soil. | 120 – 180 | 10 – 15 | 30 – 70 |
| E | A soil profile consisting of a surface alluvium layer with v_s values of type C or D and a thickness varying between about 5 m and 20 m, underlain by stiffer material with $v_s > 800$ m/s. | | | |
| S1 | Deposits consisting of or containing a layer at least 10 m thick of soft clays/silts with a high plasticity index ($PI > 40$) and high water content | < 100 (indicative) | – | 10 – 20 |
| S2 | Deposits of liquefiable soils, of sensitive clays, or any other soil profile not included in types A – E or S1 | | | |

¹⁾ If at least 75 % of the structure rests on rock and the rest on other soil conditions, and the structure has a continuous plate foundation, ground type A may be selected.

²⁾ The selection of ground type may be based either on $v_{s,30}$, N_{SPT} or c_u . $v_{s,30}$ is regarded as the most relevant parameter to be used.

³⁾ If there is doubt on which ground type to select, the most unfavourable ground type shall be selected.

Table 7.4 Ground types in Eurocode 8

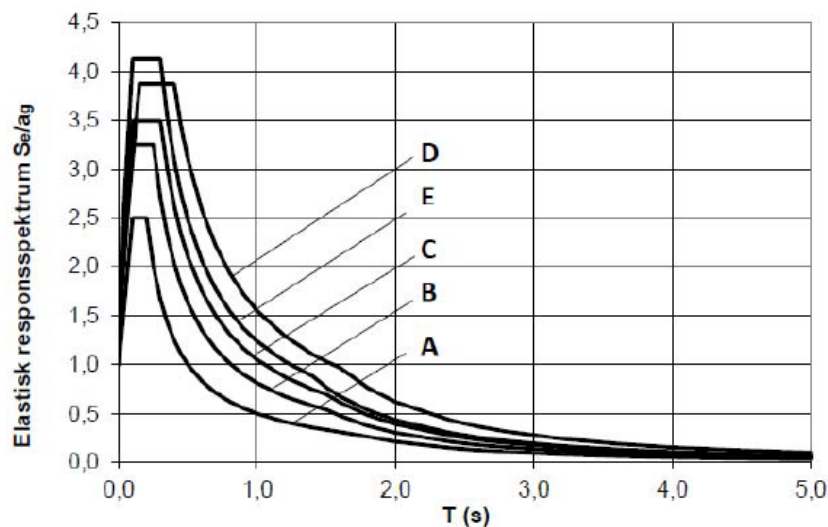


Figure 7.11 Elastic response spectrum for different ground types in Eurocode 8

The different ground types give values to parameters used to determine the design spectrum, $S_d(T)$ (Figure 7.11). The parameters and formulas for the design spectrum are given in Eurocode8 (Norge 2004). From the design spectrum, base shear force and displacement can be calculated.

$$d_g = 0.025 \cdot a_g \cdot S \cdot T_C \cdot T_D \quad (7.5)$$

where

d_g = Ground displacement

a_g = Ground acceleration

S = Soil factor

T_D = Value defining the beginning of the constant displacement response range of the spectrum

$$F_b = S_d(T_1) \cdot m \cdot \lambda \quad (7.6)$$

where

$S_d(T_1)$ = Ordinate of the design spectrum at period T_1

T_1 = Fundamental period of vibration of the building for lateral motion in the direction considered

m = Total mass of building, above the foundation or above the top rigid basement

λ = Correction factor, $\lambda = 0.85$ if $T_1 \leq 2T_C$ and the building has more than two stories, or $\lambda = 1.0$ otherwise

For buildings up to 40 m, T_1 may be approximated using following equation:

$$T_1 = C_t \cdot H^{3/4} \quad (7.7)$$

where

C_t = Moment bracing factor, C_t is 0.085 for moment resistant steel space frames, 0,075 for moment resistant space concrete frames and 0.050 for all other structures

H = Height of the building, in meters, from the foundation or from the top of a rigid basement

7.2.1 Earthquake Calculations

Calculations of ground displacement and base shear force, using the formulas given in chapter 7.2, are presented in this chapter. To demonstrate the effect of different $V_{s,30}$, values from 100-200 m/s is used in this analysis.

The clay in Tiller is sensitive. According to Table 7.4 the soil should than be described as Ground Type S2. This ground type requires special studies to provide definition of seismic action (values for S , T_B , T_C and T_D). In addition, the possibility of soil failure during seismic action shall be taken into account. However, the Association of Consulting Engineers, Norway (Løset et al. 2010) suggests an elastic response spectrums on soft and quick Norwegian clays based on depth to bedrock. For the purpose of this analysis it is assumed that the depth to bedrock is between 50 and 80 m. The resulting constants for design spectrum is given in Table 7.5.

For the purpose of this comparison, the clay is assumed not to be sensitive. The, varying the average shear wave velocity from 100 – 200 m/s means that the clay is categorized as either ground type S2, C or D (Table 7.4). The constants defining the design spectrum are given in Table 7.5. They are found in Eurocode 8 and Løset et al. (2010).

| $V_{s,30}$ | Ground Type | S | T_B | T_C | T_D |
|------------|-------------|------|-------|-------|-------|
| [m/s] | [-] | [-] | [s] | [s] | [s] |
| 100 | S2 | 1.7 | 0.2 | 0.67 | 1.5 |
| 150 | D | 1.55 | 0.15 | 0.4 | 1.6 |
| 200 | C | 1.4 | 0.1 | 0.3 | 1.5 |

Table 7.5 Ground types and corresponding properties for the design spectrum

Several parameters regarding the design building and earthquake in the analysis are selected in order to get quantifiable results. The parameters are selected on the basis of recommended values in the Eurocode 8 or by reasonable assumptions. The selected input parameters used in this analysis are presented in Table 7.6.

| | | | |
|-------------------------|-----------|----------------------|-------|
| Ground acceleration | a_g | [m/s ²] | 0.24 |
| Correction factor | λ | [-] | 1.0 |
| Building mass | m | [kg] | 16000 |
| Building height | H | [m] | 10 |
| Moment bracing constant | C_t | [sm ^{3/4}] | 0.075 |
| Behaviour factor | q | [-] | 1.0 |
| Lower bound factor | β | [-] | 0.2 |

Table 7.6 Selected input parameters

The design spectrums for elastic analysis are presented in Figure 7.12. A greater response is found at lower $V_{s,30}$.

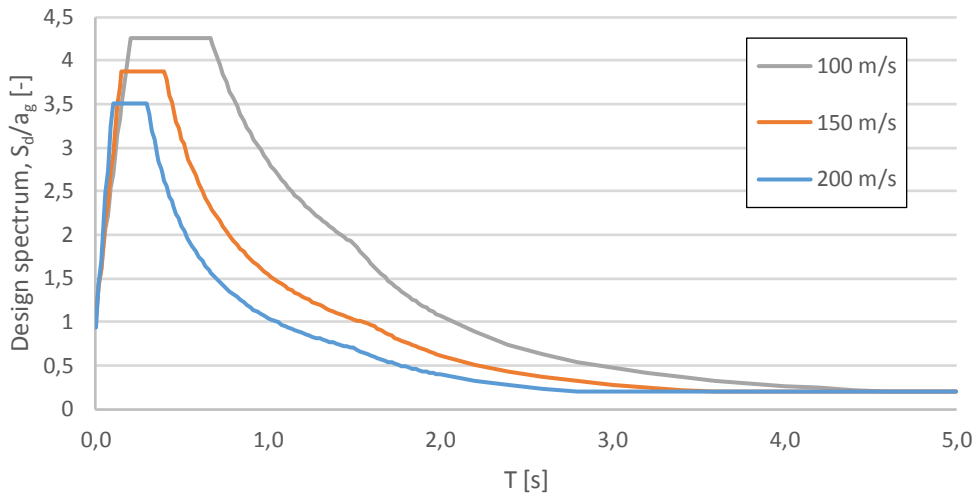


Figure 7.12 Design spectrum for elastic analysis

Based on the design spectrum, ground displacement and base shear force are calculated using the equations (7.5) and (7.6). The results are presented in Table 7.7.

| | | 100 m/s | 150 m/s | 200 m/s |
|---------------------|------|---------|---------|---------|
| Ground displacement | [mm] | 10.3 | 6.0 | 3.8 |
| Base shear force | [kN] | 220 | 120 | 81 |

Table 7.7 Results from the elastic analysis using Eurocode 8

Determining the correct ground type is vital for determining the correct earthquake design criteria according to Eurocode 8. Although this is a rough and simplified method, the results are evident. The results show higher base shear force and ground displacement at lower $V_{s,30}$. The differences in base shear force in this analysis differs by a factor of almost 3.0 for a $V_{s,30}$ ranging from 100 to 200 m/s. Base shear force using a $V_{s,30}$ of 150 and 200 m/s gave a factor around 1.5. The ground displacement decreases with around 70 and 60 % when increasing $V_{s,30}$ to 150 and 200 m/s, respectively.

7.2.2 Results from Tiller

Based on the results from Tiller, linear shear wave velocity profiles are made (Figure 7.13). Only one point is found using the crosshole test. Hence, there is not enough information to make a profile based on the crosshole test.

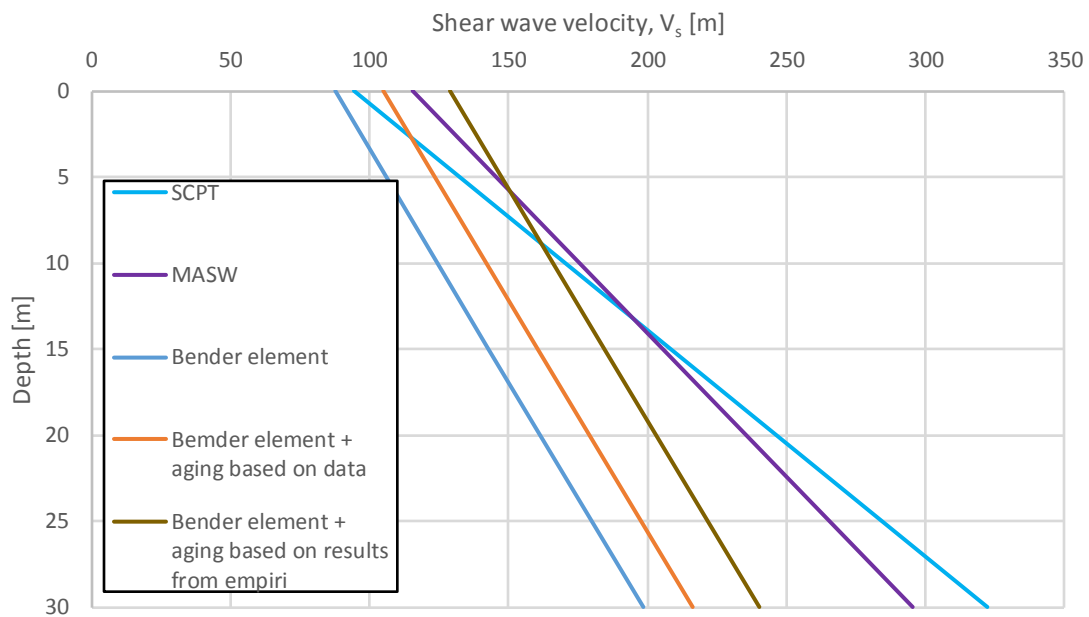


Figure 7.13 Shear wave velocity profiles based on data from Tiller investigations

The clay on Tiller is sensitive, and belong to the ground type S2. However, for the purpose of showing the consequences of the different tests, the clay is assumed to be non-sensitive. Then, the V_s profiles presented in Figure 7.13 can be used to determine the Ground types (according to Table 7.4). The results are presented in Table 7.8. The result from the original MASW results is also given.

| Method | $V_{s,30}$ | Ground type |
|---|------------|-------------|
| SCPT | 208 m/s | C |
| New MASW | 206 m/s | C |
| Original MASW | 401 m/s | B |
| Bender element | 143 m/s | D |
| Bender element + aging based on data | 161 m/s | D |
| Bender element + aging based on empiri | 185 m/s | C |

Table 7.8 Ground types at Tiller based on the different test results

In addition, by using $s_u = 0.25\sigma_{v0}'$, the average s_u is about 35 kPa. According to Table 7.4 the soil should than be a ground type D.

7.2.3 Discussion on Earthquake Calculations

It is important to note that this analysis is very simple and is only supposed to roughly show the effect of using different V_s .

The earthquake calculations show great importance of accurate measurements. The different V_s corresponds to different ground types, and the ground types are decisive when calculating loads and displacements in earthquake engineering. The effect of these differences in terms of economy in an engineering project may be major.

Based on the results from Tiller, the different tests result in ground types varying from B to D. That underlines the importance of accurate testing.

Note: The difference in results from this study are expected to be mainly due to the variation in V_s , not the other assumed parameters. In fact, an assumption of shallower depth to rock, for example, would lead to a greater response in ground type S2.

Chapter 8 Conclusions

The shear wave velocity profile at Tiller may be assumed to be linearly increasing with depth, from 125 to 230 m/s at 4 and 18 m depth, respectively. Then, $V_{s,30}$ is about 205 m/s. The final accuracy is assumed to be about 10 %.

From the test results are the invasive in situ tests considered to produce the best accuracy. However, the non-invasive MASW test produce similar results in the repeated survey, but there is uncertainty related to obtaining and interpreting its dispersion curves.

SCPT is considered to be the most reliable test conducted. The crossover method with a pseudo-interval spacing of 3 m and more produce the best results. Some variation are however seen between the two profiles. That is considered to be due to differences in the soil.

CHT at Tiller provided unclear signals for unknown reasons. The obtained results did however correspond well to the results from SCPT. Not enough results are gathered to make a profile. It is however considered to be an accurate test in general.

Bender element testing in the laboratory is giving significantly lower V_s -values compared to in situ measurements. Various sample height did not show a significant effect. Aging effect in the soil is suspected to be the most significant source of error. From the tests carried out, the aging effect is suggested differ in sensitive and non-sensitive clay. However, more investigations are needed to understand the aging effect in this soil.

Wrong value of V_s , and thus G_{max} , could have significant engineering consequences, both in settlement and earthquake calculations. In this study, the final accuracy of the V_s -profiles obtained at Tiller from SCPT and the repeated MASW survey are adequate in most cases. However, bender element testing without adjustments for aging effect and the original MASW survey under- and overestimates V_s , respectively. The consequences of using these results in geotechnical engineering may be vital.

Chapter 9

Further Work and Recommendations

Results that could be used for further comparison are obtained at Tiller. Further work on this subject could focus on evaluating and improving the tests further. In addition, the results could be compared with empirical correlations. The soil parameters at the two profiles, S5 and S6, could be more closely determined and tests at other similar sites could be conducted to see if similar results are obtained.

The consequences of variation in shear wave velocity in geotechnical engineering is an interesting subject that require a more comprehensive study.

In order to get more reliable results and simplify field work some adjustments to the equipment are suggested.

SCPT

- Accelerometers in two depths inside probe to measure the true velocity from one wave
- Wireless system to simplify the field work
- Measurements from CPT(U) to use as comparison

MASW

- Investigate if the dispersion curve in clays improves with even stronger signal (heavier sledgehammer or mechanical sources)
- Use geophones with lower frequency for acquisition to get more reliable readings at deeper depths

CHT

- To be able to use the crosshole test to make a full shear wave profile, the depth of the receivers should be adjustable

- A trigger-device would be useful to determine the first arrival of the shear wave when the signal is poor. It would also make it possible to estimate V_s with only one receiver

Bender element

- Investigate the aging effect on Tiller clay by consolidating samples in the triaxial cell for a sufficient time. Samples from both the sensitive and non-sensitive layer should be tested
- Load a sample stepwise to see if a full a shear wave profile could be obtained from one sample
- Include frequency and amplitude on the output file and enable the possibility to retrieve individual signals

Bibliography

- Anderson, D. and K. Stokoe (1978). "Shear modulus: A time-dependent soil property." Dynamic geotechnical testing, ASTM STP **654**: 66-90.
- Anderson, D. G. (1974). "Dynamic modulus of cohesive soil."
- Anderson, D. G. and R. D. Woods (1976). "Time-dependent increase in shear modulus of clay." Journal of the Geotechnical Engineering Division **102**(5): 525-537.
- Atkinson, J. (2000). "Non-linear soil stiffness in routine design." Géotechnique **50**(5): 487-508.
- Atkinson, J. and G. Salfors (1991). Experimental determination of soil properties, in Proceedings of the 10th European Conference on Soil Mechanics and Foundation Engineering, AA Balkema, Rotterdam.
- Benz, T. (2007). Small-strain stiffness of soils and its numerical consequences, Univ. Stuttgart, Inst. f. Geotechnik.
- Brinkgreve, R. and W. BROERE (2006). Plaxis material models manual, Delft:[sn].
- Burland, J. (1989). "Ninth Laurits Bjerrum Memorial Lecture:" Small is beautiful"-the stiffness of soils at small strains." Canadian Geotechnical Journal **26**(4): 499-516.
- Butler, D. K. and J. R. Curro Jr (1981). "Crosshole seismic testing-Procedures and pitfalls." Geophysics **46**(1): 23-29.
- Chan, K., et al. (2010). "Effect of bender element installation in clay samples." Géotechnique **60**(4): 287-291.

- Comina, C., et al. (2010). "Reliability of VS, 30 evaluation from surface-wave tests." Journal of Geotechnical and Geoenvironmental Engineering **137**(6): 579-586.
- Dyvik, R. and C. Madshus (1985). Laboratory Measurement of G_{max} Using Bender Elements. Proceedings of ASCE Annual Convention: Advances in the Art of Testing Soils under Cyclic Conditions, Detroit.
- Eiksund, G. (2013). Dynamic Soil Properties. Lecture in PHD course BA8305 Geodynamics, NTNU.
- Gylland, A., et al. (2013). "Characterisation and engineering properties of Tiller clay." Engineering Geology **164**: 86-100.
- Hardin, B. and F. Richart Jr (1963). "Elastic wave velocities in granular soils." Journal of Soil Mechanics & Foundations Div **89**(Proc. Paper 3407).
- Hardin, B. O. and W. Black (1969). "Closure on vibration modulus of normally consolidated clay." Journal of Soil Mechanics & Foundations Div.
- Hardin, B. O. and V. P. Drnevich (1972). "Shear modulus and damping in soils." Journal of the Soil Mechanics and Foundations Division **98**(7): 667-692.
- Ibrahim, A., et al. (2011). Determination of very small strain shear modulus of Auckland residual soils using bender elements. W: Proceedings of the 9th Pacific Conference on Earthquake Engineering. Building an Earthquake-Resilient Society, Auckland.
- Janbu, N. (1963). "Soil compressibility as determined by oedometer and triaxial tests." Proc. ECSMFE Wiesbaden **1**: 19-25.
- Knutsen, M. (2014). On Determination on G_{max} by Bender Element and Cross-Hole Testing. Civil and Transport Engineering. Trondheim, NTNU: 243.
- Kramer, S. (1996). "Geotechnical earthquake engineering. ." New Jersey.

- Lai, C. G., et al. (2005). "Propagation of data uncertainty in surface wave inversion." Journal of Environmental & Engineering Geophysics **10**(2): 219-228.
- Lee, J.-S. and J. C. Santamarina (2005). "Bender elements: performance and signal interpretation." Journal of Geotechnical and Geoenvironmental Engineering **131**(9): 1063-1070.
- Long, M. and S. Donohue (2007). "In situ shear wave velocity from multichannel analysis of surface waves (MASW) tests at eight Norwegian research sites." Canadian Geotechnical Journal **44**(5): 533-544.
- Long, M. and S. Donohue (2010). "Characterization of Norwegian marine clays with combined shear wave velocity and piezocone cone penetration test (CPTU) data." Canadian Geotechnical Journal **47**(7): 709-718.
- Lunne, T., et al. (2006). "Effects of sample disturbance and consolidation procedures on measured shear strength of soft marine Norwegian clays." Canadian Geotechnical Journal **43**(7): 726-750.
- Løset, Ø., et al. (2010). Dimensjonering for Jordskjelv, RIF Rådgivende Ingeniørers Forening.
- Moss, R. E. S. (2008). "Quantifying measurement uncertainty of thirty-meter shear-wave velocity." Bulletin of the Seismological Society of America **98**(3): 1399-1411.
- Norge, S. (2004). "NS-EN 1998-1: 2004+ NA: 2008 Eurokode 8: Prosjektering av konstruksjoner for seismisk påvirkning Del 1: Allmenne regler, seismiske laster og regler for bygninger." Standard Norge.
- Norges Geoteknisk Forening, N. (1982). Veiledning for symboler og definisjoner I geoteknikk, presentasjon av geotekniske undersøkelser, Melding.
- O'Rourke (2015). Report on the MASW surveys at Klett, Byneset, Tiller, Dragvoll & Rosten-Saupstad for the Norwegian Geotechnical Institute.

Park, C. B., et al. (1999). "Multichannel analysis of surface waves." Geophysics **64**(3): 800-808.

Robertson, P. K., et al. (1986). "Seismic CPT to measure in situ shear wave velocity." Journal of Geotechnical Engineering **112**(8): 791-803.

Sanchez-Salinerio, I., et al. (1986). Analytical studies of body wave propagation and attenuation, DTIC Document.

Schmertmann, J. H. (1991). "The mechanical aging of soils." Journal of Geotechnical Engineering **117**(9): 1288-1330.

Simpson, B. (1992). "Thirty-second Rankine Lecture: Retaining structures: displacement and design." Géotechnique **42**: 539-539.

Stokoe, K. H. and F. Richart (1974). "Dynamic response of embedded machine foundations." Journal of Geotechnical and Geoenvironmental Engineering **100**(Proc Paper 10499).

Stokoe, K. H. and R. D. Woods (1972). "In situ shear wave velocity by cross-hole method." Journal of the Soil Mechanics and Foundations Division **98**(5): 443-460.

Sully, J. and R. Campanella (1995). "Evaluation of in situ anisotropy from crosshole and downhole shear wave velocity measurements." Géotechnique **45**(2): 267-238.

Tanimoto, K. and M. Kurzeme (1973). "IN SITU SHEAR WAVE VELOCITY BY CROSS-HOLE METHOD." Journal of Soil Mechanics & Foundations Div **99**(sm 4).

Tovslid, H. (2015). Lagringseffekt for 54mm fra Tiller, NTNU. **Master**.

Vucetic, M. and R. Dobry (1991). "Effect of soil plasticity on cyclic response." Journal of Geotechnical Engineering **117**(1): 89-107.

Wang, Y., et al. (2007). "Measurement biases in the bender element test." Journal of Geotechnical and Geoenvironmental Engineering **133**(5): 564-574.

List of Figures

| | |
|--|----|
| Figure 2.1 Particle movement of body waves Benz (2007) | 5 |
| Figure 2.2 Torque and rotation of a one dimensional rod (Kramer 1996) | 6 |
| Figure 2.3 Particle movement in a Rayleigh wave (Eiksund 2013) | 8 |
| Figure 2.4 Schematic figure of a thin element in a Kelvin-Voigt solid (Kramer 1996) | 9 |
| Figure 2.5 Characteristic stiffness-strain behaviour and definition of strain ranges (Atkinson and Sallfors 1991) | 11 |
| Figure 2.6 PI-chart of the stiffness reduction curve (Vucetic and Dobry 1991) | 15 |
| Figure 2.7 Phases and modulus-time response (Anderson and Stokoe, 1978) | 17 |
| Figure 3.1 Location of the Tiller site..... | 19 |
| Figure 3.2 Suggested layering at the Tiller site (Gylland et al. 2013) | 20 |
| Figure 3.3 Overview of Tiller and approximate locations of performed site investigations.... | 21 |
| Figure 4.1 Signal output from one hit using SCPT | 25 |
| Figure 4.2 Setup of the SCPT (Photo: Eide, H) | 25 |
| Figure 4.3 Illustration of polarized waves and usage of crossover method (Sully and Campanella 1995)..... | 26 |
| Figure 4.4 Schematic figure of the crosshole method using two receivers (Sully and Campanella 1995)..... | 27 |
| Figure 4.5 Schematic figure of the crosshole test (Knutsen, 2014) | 28 |
| Figure 4.6 Clear signals from the crosshole test | 29 |
| Figure 4.7 Setup of the crosshole test at Tiller (Photo: Eide, H) | 30 |
| Figure 4.8 The accelerometer used in the crosshole test (Photo: Eide, H)..... | 30 |
| Figure 4.9 Schematic figure of the MASW setup | 31 |
| Figure 4.10 Example of shot gather (a), dispersion image (b) and dispersion curves with associated root mean square error (c) from a MASW (Donohue et al. 2012)..... | 32 |
| Figure 4.11 MASW setup at Klerr (Photo: Eide, H) | 33 |
| Figure 4.12 Movement of a piezoelectric bender element (Kramer 1996) | 34 |
| Figure 4.13 Schematic figure of a bender element setup in a triaxial-cell (Ibrahim et al. 2011) | 35 |
| Figure 4.14 Piezoelectric bender element fitted into modified pedestal (Photo: Eide, H)..... | 36 |
| Figure 4.15 Screenshot during bender element testing | 37 |

| | |
|--|----|
| Figure 4.16 Example of sample after testing (Photo: Eide, H) | 37 |
| Figure 5.1 SCPT-results using cross-correlation method in processing | 41 |
| Figure 5.2 SCPT-results using crossover method and 0.5m (a) and 5m (b) pseudo-interval spacing..... | 42 |
| Figure 5.3 Average values from SCPT investigations from crossover method with 3.0 m pseudo-interval spacing..... | 43 |
| Figure 5.4 Signals from the first vertical hit in x- (a) and y-direction (b)..... | 44 |
| Figure 5.5 Dispersion curve from best shot at profile S5A (a), S6A (b), S5 (c) and S6 (d) at Tiller (O'Rourke 2015)..... | 47 |
| Figure 5.6 Comparison between original (with several methods of processing) and repeated MASW results at profile S5 (a) and S6 (b) | 48 |
| Figure 5.7 Result from the repeated MASW survey | 49 |
| Figure 5.8 Development of V_s during consolidation for sample #1-5 | 51 |
| Figure 5.9 Development of V_s during consolidation for sample #6-8 | 52 |
| Figure 5.10 Development of V_s for sample#8 during consolidation..... | 52 |
| Figure 5.11 Shear wave velocity development vs. log time..... | 53 |
| Figure 5.12 Shear wave velocity development of sample #8 after the end of primary consolidation | 53 |
| Figure 5.13 Normalized development of the shear wave velocity after end of primary consolidation of sample #8..... | 54 |
| Figure 5.14 Development of the shear wave velocity in sample #7 against log time | 56 |
| Figure 6.1 Summary of all obtained data from Tiller | 57 |
| Figure 6.2 Comparison of results from profile S5 (a) and S6 (b) | 59 |
| Figure 6.3 Average shear wave velocity results from Tiller | 60 |
| Figure 6.4 Crosshole signal in z-direction from Esp (a) and Tiller (b)..... | 64 |
| Figure 6.5 Illustration of different signal paths (Knutson 2014)..... | 65 |
| Figure 6.6 MASW-data from Tiller S6 with different processing | 67 |
| Figure 6.7 Received signals from sample #5 at frequencies 1.4 kHz (a), 1.6kHz (b), 1.8 kHz (c), 2.8kHz (d) and 3.6 kHz (e)..... | 69 |
| Figure 6.8 Measure of sample quality based on relative dissipation of pore waver | 72 |
| Figure 7.1 Tangent and secant reduction curves used in PLAXIS material model Hardening Soil with Small-Strain Stiffness (Brinkgreve and BROERE 2006) | 74 |
| Figure 7.2 Normalized tangent shear modulus reduction curve for different shear wave velocities..... | 75 |

| | |
|---|-------|
| Figure 7.3 PLAXIS model setup and soil parameters..... | 76 |
| Figure 7.4 Example of deformed mesh of the drained analysis | 76 |
| Figure 7.5 Development of total displacement $ u $ in point (0,0) during loading | 77 |
| Figure 7.6 Development of horizontal displacement in point C (20m, 0m) | 78 |
| Figure 7.7 Horizontal displacement in the drained analysis | 79 |
| Figure 7.8 G/G_{ur} after consolidation with $V_s=150$ m/s (a) and $V_s=200$ m/s (b)..... | 79 |
| Figure 7.9 Example of a deformed mesh $ u $ of an undrained analysis..... | 80 |
| Figure 7.10 Excess pore pressure in undrained loading using $V_s=100$ m/s (a) and $V_s=250$ m/s (b) | 81 |
| Figure 7.11 Elastic response spectrum for different ground types in Eurocode 8 | 83 |
| Figure 7.12 Design spectrum for elastic analysis | 87 |
| Figure 7.13 Shear wave velocity profiles based on data from Tiller investigations | 88 |
| Figure 0.1 Example of ERT-profile with interpreted V_p (Donohue et al. 2012)..... | XI |
| Figure 0.2 Development of small-strain stiffness with time after primary consolidation (Seng and Tanaka, 2012)..... | XIX |
| Figure 0.3 Special bender element setup to investigate V_s anisotropy (Pennington et al. 1997) | XX |
| Figure 0.4 Visualisation of measurements vs. correlation function (Mayne 2007b) | XXIII |
| Figure 0.5 G_{max} to RD for ten different sands (Brinkgreve 2010) | XXIV |

List of Tables

| | |
|--|----|
| Table 2.1 Parameters affecting G_{\max} (Benz, 2007) | 13 |
| Table 3.1 Tiller soil parameters used in this work (Gylland et al. 2013) and (Tovslid 2015) | 21 |
| Table 4.1 Stages of consolidation for sample #1-5 | 38 |
| Table 4.2 Stages of consolidation for sample #7 | 38 |
| Table 4.3 Stages of consolidation for sample #8 | 39 |
| Table 5.1 Result from bender element test on samples from same depth with various height | 50 |
| Table 5.2 Predicted aging effect using values from both laboratory data and an empirical equation..... | 55 |
| Table 5.3 Shear wave velocity from bender element and its predicted development based on laboratory data and empirical formulas..... | 56 |
| Table 6.1 Suggested minimum frequency to avoid near-field effect with $V_s=100$ m/s | 68 |
| Table 6.2 Suggested minimum frequency to avoid near-field effect with $V_s=150$ m/s | 68 |
| Table 6.3 Results from Knutsen (2014) and corrected V_s -value assuming system delay | 70 |
| Table 6.4 Sample quality based on $\Delta e/e_0$ (Lunne et al. 2006) | 71 |
| Table 7.1 Maximum deformation using different V_s in a drained analysis..... | 77 |
| Table 7.2 Horizontal displacement in point (20m, 0m) | 78 |
| Table 7.3 Maximum deformation using different V_s in a undrained analysis..... | 80 |
| Table 7.4 Ground types in Eurocode 8..... | 83 |
| Table 7.5 Ground types and corresponding properties for the design spectrum..... | 86 |
| Table 7.6 Selected input parameters | 86 |
| Table 7.7 Results from the elastic analysis using Eurocode 8 | 87 |
| Table 7.8 Ground types at Tiller based on the different test results..... | 89 |

Appendix

Appendix A

A.1 Conducted Field and Laboratory work

A summary of the tests conducted (or assisted) by the author during the spring of 2015:

| Site | Conducted tests |
|------------|---|
| Tiller | 2 SCPT, 1 CHT |
| Esp | 1 SCPT, 1 CHT |
| Klett | 1 SCPT, 3 MASW |
| Klett2 | 2 ERT |
| Nidarvoll | 2 ERT |
| Laboratory | 10 Bender element tests (2 practice samples) |

Appendix B

B.1 P-wave

Assuming a constrained infinite rod, with only axial deformation the equilibrium equation is given as:

$$(\sigma_{x_0} + \frac{\delta\sigma_x}{\delta x} dx)A - \sigma_{x_0}A = \rho A \frac{\delta^2 u}{\delta t^2} dx$$

which may be simplified into the one-dimensional equation of motion:

$$\frac{\delta\sigma_x}{\delta x} = \rho \frac{\delta^2 u}{\delta t^2}$$

by using the relations $\sigma_x = M\varepsilon_x$ and $\varepsilon_x = \frac{\delta u}{\delta x}$, it may be written as:

$$\frac{\delta^2 u}{\delta t^2} = \frac{M}{\rho} \frac{\delta^2 u}{\delta x^2}$$

An alternative way of writing the one-dimensional equation of motion is:

$$\frac{\delta^2 u}{\delta t^2} = V_p^2 \frac{\delta^2 u}{\delta x^2}$$

Hence, following relation may be made between the rod stiffness, density and wave propagation:

$$V_p = \sqrt{M\rho}$$

Appendix C

C.1 Bender Element Results

Sample #1

| <i>Time</i> | σ'_1 | σ'_3 | V | d | t_s | V_s | G_{max} |
|-------------|-------------|-------------|--------------------|------|-------|-------|-----------|
| [hr] | [kPa] | [kPa] | [cm ³] | [mm] | [ms] | [m/s] | [MPa] |
| 0 | 0 | 0 | 0 | 0 | – | – | – |
| 3 | 41,1 | 28,1 | 5,0 | 1,6 | 1 | 93,4 | 16,6 |
| 18,6 | 147,3 | 102,3 | 14,6 | 3,7 | 0,66 | 138,3 | 36,4 |
| 22,2 | 41,4 | 28,4 | 14,6 | 3,65 | 0,75 | 121,8 | 28,2 |

Sample #2

| <i>Time</i> | σ'_1 | σ'_3 | V | d | t_s | V_s | G_{max} |
|-------------|-------------|-------------|--------------------|------|-------|-------|-----------|
| [hr] | [kPa] | [kPa] | [cm ³] | [mm] | [ms] | [m/s] | [MPa] |
| 0 | 0 | 0 | 0 | 0 | – | – | – |
| 2,7 | 41,2 | 28,2 | 6 | 1,4 | 0,955 | 98,0 | 18,3 |
| 17,5 | 149,2 | 104,2 | 14,4 | 3,2 | 0,65 | 141,2 | 37,9 |
| 21,4 | 42,8 | 29,8 | 13,8 | 3,2 | 0,82 | 112,0 | 23,8 |

Sample #3

| <i>Time</i> | σ'_1 | σ'_3 | V | d | t_s | V_s | G_{max} |
|-------------|-------------|-------------|--------------------|------|-------|-------|-----------|
| [hr] | [kPa] | [kPa] | [cm ³] | [mm] | [ms] | [m/s] | [MPa] |
| 0 | 0 | 0 | 0 | 0 | – | – | – |
| 3,5 | 42,7 | 29,7 | 5 | 1,3 | 0,4 | 109,3 | 22,7 |
| 14,4 | 150 | 105 | 10,5 | 2,5 | 0,305 | 139,3 | 36,9 |
| 16,7 | 42,2 | 29,2 | – | 2,6 | 0,375 | 113,1 | 24,3 |

Sample #4

| <i>Time</i> | σ'_1 | σ'_3 | V | d | t_s | V_s | G_{max} |
|-------------|-------------|-------------|--------------------|------|-------|-------|-----------|
| [hr] | [kPa] | [kPa] | [cm ³] | [mm] | [ms] | [m/s] | [MPa] |
| 0 | 0 | 0 | 0 | 0 | – | – | – |
| 2,6 | 44 | 31 | 3,8 | 1,9 | 1,17 | 96,6 | 17,7 |
| 17,2 | 149,3 | 104,3 | 12,5 | 3,3 | 0,825 | 139,3 | 36,9 |
| 20,8 | 43,2 | 30,2 | 11,1 | 3,3 | 1,01 | 113,8 | 24,6 |

Sample #5

| <i>Time</i> | σ'_1 | σ'_3 | V | d | t_s | V_s | G_{max} |
|-------------|-------------|-------------|--------------------|------|-------|-------|-----------|
| [hr] | [kPa] | [kPa] | [cm ³] | [mm] | [ms] | [m/s] | [MPa] |
| 0 | 0 | 0 | 0 | 0 | – | – | – |
| 2,7 | 42 | 29 | 4 | 0,8 | 0,41 | 110,2 | 23,1 |
| 17,6 | 149,8 | 104,8 | 8,9 | 1,7 | 0,32 | 138,4 | 36,4 |
| 20,7 | 42,3 | 29,3 | 8,3 | 1,7 | 0,395 | 112,2 | 23,9 |

Sample #6

| <i>Time</i> | σ'_1 | σ'_3 | V | d | t_s | V_s | G_{max} |
|-------------|-------------|-------------|--------------------|------|-------|-------|-----------|
| [hr] | [kPa] | [kPa] | [cm ³] | [mm] | [ms] | [m/s] | [MPa] |

| | | | | | | | |
|-----|-----|------|------|---|-------|------|------|
| 0 | 0 | 0 | 0 | 0 | – | – | – |
| 5,7 | 100 | 70,1 | 10,1 | 9 | 0,915 | 94,0 | 16,8 |

Sample #7

| <i>Time</i> | σ'_1 | σ'_3 | V | d | t_s | V_s | G_{max} |
|-------------|-------------|-------------|--------------------|------|-------|-------|-----------|
| [hr] | [kPa] | [kPa] | [cm ³] | [mm] | [ms] | [m/s] | [MPa] |
| 0 | 0 | 0 | 0 | 0 | – | – | – |
| 21,6 | 116,5 | 81,5 | 15 | 6,22 | 0,745 | 119,2 | 27,0 |
| 25,7 | 149,7 | 104,7 | 16 | 6,45 | 0,715 | 123,8 | 29,1 |
| 28,1 | 117,7 | 82,7 | 16,2 | 6,45 | 0,745 | 118,9 | 26,8 |

Sample #8

| <i>Time</i> | σ'_1 | σ'_3 | V | d | t_s | V_s | G_{max} |
|-------------|-------------|-------------|--------------------|------|-------|-------|-----------|
| [hr] | [kPa] | [kPa] | [cm ³] | [mm] | [ms] | [m/s] | [MPa] |
| 0 | 0 | 0 | 0 | 0 | – | – | – |
| 21,6 | 73,8 | 51,8 | 7,5 | 1,2 | 0,78 | 120,3 | 27,5 |
| 25,1 | 149,9 | 104,9 | 10,3 | 1,8 | 0,675 | 138,1 | 36,2 |
| 46,3 | 151,3 | 129,3 | 29,5 | 2,9 | 0,625 | 147,4 | 41,3 |

C.2 Noticeable Incidents during Testing

The standard sample to be tested in the triaxial apparatus has diameter of 54mm and height of a 100mm. Bedding samples with different heights proved challenging, due to various equipment like bedding-mould and rubber skin not fitting. Below are any incidents that may be of significance in the individual tests presented.

Sample #1

Unaware of the frequency dependency.

Sample #2

No significant incidents occurred.

Sample #3

A custom made bedding-mould was used. Some more disturbance is expected. The software had problems identifying the first arrival of the shear wave during consolidation stage (1). Software/computer froze after 14.4 hr. No data was collected, but the cell pressure in the cell remained the same. This was discovered some four hours later. When the software was restarted, the test continued at in situ stress level. The total deformation was however lost, and assumed to not change.

Sample #4

At first a sample with a height of 150 mm was supposed to be tested, but it did not fit in the apparatus. After trimming the sample to 120 mm, it was still too high to fit in the load cell, but another load cell in steel fitted.

Sample #5

A custom made bedding-mould was used. Some more disturbance is expected. The software had problems identifying the first arrival of the shear wave during consolidation stage (1).

Sample 6

During consolidation it was noticed that an O-ring was not strapped around the pedestal but rather around the sample. This disturbance led to the sample failing during consolidation.

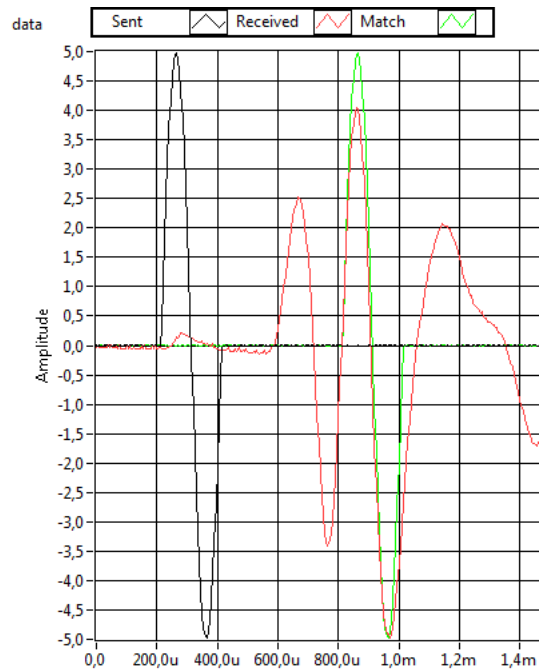
Sample 7

After bedding the sample and the consolidation had started running, it was discovered that a paper filter was missing. During the consolidation the clay started entering and clogging some tubes. This led to problem with drainage as well as the sample got a big cavity.

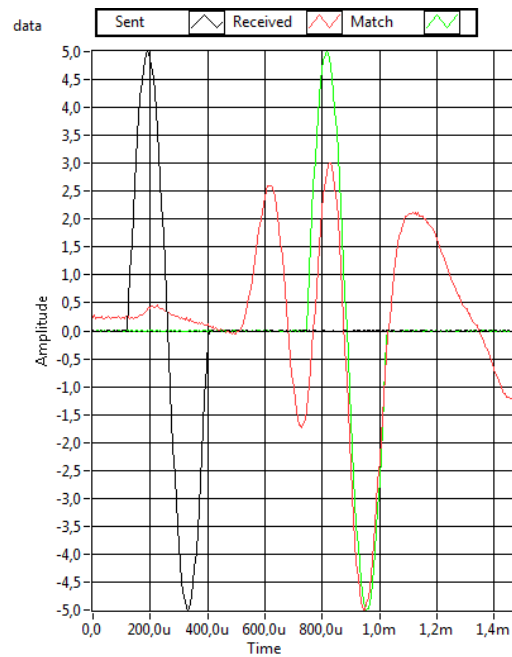
Sample #8

Software/computer froze after 46 hr. No more data was collected after this point.

C.3 Signal Interpretation



Signal from sample #3 after primary consolidation



Signal from sample#5 after primary consolidation

Appendix D

D.1 Other Tests

Down Hole Seismic

For the down hole seismic method only one borehole is needed. The shear wave source is placed at the surface while a string of receivers are in the borehole.

This method requires only one borehole per reading, but it measures the vertical wave propagation. The soil is usually layered more or less horizontally, and thus back calculation has to be done to find the shear wave velocity in the different layers.

Suspension Logging

In suspension logging both the shear wave source and the receiver are placed in the same borehole. This method focuses on the propagation velocities of waves that travel along the borehole, not the propagation velocities of direct waves. It may be used to significant depths and have a resolution of

Retardation of Drop-Weight

A heavy pounder is used for dynamic deep compaction (DDC) in non-cohesive material. An accelerometer is connected to the heavy pounder, and measure the retardation during penetration of the heavy tamper into the soil surface. From the force-penetration curves, G_{max} may be estimated.

Local Measurements

This method does not measure the shear wave velocity but rather the deformation in a triaxial test. Small-strain stiffness is a challenge to measure using traditional triaxial testing, where the deformation is measured by the relative distance between the top cap and base. Using local strain transducers however, very-small stain can be measured accurately, not depending on the sample bedding imperfections.

However, local measurements are rather expensive to use on a regular basis.

Resonant Column and Torsional Shear

A sample is placed in a device that is able to also load the sample torsionally in addition to load it triaxially,. A non-destructive cyclic test, where the sample is subjected to vibrations, makes it possible to find the G_{\max} .

The difference between the resonant column and the torsional shear test is mainly the frequency and amplitude of loading.

Accelerometer

The same principal as the in situ crosshole method may be used in the laboratory. Two accelerometers with a known fixed distance are placed in a bin filled with soil. The accelerometers measure acceleration in the soil. The soil bin is exposed to a force creating shear waves and the accelerators measure the arrival time of the shear waves. From these measurements the shear wave velocity may be calculated.

D.2 Electrical Resistivity Tomography (ERT)

General

Electrical resistance tomography is a technique for imaging the subsurface electrical structure using conduction currents. From a series of electrodes, low-frequency electrical current is injected into the subsurface, and the resulting potential distribution is measured. A large variety of different source and receiver orientations are used to sample the target volume from many different views. From that data, a computer model of the electrical resistivity distribution is found that produces, to within some predetermined tolerance, the measured potential field. (Ramirez et al. 2000)

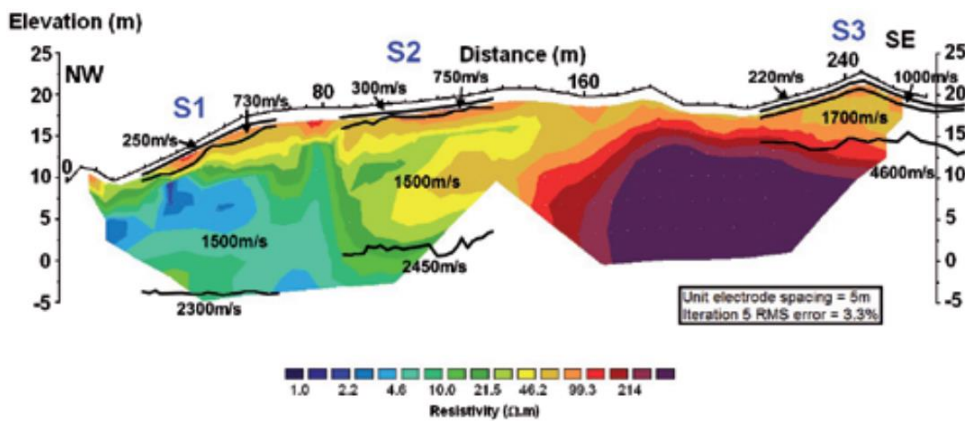


Figure 0.1 Example of ERT-profile with interpreted V_p (Donohue et al. 2012)

Due to the effectiveness and low cost of using ERT to map large areas, it may be used in combination with other in situ test to determine the V_s of a large site. If combined with e.g. SCPT, the number of boreholes needed may be significantly reduced.

Testing procedure

During the MASW testing, Apex was also conducting ERT at different sites in Trondheim. The author assisted Apex on making two ERT-profiles at both Klett and Nidarvoll sites.

Appendix E

E.1 Multifunction DAX Specifications


(from National Instruments web page on USB-6210)

| General | |
|----------------------------------|----------------------------|
| Product Family | Multifunction DAQ |
| Measurement Type | Voltage |
| Form Factor | USB |
| Operating System / Target | Linux Mac OS Windows |
| RoHS Compliant | Yes |
| Isolation Type | None |

| Physical Specifications | |
|--------------------------------|-----------------|
| Length | 16.9 cm |
| Width | 9.4 cm |
| Height | 3.1 cm |
| I / O Connector | Screw terminals |
| USB Power | Bus-Powered |

| Analog Input | |
|--------------------------------|------------------|
| Single-Ended Channels | 16 |
| Differential Channels | 8 |
| Analog Input Resolution | 16 bits |
| Maximum Voltage Range | |
| Range | -10 V - 10 V |
| Accuracy | 2.69 mV |
| Sensitivity | 91.6 μ V |
| Minimum Voltage Range | |
| Range | -200 mV - 200 mV |
| Accuracy | 0.088 mV |
| Sensitivity | 4.8 μ V |
| Number of Ranges | 4 |
| Simultaneous Sampling ⓘ | No |
| On-Board Memory | 4095 samples |

| Analog Output | |
|--|---------------------|
| Number of Channels | 0 |
| Digital I / O | |
| Bidirectional Channels | 0 |
| Input-Only Channels | 4 |
| Output-Only Channels | 4 |
| Timing | Software |
| Logic Levels | TTL |
| Programmable Input Filters | No |
| Supports Programmable Power-Up States? | Yes |
| Digital Input | |
| Input Type | Sinking Sourcing |
| Maximum Voltage Range | 0 V - 5.25 V |

| Counters / Timers | |
|--|---------|
| Watchdog Timer  | No |
| Counters | 2 |
| Buffered Operations | Yes |
| Debouncing / Glitch Removal | Yes |
| Max Source Frequency | 80 MHz |
| Pulse Generation | Yes |
| Size | 32 bits |
| Timebase Stability | 50 ppm |
| Logic Levels | TTL |
| Timing / Triggering / Synchronization | |
| Triggering | Digital |

E.2 Accelerometer Specifications

(From rs-online.com product number 759-1998)

| | |
|----------------------------------|---------------------------|
| Dimensions | 4.15 x 4.15 x 1.5mm |
| Height | 1.5mm |
| Length | 4.15mm |
| Maximum Frequency Response | 1600Hz |
| Maximum Operating Supply Voltage | 3.6 V |
| Maximum Operating Temperature | +85 °C |
| Minimum Operating Supply Voltage | 1.8 V |
| Minimum Operating Temperature | -40 °C |
| Mounting Type | Surface Mount |
| Noise | 250mg/ $\sqrt{\text{Hz}}$ |
| Number of Axis | 3 |
| Package Type | LFCSP LQ |
| Pin Count | 16 |
| Sensitivity | 192mV/g |
| Technology | Analogue |
| Width | 4.15mm |

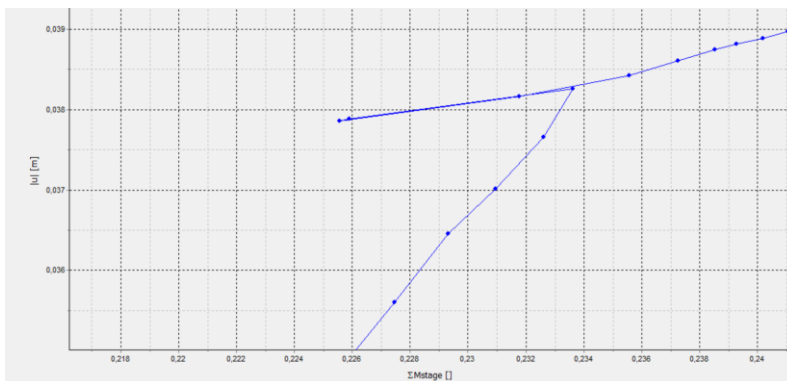
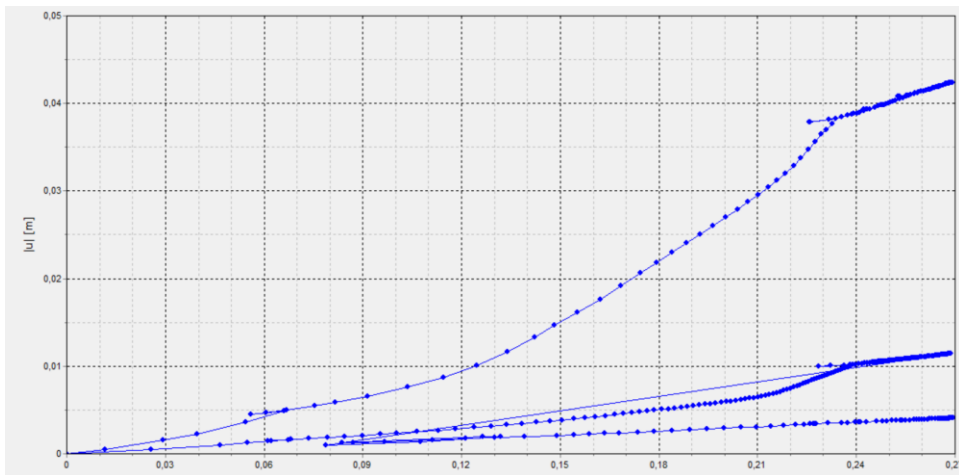
Appendix F

F.1 Settlement Calculations

Undrained $q=200\text{kPa}$

| Test | $ u $ [mm] | % of $ u _{HS}$ |
|-------------------|------------|-----------------|
| HS | 108 | 100,0 % |
| HSSsmall -100 m/s | 42 | 38,9 % |
| HSSsmall -150 m/s | 16 | 14,8 % |
| HSSsmall -200 m/s | 4,1 | 3,8 % |
| HSSsmall -250 m/s | 2,6 | 2,4 % |

Total displacement in undrained analysis when loaded to failure ($\approx 54\text{kPa}$)



| Property | Unit | Value |
|-----------------------|-------------------|-------------------------------------|
| Stiffness | | |
| E_{50}^{ref} | kN/m ² | 2000 |
| E_{oed}^{ref} | kN/m ² | 2000 |
| E_{ur}^{ref} | kN/m ² | 6000 |
| power (m) | | 1,000 |
| Alternatives | | |
| Use alternatives | | <input type="checkbox"/> |
| C_c | | 0,2380 |
| C_s | | 0,07141 |
| e_{init} | | 1,070 |
| Strength | | |
| c'_{ref} | kN/m ² | 6,000 |
| ϕ' (phi) | ° | 29,00 |
| ψ (psi) | ° | 0,000 |
| Small strain | | |
| $\gamma_{0.7}$ | | 0,1000E-3 |
| G_0^{ref} | kN/m ² | 42,75E3 |
| Advanced | | |
| Set to default values | | <input checked="" type="checkbox"/> |
| Stiffness | | |
| ν'_{ur} | | 0,2000 |

Appendix G

G.1 Westerlund on Diagenesis

Westerlund (1978) made shear wave investigations on three clay sites in Trondheim. He conducted both the crosshole method in field and resonant column test in the lab. Based on his data, Westerlund investigated the time effect after primary consolidation based on Anderson (1974). The obtained theoretical values for ΔV_s fitted well with the observed results from the lab.

Westerlund (1978) used the time 20 years to estimate the in situ situation. His results fitted fairly well after the time adjustment, despite using equipment with different strain range in field and lab.

G.2 Aging Effect

Seng and Tanaka (2012) presented data on clay samples from Anderson and Woods (1976) and Lohani et al. (2001) in a normalized plot.

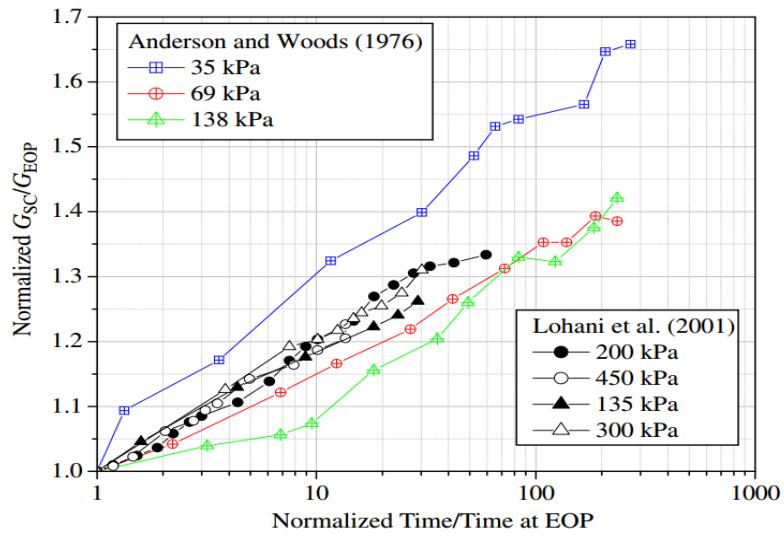


Figure 0.2 Development of small-strain stiffness with time after primary consolidation (Seng and Tanaka, 2012)

Appendix H

H.1 Anisotropy in Gault Clay

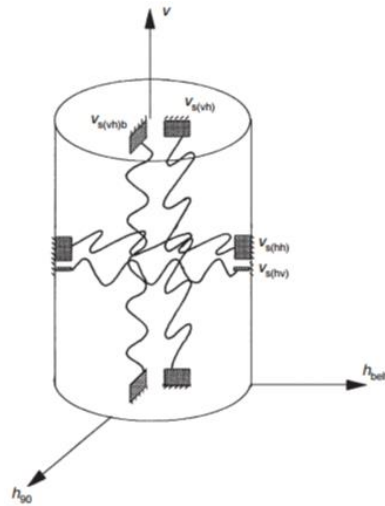


Figure 0.3 Special bender element setup to investigate V_s anisotropy (Pennington et al. 1997)

Pennington et al (1997) investigated anisotropy of small-strain shear stiffness in Gault Clay. A triaxial device with incorporated bender elements to propagate and receive both vertical and horizontal propagating shear waves was developed (Figure 0.3). In the horizontal direction, shear waves with particle motion in both horizontal and vertical direction was made. 100mm triaxial samples of both reconstituted and natural Gault Clay samples were tested to investigate the material anisotropic small-strain stiffness. In situ investigation, by seismic cone and cross-hole method, was available as reference.

Gault Clay is a very stiff, heavily overconsolidated clay deposit with estimated K_0' and OCR of 2.1 and 30 respectively. For the reconstituted samples, $V_{s(vh)}$ and $V_{s(hv)}$ were virtually consistent, indicating the assumption of a cross-anisotropic material to be valid. However, $V_{s(hh)}/V_{s(hv)}$ was found to be in the order of 1.2. The soil fabric is probably the cause. The natural samples and the in situ measurements showed $V_{s(vh)} < V_{s(hv)} < V_{s(hh)}$. That is probably due to the stress history of the Gault Clay.

Appendix J

J.1 Empirical Correlations

Several correlations have been made in order to estimate G_{max} , based on different parameters. Some make a rough estimate based on few parameters, while others give more accurate estimates and requires more parameters.

The formulas for determining G_{max} is usually given on the basis of the modified Hardin & Black equation (Hardin, 1978):

$$G_{max} = A f(e)OCR^k \left(\frac{p'}{p_{ref}} \right)^n$$

where

G_{max} = Small-strain stiffness in GPa

OCR = Over consolidation ratio

p' = Effective mean stress in kPa

p_{ref} = Reference pressure of 100kPa

$f(e)$ = Function of the void ratio, e

A, k, n = Constants given to get the best correlation for different soils. For non-cohesive soils, the factor k will be 0.

In addition to the correlations referred to in this chapter, correlations in respect to several other parameters have been made, e.g. dry and saturated unit weight and SPT.

Cone Penetration Resistance, q_c , is the resistance measured using CPTU. The q_c depends, like G_{max} and G_{oed} on the vertical and horizontal effective stress and soil density. This suggests that a correlation could be made between these parameters. However, it is important to mark that the parameters depend differently on the stress and density condition, and a unique correlation is not to be expected.

Rix and Stokoe (1992) presented a paper where the accuracy of the correlation between G_{max} and q_c for sands was investigated. They found that the G_{max} to q_c ratio decreased as the q_c (or relative density) increased. However the ratio also differed for different sands and Rix and Stokoe (1992) concluded some other factors not included influence the G_{max} to q_c ratio and more work has to be done to identify these. The average values of the ratio resulted in following equation:

$$\frac{G_{max}}{q_c} = 1634 \left[\frac{q_c}{\sqrt{\sigma_v'}} \right]^{-0.75}$$

Regarding clays Mayne & Rix (1995) derived following empirical formula:

$$V_s = 1.75q_c^{0.627}$$

Later Long & Donohue (2010) updated the equation based on results from ten Norwegian clays and proposed following relation:

$$V_s = 2.944q_c^{0.613}$$

It has shown a better correlation with Norwegian clays.

Other parameters have also been introduced to the correlation between q_c and G_{max} to obtain more accurate results. Some of the most common parameters to include are void ratio, e_0 , OCR, plasticity index, I_p or CPTU pore pressure parameter B_q . To use the corrected cone tip resistance, q_t , has also given good results.

Long & Donohue (2010) proposed the following more advanced and accurate relations:

$$G_{max} = 4.39q_t^{1.225}(1 + B_q)^{2.53}$$

$$V_s = 1.961q_t^{0.579}(1 + B_q)^{1.202}$$

Where B_q is defined by Lunne et al (1997) as:

$$B_q = \frac{u_2 - u_0}{q_t - \sigma_{vo}} = \frac{\Delta u}{q_{net}}$$

Mayne (2007b) suggested following relation valid for most soil types:

$$G_{max} \approx 50p_{ref} \left[\frac{q_t - \sigma_{vo}}{p_{ref}} \right]^{m^*}$$

where p_{ref} is reference pressure at 100kPa, σ_{vo} is total overburden stress and m^* is a variable depending on soil type. $m^* = 0.6$ for clean quartz sands, 0.8 for silts and 1.0 for intact clays of low to medium sensitivity.

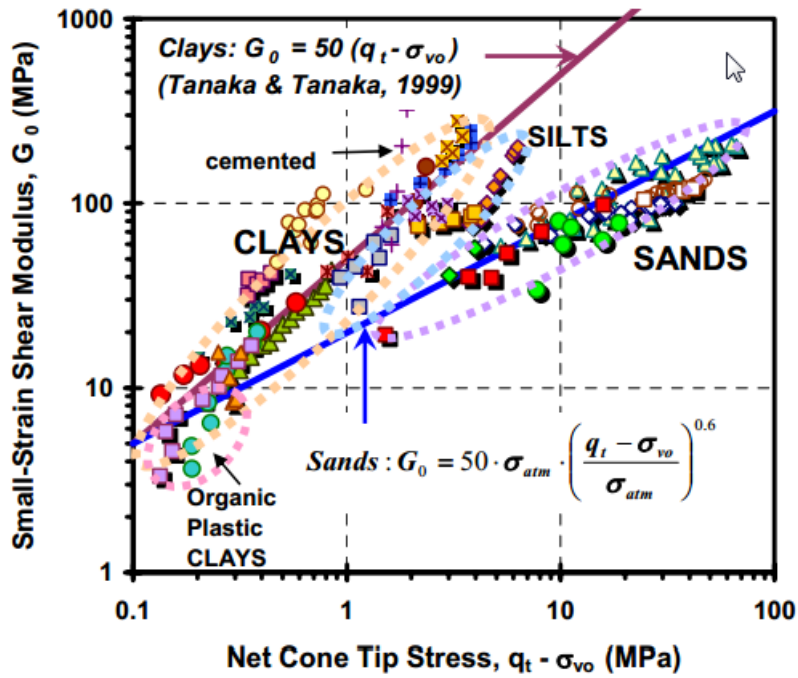


Figure 0.4 Visualisation of measurements vs. correlation function (Mayne 2007b)

Brinkgreve (2010) proposed various empirical formulas for calculating the reference stiffness parameters for (quartz) sands. His proposed formulas were supposed to be simple, in the way that they include few parameters. They are supposed to be used as a first approximation in advanced models and hence not very accurate. The formulas are linearly dependent on the relative density (RD), defined as: $RD = \frac{e_{max} - e}{e_{max} - e_{min}}$, where e is the void ratio. The formula for

G_{max}^{ref} and E_{oed}^{ref} are given in below.

$$G_{max}^{ref} = 60 + 68RD$$

$$E_{oed}^{ref} = 60RD$$

Where the values are given in MPa.

The formula for G_{max}^{ref} where based on the result from ten different sands, shown in Figure 0.5.

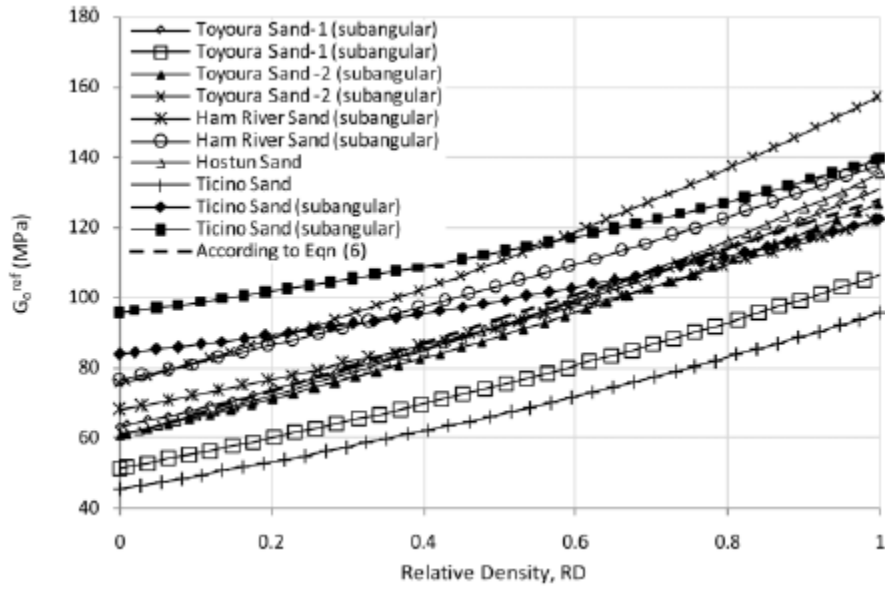


Figure 0.5 G_{max} to RD for ten different sands (Brinkgreve 2010)